GEORGIA INSTITUTE OF TECHNOLOGY
OFFICE OF CONTRACT ADMINISTRATION
SPONSORED PROJECT INITIATION

Date: March 6, 1979

Project Title: Computer Simulation of Locking Material Protected Structure Response to Mine Blast

Project No: E-16-638

Project Director: Dr. S. V. Hanagud

Sponsor: Army Materials and Mechanics Research Center

Agreement Period: From 2/12/79 Until ~~8/11/80~~ 8/11/81 ~~7/1/81~~

Type Agreement: Contract No. DAAG46-79-C-0014

Amount: $49,958 (Army)
2,453 (GIT E-16-335)
$52,411 Total

Reports Required: Interim Reports, Final Report

Sponsor Contact Person (s):

Technical Matters

Mr. Jiro Adachi
Army Materials & Mechanics Res. Ctr.
ATTN: DRXMR-AP
Watertown, MA 02172
(617) 923-3303

Contractual Matters
(thru OCA)

Mr. Thomas A. Bryant
Office of Naval Research
Resident Representative
Georgia Institute of Technology
325 Hinman Research Building
Atlanta, GA 30332

Defense Priority Rating: DO-C9 under DMS Reg. 1

Assigned to: Aerospace Engineering (School/Laboratory)

COPIES TO:

- Project Director
- Division Chief (EES)
- School/Laboratory Director
- Dean/Director—EES
- Accounting Office
- Procurement Office
- Security Coordinator (OCA)
- ✓Reports Coordinator (OCA)
- Library, Technical Reports Section
- EES Information Office
- EES Reports & Procedures
- Project File (OCA)
- Project Code (GTRI)
- Other

GEORGIA INSTITUTE OF TECHNOLOGY OFFICE OF CONTRACT ADMINISTRATION

SPONSORED PROJECT TERMINATION SHEET

Date 6/15/82

Project Title: Computer Simulation of Locking Material Protected Structure Response to Mine Blast

Project No: E-16-638

Project Director: Dr. S. V. Hanagud

Sponsor: Army Materials and Mechanics Research Center

Effective Termination Date: 8/11/81

Clearance of Accounting Charges: 8/11/81

Grant/Contract Closeout Actions Remaining:

- [ ] Final Invoice and Closing Documents
- [ ] Final Fiscal Report
- [x] Final Report of Inventions
- [x] Govt. Property Inventory & Related Certificate
- [ ] Classified Material Certificate
- [ ] Other _____

Assigned to: Aerospace Engineering (School/Laboratory)

COPIES TO:

Administrative Coordinator	Research Security Services	EES Public Relations (2)
Research Property Management	~~Reports Coordinator (OCA)~~	Computer Input
Accounting	Legal Services (OCA)	Project File
Procurement/EES Supply Services	Library	Other _____

FORM OCA 10:781

FINAL REPORT
E-16-638

COMPUTER SIMULATION FOR THE TRANSIENT DYNAMIC RESPONSE OF LOCKING MATERIALS

BY

S. Hanagud, Principal Investigator

and

Research Assistants:

N. Abhyankar

S. Chandra Shekhara

H.P. Chen

R. L. Latham

SUMMARY

The concept of a locking material and the potential effectiveness of the locking material for possible use as a coutermeasure to specified mine blasts have been investigated in the report. The effectiveness of the countermeasure has been demonstrated by the use of analytical methods and second order accurate computer codes. Computer codes have been developed to investigate and evaluate such a design that uses the countermeasures. The computer codes include programs in one space dimension, three space dimensions, axisymmetric coordinates and state space approach.

As a result of the investigation, specific design parameters, candidate materials and fields for further study have been identified.

TABLE OF CONTENTS

I. INTRODUCTION

This report presents the results to date of investigations concerning the development of a countermeasure to mine blasts. In particular, the investigations have been conducted to develop computer simulation techniques that are capable of simulating the transient dynamic response of Locking materials[1,2] or locking material - structure combinations. These developed techniques have been used to

(a) examine if a locking material shield has the potential of protecting a given structure from dynamic loads that have a time history similar to that of mine blasts, and

(b) provide a tool for designing the locking material shield - structure combination.

Terms, such as foams, distended materials[3] or nonreactive porous solids[4], have been used to describe the locking materials. Typically, a locking material is characterized by a hydrostatic pressure -density curve similar to that shown in Figure 1. The model described in Figure 1 is an idealized behavior. In practice, a more realistic model may be necessary. A material, which follows the model shown in Figure 2 behaves like an elastic solid below a pressure p_E. For pressure, $p > p_E$, the pore spaces collapse and the material locks, at a density ρ_l . The subsequent behavior of the material is that of an incompressible material. In practical shock interaction and attenuation calculations by numerical techniques, the model shown in Figure 1 is replaced by a pressure-density relationship similar to those shown in Figures 2 or 3. In Figure 3, after reaching the locking density, the material is assumed to follow a pressure-density behavior of the corresponding solid. Furthermore, unloading will follow different paths as shown in the Figures 2 and 3. Such unloading paths are necessary to reflect the fact that a collapsed porous space can not be recovered. An exception to this rule is the graphite foam[3].

The theoretical foundation for expecting a locking material to be an effective peak stress attenuator or a countermeasure to mine blasts can be summarized as follows. Materials, that approximate a pressure-density behavior of Figures 1, 2 or 3, imply a large ratio of unloading or rarefaction wave velocity to the loading or shock velocity. The large ratio is the result of the fact that the velocity of the loading shockwave is related to the slope of the straight line connecting the initial and final states. The velocity of the unloading wave or rarefaction wave is related to the slope of the pressure-density curve for

the solid at the locked state. The attenuation is caused by the unloading or rarefaction wave overtaking the loading shock wave because of the relatively higher velocity of the unloading waves. In practical situations, the effects of shear stresses and yielding need to be considered.

Candidate Materials

In principle, locking material can be produced from any parent solid material. The needed process of production requires the formation of a nonreactive porous solid of a density lower than that of the parent material. A commercial aluminum locking material MO-AK (Emerson and Cummings) has been available in the past. This is usually inhomogeneous. Homogeneous aluminum locking material can be produced by techniques[3] such as hot pressing of aluminum powders, cold pressing of aluminum powders followed by sintering or a repeated sequence hot pressing that is followed by sintering of aluminum powders and the use of silica microballons. Commercially, graphite locking materials are available from companies such as National Carbon Company. Of course, a very common locking material of comparatively low threshold pressure capability that is easily available is styro-foam. Depending on the environment and the peak stresses that need to be attenuated, different types of locking material can be chosen or designed for a particular application. For example, in the case of a tank that is subjected to mine blasts, a locking material made of steel may be an interesting possibility. In some cases, a combination of different locking materials or a sandwich construction may be more practical.

Theoretical Foundation

Consider a locking material in a state of one dimensional strain along x-axis. A pressure-density relationship as shown in Figure 4 has been assumed. Initially, stresses and velocities, in the region $x \geq 0$, have been assumed to be equal to zero. At time $t = 0$, it is assumed that a stress $-\sigma_x = \bar{\sigma}$ is applied at the left boundary. The left boundary is initially at $x = x_0(t=0) = 0$. The applied stress is maintained at the left boundary for $0 < t < t_1$ as shown in Figure 5. In addition to the pressure density behavior, the behavior in shear is assumed to be elastic-plastic with the following yield condition.

$$(\sigma_1 - \sigma_2)^2 + (\sigma_2 - \sigma_3)^2 + (\sigma_3 - \sigma_1)^2 = 2Y^2 \qquad (1)$$

In this equation, σ_1, σ_2, σ_3 are the principal stresses and Y is the yield stress in simple tension. For the assumed one-dimensional strain conditions, a σ_x- ρ relationship can be derived from the pressure-density relationship and the assumed yield condition. The resulting σ_x- ρ relationship is as illustrated in Figure 6. The slope of the σ_x- ρ curve for $\rho \gtrsim \rho_1$ is derived from the mechanical behavior of the solid that constitutes the parent material for the given locking material of initial density ρ_0. For example, ρ_0 for an aluminum locking material can be in the range of 1.1 gms/c.c. to 2.3 gms/c.c. The value of ρ_1 is approximately equal to 2.7 gms/c.c. In practice, ρ_1 is usually slightly below the value of the solid density of the parent material.

For $t > 0$, the applied stress at the left boundary results in two stress waves propagating in the positive x-direction. The first wave is an elastic forerunner that carries the stress discontinuity that corresponds to $\tilde{Y}^*$. The second wave is a shock wave that carries the stress discontinuity that corresponds to the difference between $\bar{\sigma}$ and $\tilde{Y}^*$. The shockwave velocity is denoted by $\dot{k}$. The following jump conditions are valid across the elastic forerunner and the shock wave.

$$\rho_o (\dot{k}_e - v_o) = \rho_e (\dot{k}_e - v_e) \qquad (2)$$

$$\tilde{Y} = -\rho_e (\dot{k}_e - v_e) v_e + \rho_o (\dot{k}_e - v_o) v_o \qquad (3)$$

$$\rho_1 (\dot{k}_1 - v_1) = \rho_e (\dot{k}_1 - v_e) \qquad (4)$$

$$\bar{\sigma} - \tilde{Y} = -\rho_1 (\dot{k}_1 - v_1) v_1 + \rho_e (\dot{k}_1 - v_e) v_e \qquad (5)$$

In these equations, v_e and v_0 are the particle velocities ahead of the elastic forerunner wave and behind the forerunner wave respectively. The velocity of elastic forerunner wave itself is equal to $\dot{k}_e$. In a similar way, v_1 is the particle velocity behind the shock wave. From initial conditions, $v_0 = 0$. From equations (4) and (5) the shock wave velocity $\dot{k}_1$ is given by the following equation.

$$\dot{k}_1 = v_e + \sqrt{\frac{\bar{\sigma} - \tilde{Y}}{\rho_e (1 - \frac{\rho_e}{\rho_1})}}$$

---

* $\tilde{Y} = \left(\frac{K}{2G} + \frac{2}{3} \right) Y$

usually, v_e is very small and

$$\rho_e \approx \rho_0$$

Then

$$\dot{K}_\ell = \sqrt{\frac{\bar{\sigma} - Y}{\rho_0 \left(1 - \frac{\rho_0}{\rho_\ell}\right)}}$$

This is the velocity of the loading shock wave in the locking material. For example, for aluminum locking material of initial density $\rho_0 = 1.5$ gms/c.c., $\rho_\ell = 2.7$ gms/c.c., Y = 37,500 psi and $\bar{\sigma}$ = 125,000 psi the velocity of the loading shock wave is 3354 feet per second which is approximately 20% of the longitudinal elastic wave velocity in solid aluminum. Similarly for $\bar{\sigma}$ = 525,000 psi the velocity of the loading shock wave is approximately 44% of the longitudinal elastic wave velocity of the solid aluminium. These examples qualitatively illustrate the slow loading velocities in a locking material of low initial density. However, it is to be noted that the shock wave velocity in a solid is slower [illegible]dinal elastic wave velocity. Even then, the shock wave velocity can be shown to be slower in locking materials than in the corresponding solid.

Experimental Background

In the past, experimental investigations have been conducted[3] on several locking materials. In these investigations, metals, plastics, graphite and ceramics have been used as parent materials to produce locking materials. Experiments have been conducted by using light gas guns and flyer plates. In these experiments, attempts have been made to simulate conditions of one dimensional strain. In the point of view of the present study, a significant result, from these studies, concerns a comparison of the shock wave velocities in locking materials with the corresponding wave velocities of solid materials.

In most of these studies, a two wave pattern has been observed in locking materials and solids. In locking materials, a forerunner wave carries stresses in the material before the phase transition from the initial density ρ_0 to the locked density ρ_ℓ. The second slow wave corresponds to the shock wave that was discussed in the previous section. This shock wave carries stresses that exceed the stresses necessary for phase transition. Solid materials also exhibit a two wave pattern. In this case, the stresses carried by the forerunner wave

correspond to the yield limit and the elastic behavior of the solid before yield. This forerunner wave travels at a velocity corresponding to the longitudinal wave velocity. The second wave carries stresses that exceed the elastic limit. The experiments confirm the fact that this second wave in the solid is much faster than the second shock wave in the locking material. For example, in Aluminum locking materials of initial density ρ_0 = 2.1 gms/c.c., the second shock wave velocity varied from 0.7 to 1.29 mm/μsec. The second wave velocity, in the corresponding solid was in the range of 4.62 mm/μsec. Similarly, the first wave velocities, in the locking materials, was smaller than the first wave velocities in the corresponding solid. The first wave velocities, in aluminum locking materials of initial density ρ_0 = 2.1 gms/c.c., varied in the range 1.6 mm/ μsec to 2.0 mm/μsec. The corresponding first wave in the solid travelled with a velocity of 6.11 mm/ μsec.

The theoretical foundation and the results of the experimental studies confirm the potential benefits that can be derived from locking materials when they are used as protective structures.

II. RESEARCH PLAN

Problems Associated With Engineering Design

In the point of view of engineering designs, the results of this project should provide tools to design a countermeasure or a protective structure for mine blasts that will be specified. In this report, however, the protective structure for the mine blasts is assumed to be made of a locking material. Specifically, such a design involves the selection of a parent material from which the locking material is produced, the thickness of the protective structure, other geometrical parameters and methods of joining the countermeasure to the structure. In addition, the selection of an initial density for the locking material and the specification of the desired microstructure constitute important aspects of the design. The selected initial density, the specified production technique and the resulting microstructure, usually, determine the range of pressures at which the phase transition takes place from the initial density to the locked density. The microstructure is also responsible for the elastic stress-strain behavior and the associated yield conditions.

An essential design tool, for the selection of the various design parameters, is a computer simulation that is capable of providing the transient dynamic response of the locking material or the locking material and structure combinations. The specified mine blasts and the various design parameters can be supplied as an input to the resulting computer program. The output can be obtained as deformations and stresses at various locations as a function of the time. The output data can then be used

(a) to check if the selected design parameters provide the desired margin of safety for various failure modes,
(b) to iterate or to modify the design parameters and
(c) to establish the damage tolerance and reliability of the design.

The primary objectives of the reported investigations is to develop such computer simulations and the resulting computer programs. To date, most of the reported investigations have been restricted to one space dimension and time. The results have been mainly used to simulate the experimental results. The programs have not been used to study the effectiveness of the locking material as a countermeasure to resist mine blasts. A study of the transient-dynamic response of a locking material that involved two space dimensions and time has been reported by the author[4]. This study described the impact of compactible plates under axisymmetric conditions. The constitutive relationship that was used for the

compactible plate is very specialized and cannot be easily generalized for the locking materials of concern here. The one dimensional analysis and the compactible plate analysis have used the finite difference technique developed by Von Neuman and Richtmyer[5,6]. This finite difference scheme is similar to that used in the Hemp code[7]. Certain difficulties were encountered in the application of the Von Neuman's approach to locking materials.

(1) Very small time steps were needed to account for the phase transition from the initial density to the locked density. Oscillations, overshoots and undershoots were excessive.
(2) An accurate computer simulation of the precursor wave was very difficult.
(3) Computational efficiency and the level of accuracy decreased when two or more space dimensions were considered. Similar problems were encountered in considering multiple reflections.

Other investigators[3,4] also experienced similar difficulties in applying the Von Neumann's technique to the study of the dynamic response of locking materials and phase transition.

In order to remove these difficulties and develop the needed computer simulation techniques for transient dynamic response of locking materials, the following research plan was adapted.

(1) The first step was to prepare a state of the art review of finite difference methods for the numerical solution of hyperbolic differential equations.
(2) The second step was to select a computationally efficient and accurate finite difference method.
(3) The next step was to investigate the application of the method to solid mechanics and structures problem by analyzing problems with known solutions.
(4) The selected second order accurate method was then applied to study the transient response of locking material structures under the conditions of one dimensional strain. The purpose of the analysis was to demonstrate the capability of locking material as a counter measure to mine blasts.
(5) Then a computer simulation of locking material was developed under conditions of axisymmetry and finite deformations.
(6) Later a new technique called "state space" approach has been developed. In this method the differential equations in r-z directions have been reduced to differential equations in r coordinate only.

III. STATE OF THE ART REVIEW

Von Neumann's Technique

The field of analysis of the transient dynamic response of the elastic-plastic-locking materials is in the general field that is concerned with seeking solutions to nonlinear hyperbolic systems with prescribed initial values. In the past, it has been possible to obtain very few analytical solutions in these fields. As a consequence, alternative methods of solution have been sought for many practical problems. These alternative methods include numerical solutions by the method of characteristics and transform techniques. The method of characteristics is very cumbersome and the difficulty increases when more than one space dimension is considered. The transform techniques have limitations when applied to nonlinear problems and structures with finite boundaries.

Some of these difficulties have been removed by using the Von Neumann's technique[5,6] to study the dynamic response of solids. The Von Neumann's technique is a very significant contribution to the field of the numerical solution of hyperbolic problems and has been often quoted as "New Math of Mechanics".[8] A classic application of the New Math to problems in solid mechanics is in the form of Hemp Code[7] which has been successfully applied to solve many practical problems. However, even the Von Neumann's technique has some limitations. Some of these limitations are the computational efficiency, orders of accuracy, the spread of contact discontinuities and wave fronts over a finite width, oscillations behind the discontinuities, overshoots, undershoots, practical programming difficulties in applications to structural dynamics problems and limitation on the size of the multidimensional finite difference grids.

Further Developments

The pioneering work of Von Neumann[5] and Richtmyer[6] provided a finite difference technique for hyperbolic problems. In this technique, discontinuities are calculated as a part of the solution instead of employing methods such as "shock fitting" at the internal boundaries. The stability of the computations is accomplished, in this technique, by the use of an artificial viscosity. The resulting method has been applied to many practical problems including solid mechanics problems[7,9,10] to provide results to a first order of accuracy. This finite difference technique and other techniques can be evaluated on the basis of the following criteria.

(1) accuracy
(2) simplicity
(3) computational efficiency
(4) steepness of shock fronts
(5) reduction of diffusion across contact discontinuities
(6) reduction of smearing of shock and contact discontinuities
(7) removal of oscillations behind the shock front
(8) elimination of overshoots and undershoots at shock and other discontinuity fronts
(9) preservation of consistent accuracy in implementation of the boundary conditions
(10) efficient extension to multi-dimensional problems

In the original Von Neumann's technique, large number of finite difference grid points are necessary to insure accuracy in multidimensional problems. As discussed before, an artificial viscosity is necessary to achieve stability. This artificial viscosity and other diffusion, inherent in finite difference methods, have lead to the spread of shock fronts and smearing of contact discontinuities. Oscillations, overshoots and undershoots constitute a set of unavoidable problems. Attempts to decrease oscillations, overshoots and undershoots by the use of an additional amount of artificial viscosity only result in additional smearing of contact discontinuities. Computational efficiency is severely affected in two and three space dimensional problems.

As a first step toward solving these problems, Lax[11] introduced a second order accurate finite difference scheme for hyperbolic differential equations in one space dimension. For example, for a differential equation of the type

$$u_t = A\, u_x$$

the second order accurate finite difference operator is

$$L_x^K = I + K A \Delta_0 + \frac{K^2}{2} A^2 \Delta_{+-}$$

In this equation, K represents the time increment. The quantities Δ_0 and Δ_{+-} represent spatial central finite difference approximations for first and second order derivatives. Even though, it appeared to be very simple, attempts to extend the celebrated Lax's operator to two and three space dimensional problems resulted in numerical procedures that are not

optimally stable in the sense of Courant Levy and Friedrichs[12] stability criteria. This resulted in the necessity for smaller time steps which negates any advantage of the second order accurate finite difference schemes from the point of view of computational efficiency. The simplicity and programming convenience are also affected in these schemes for multidimensions.

In 1968 Strang[13] introduced an optimally stable, second order accurate finite difference procedure for two space dimensions.

In two space dimensions, this optimally stable scheme can be written as follows:

$$L^{K}_{xy} = \frac{1}{2} \left(L^{K}_{x} L^{K}_{y} + L^{K}_{y} L^{K}_{x} \right)$$

or

$$L^{K}_{xy} = \frac{1}{2} L^{K/2}_{x} L^{K}_{y} L^{K/2}_{x}$$

In either of these forms, the multidimensional operators are composed of successive operations of one dimensional Lax type of second order accurate operators in x or y directions. This means, that at any given sequence of computations, only a locally one dimensional operator is being used. The use of locally one dimensional operator means that large grid sizes can be used for multidimensional problems. During a specified computational sequence, only limited amount of data that are needed to perform the locally one dimensional operator, need be kept in the active memory.

The Strang type of second order accurate finite difference scheme for hyperbolic problems has been extended to consider

(a) more than two space dimensions,
(b) equations in a nonconservative form and
(c) nonlinear problems.

by Gottlieb[14], Gourlay[15], and Morris[16] and others[17-21].

For example, equations of the type

$$\{u_t\} = \sum_{j=1}^{d} A_j \{u\} \frac{\partial}{\partial x_j} \{u\}$$

can be considered. In this equation d represents the number of space dimensions. Another significant contribution in seventies[15,16] was the recognition of the fact that the computational sequence can be rearranged to provide second order accuracy at every other time step i.e.,

$$\{u\}^{t+2\Delta t} = L_{x_1} L_{x_2} L_{x_2} L_{x_1} \{u\}^{t} + O(h^3) \tag{6}$$

for a two dimensional problem.

In summary, the second order accuracy, optimal stability i.e.,

$$\frac{\Delta t}{\Delta x_j} |a_j| \leq 1 \tag{7}$$

or larger time steps, locally one dimensional operators and reduction of the number of computations by preserving the second order accuracy only at every other step have significantly contributed toward the development of computationally efficient finite difference schemes for hyperbolic differential equations. Other important contributions that have helped in simplifying the practical aspects of programming are the development of two step formulation for the one dimensional second order finite difference operator[15-21] and the introduction of the concept of point condition codes[10].

However, there are additional problems involving oscillations behind a wave front, undershoots, overshoots and smearing of contact discontinuities and shock fronts. Attempts have been made to improve this situation by Glimm[22], Chorin[23], Harten[24,25] and Sod[26]. Achievement of consistent accuracy at the boundaries[27,28] is also another recognized problem.

IV. PRELIMINARY WORK

Even though these developments have been extensively discussed in mathematical journals and reports, there are very few applications of these techniques in the field of solid mechanics and structures. Only the original Von Neumann's scheme has been applied to many problems. Some preliminary investigations leading to the applications of these new developments, involving second order accuracy, optimal stability, computational efficiency etc., to solid mechanics problems have been conducted at Georgia Institute of Technology.

As a first step, a three dimensional linear elastodynamic problem has been solved. In particular, the problem of a suddenly applied point load moving at a constant velocity on the surface of a linear elastic half space, has been simulated. This problem has also been solved by Gakenheimer and Miklovitz[29,30] and numerical results have been calculated for the case of zero velocity of the point load. The method, that has been used by Gakenheimer and Miklovitz consists of integral transform techniques followed by inversion procedures by the use of Cagniard de Hoop method. These numerical results have been compared with the results obtained at Georgia Institute of Technology by the use of a second order accurate Gottlieb-Strang type of finite difference scheme.

The equations of motion for the three dimensional linear elastodynamic problem can be written as follows:

$$\frac{\partial}{\partial t}\underset{\sim}{u} + \sum_{i=1}^{3} A_i \frac{\partial}{\partial x_i}\underset{\sim}{u} = 0 \tag{8}$$

$$\underset{\sim}{u}^T = \left[\rho u_t^1 , \rho u_t^2 , \rho u_t^3 , \sigma_{11} , \sigma_{22} , \sigma_{33} , \sigma_{12} , \sigma_{23} , \sigma_{31} \right] \tag{9}$$

$$A_1 = \begin{bmatrix}
0 & 0 & 0 & -1 & 0 & 0 & 0 & 0 & 0 \\
0 & 0 & 0 & 0 & 0 & 0 & -1 & 0 & 0 \\
0 & 0 & 0 & 0 & 0 & 0 & 0 & 0 & -1 \\
-(\lambda+2\mu)/\rho & 0 & 0 & 0 & 0 & 0 & 0 & 0 & 0 \\
-\lambda/\rho & 0 & 0 & 0 & 0 & 0 & 0 & 0 & 0 \\
-\lambda/\rho & 0 & 0 & 0 & 0 & 0 & 0 & 0 & 0 \\
0 & -\mu/\rho & 0 & 0 & 0 & 0 & 0 & 0 & 0 \\
0 & 0 & 0 & 0 & 0 & 0 & 0 & 0 & 0 \\
0 & 0 & -\mu/\rho & 0 & 0 & 0 & 0 & 0 & 0
\end{bmatrix}$$

$$A_2 = \begin{bmatrix}
0 & 0 & 0 & 0 & 0 & 0 & -1 & 0 & 0 \\
0 & 0 & 0 & 0 & -1 & 0 & 0 & 0 & 0 \\
0 & 0 & 0 & 0 & 0 & 0 & 0 & 0 & -1 \\
0 & -\lambda/\rho & 0 & 0 & 0 & 0 & 0 & 0 & 0 \\
0 & -(\lambda+2\mu)/\rho & 0 & 0 & 0 & 0 & 0 & 0 & 0 \\
0 & -\lambda/\rho & 0 & 0 & 0 & 0 & 0 & 0 & 0 \\
-\mu/\rho & 0 & 0 & 0 & 0 & 0 & 0 & 0 & 0 \\
0 & 0 & -\mu/\rho & 0 & 0 & 0 & 0 & 0 & 0 \\
0 & 0 & 0 & 0 & 0 & 0 & 0 & 0 & 0
\end{bmatrix}$$

$$A_3 = \begin{bmatrix}
0 & 0 & 0 & 0 & 0 & 0 & 0 & 0 & -1 \\
0 & 0 & 0 & 0 & 0 & 0 & 0 & -1 & 0 \\
0 & 0 & 0 & 0 & 0 & -1 & 0 & 0 & 0 \\
0 & 0 & -\lambda/\rho & 0 & 0 & 0 & 0 & 0 & 0 \\
0 & 0 & -\lambda/\rho & 0 & 0 & 0 & 0 & 0 & 0 \\
0 & 0 & -(\lambda+2\mu)/\rho & 0 & 0 & 0 & 0 & 0 & 0 \\
0 & 0 & 0 & 0 & 0 & 0 & 0 & 0 & 0 \\
0 & -\mu/\rho & 0 & 0 & 0 & 0 & 0 & 0 & 0 \\
-\mu/\rho & 0 & 0 & 0 & 0 & 0 & 0 & 0 & 0
\end{bmatrix}$$

The original Lax operator for this problem consists of

$$L_{x_1 x_2 x_3} = I + \Delta t \left(A\Delta_0^1 + B\Delta_0^2 + C\Delta_0^3 \right) + \frac{\Delta t^2}{2} \left\{ A^2 \Delta_{+-}^1 + B^2 \Delta_{+-}^2 + C^2 \Delta_{+-}^3 + (AB + BA)\ \Delta_0^1 \Delta_0^2 + (BC + CB)\ \Delta_0^2 \Delta_0^3 + (CA + AC)\ \Delta_0^3 \Delta_0^1 \right\} \tag{10}$$

This operator is cumbersome and not optimally stable. The maximum value of time step is restricted by the following equation

$$\frac{\Delta t}{\Delta x} \left| \mu_i \right|_{max} \leq \frac{1}{3\sqrt{3}} \tag{11}$$

The quantity $|\mu_i|_{max}$ represents the maximum magnitude of the eigenvalues of A_i. In an optimally stable scheme, the right hand side which is also often called Courant, Friedrichs, and Levy number (CFL) should be 1 instead of $1/3\sqrt{3}$. In the non-optimally stable scheme the maximum time step is approximately 1/5 of the time step that can be used in an optimally stable scheme. The Gottieb-Strang scheme that has been used in this preliminary work is an optimally stable scheme and CFL = 0.98 has been used. In this scheme, the value of u^{n+2} is obtained by using the following equation

$$\underset{\sim}{u}^{(n+2)\Delta t} = \prod_{i=0}^{2} L_{x_{3-i}} \prod_{i=1}^{3} L_{x_i}\, \underset{\sim}{u}^{n\Delta t} \tag{12}$$

$$L_{x_i} = I + \Delta t\, A_i \Delta_0 + \frac{\Delta t^2}{2} A_i \Delta_{+-}$$

for the partial differential equation

$$\frac{\partial}{\partial t}\{u\} = A_i \frac{\partial}{\partial x_i}\{u\}$$

Even the operator L_{xi} is split into two steps. There are many two step formulations that are available.

In order to compare the numerical results with those from Gakenheimer and Miklovitz,[29,30] an elastic body of the size .08"x.08"x.04" is considered. This body constitutes a finite elastic space when compared to the elastic half space considered by Gakenheimer and Miklovitz. Therefore, the solutions are expected to agree only for a limited interval of time. Because of symmetry, only one quarter of the body is considered as shown in Figure 7. The approximation of the point load directions is also shown in Figure 7. A value of $\Delta x = \Delta y = \Delta z = .002"$ has been selected.

The values of the Lame's constants λ and μ are selected such that the ratio of dilatational velocity c_p to shear wave velocity c_s, is equal to $\sqrt{3}$. The results from the finite difference procedure are converted to the axisymmetric coordinate r-z as shown in Figure 8. The angle φ is measured from z-axis. The displacement and time are nondimensionalized as follows:

$$V_r(d, \varphi, \tau) = \frac{\pi^2 \mu d}{H} u_r(d, \varphi, \tau) \tag{14}$$

$$V_z(d, \varphi, \tau) = \frac{\pi^2 \mu d}{H} u_z(d, \varphi, \tau) \tag{15}$$

$$\tau = \frac{c_p t}{d} \tag{16}$$

In the equations u_r, u_z are the dimensional displacements in r and z directions, H is the applied load, μ is the Lame's constant,

$$d = \sqrt{r^2 + z^2} \tag{17}$$

and

$$\varphi = \tan^{-1} \frac{r}{z} \tag{18}$$

Figure 9a is a plot of v_z versus τ for $\varphi = 0$. Similarly Figure 9b is a plot of v_z versus τ for $\varphi = 30^\circ$ and 60°. The full lines are from Gakenheimer and Miklovitz [29] . The dots represent the results from the numerical solutions. The agreement is very good in the interval of time before the reflections from the boundaries change the solution.

The developed second order accurate computationally efficient finite difference scheme has also been modified to study a linear elastodynamic fracture problem. This problem consists of a rectangular plate of the size 1.6"x.8" containing a central crack of the size .226". This plate is impulsively loaded by a step input load of 10,000 psi at the boundaries that are parallel to the longitudinal direction of the crack. A modulus of elasticity $.2966 \times 10^8$ psi and $\nu = 0.296$ have been assumed. The Courant-Levy-Fredrichs stability number of 0.98 has been used. The variation of a nondimensionalized stress intensity factor $\tilde{K}_I$ with time has been illustrated in Figure 10. The nondimensionalized stress intensity factor $\tilde{K}_I$ has been defined as follows:

$$\tilde{K}_I = \frac{K_I}{H\sqrt{a}} \qquad (19)$$

In this equation '2a' is the length of the crack and H is the applied stress at the boundary.

V. ANALYSIS UNDER CONDITIONS OF ONE DIMENSIONAL STRAIN

The analysis in this chapter deals with the case of one dimensional strain and different end conditions. Provision is made to consider large deformations and an elastic-plastic behavior of the locking material. The initial positions of the body are selected as Lagrangian coordinates and the equations of motion are written accordingly. A locking material behavior is considered for the pressure-density relationship.

The numerical integration of the field equations is carried out by Strang-Gottlieb technique (C-9). A predictor equation is written for a half time step. A corrector equation then yields the values of the unknowns up to 2nd order accuracy in time at every even time step.

Notation

$\sigma_x, \sigma_y, \sigma_z$	Axial Stresses
s_x, s_y, s_z	Deviator Stresses
p	Pressure
ρ	Density
V	Specific Volume
ρ_ℓ	Solid Density
ρ_0	Initial density
u	Velocity in x-direction
G	Shear modulus for the material
K	Bulk modulus for the material
$(\dot{})$	Time derivative

Field Equations

The equation of motion and the equation representing the conservation of mass can be written as follows:

$$\frac{\partial \sigma_x}{\partial x} = \rho \frac{\partial u}{\partial t} \qquad (20)$$

$$\dot{\rho} = -\rho \frac{\partial u}{\partial x} \qquad (21)$$

It is further assumed that the stress tensor can be separated into pressure and stress deviators. Then,

$$\sigma_x = -p + S_x \tag{22}$$

$$\sigma_y = \sigma_z = -p + S_y \tag{23}$$

Before yielding, the stress deviator rate is related to the strain deviator rate. Then,

$$\dot{S}_x = \frac{4G}{3}\frac{\dot{V}}{V} \tag{24}$$

$$\dot{S}_y = \dot{S}_z = -\frac{2G}{3}\frac{\dot{V}}{V} \tag{25}$$

The pressure-density relation for a locking material is assumed in the following form: (see Figure 11).

$$\begin{aligned} p &= f_1(\rho) && \rho_o < \rho < \rho_1 \\ p &= f_2(\rho) && \rho_1 < \rho < \rho_l \\ p &= f_3(\rho) && \rho_l < \rho \end{aligned} \tag{26}$$

The following yield condition is used

$$S_x^2 + 2S_y^2 - \frac{2}{3}Y^2 \leq 0 \tag{27}$$

The final set of equations to be integrated can be written as follows:

$$\frac{\partial u}{\partial t} = \frac{1}{\rho}\frac{\partial \sigma_x}{\partial x} \tag{28}$$

$$\frac{\partial \rho}{\partial t} = -\rho\frac{\partial u}{\partial x} \tag{29}$$

$$\frac{\partial \sigma_x}{\partial t} = \left(\rho\frac{\partial f}{\partial \rho} + \frac{4G}{3}\right)\frac{\partial u}{\partial x} \tag{30}$$

$$\frac{\partial \sigma_y}{\partial t} = \left(\rho\frac{\partial f}{\partial \rho} - \frac{2G}{3}\right)\frac{\partial u}{\partial x} \tag{31}$$

In a matrix form, these equations can be rewritten as follows:

$$\frac{\partial}{\partial t}\{\underset{\sim}{u}\} = [A(\rho)]\ \frac{\partial}{\partial x}\{\underset{\sim}{u}\} \tag{32}$$

where

$$\{\underset{\sim}{u}\} = \begin{Bmatrix} u \\ \rho \\ \sigma_x \\ \sigma_y \end{Bmatrix} \tag{33}$$

and

$$[A(\rho)] = \begin{bmatrix} 0 & 0 & 1/\rho & 0 \\ -\rho & 0 & 0 & 0 \\ \rho\frac{\partial f}{\partial \rho} + \frac{4G}{3} & 0 & 0 & 0 \\ \rho\frac{\partial f}{\partial \rho} - \frac{2G}{3} & 0 & 0 & 0 \end{bmatrix} \tag{34}$$

The Finite Difference Scheme

The given continuum is divided into N number of Lagrangian cells. These cells are denoted by a subscript j (j=1 to N). Each cell is of width Δx^0 at time t=0. The field variables for the cell j at time t is denoted by $\underset{\sim}{u}_j^t$. If all the field variables are known at a given time t, the corresponding values of the field variables at time $t+\Delta t$ can be determined in the following way by using the Gottlieb-Strang scheme

$$\underset{\sim}{u}_j^* = \gamma \underset{\sim}{u}_j^t + \frac{\Delta t}{2\Delta x} A(\gamma \underset{\sim}{u}_j^t)\ \delta \underset{\sim}{u}_j^t \tag{35}$$

$$\underset{\sim}{u}_j^{t+\Delta t} = \underset{\sim}{u}_j^t + \frac{\Delta t}{\Delta x} A(\gamma \underset{\sim}{u}_j^*)\ \delta \underset{\sim}{u}_j^* \tag{36}$$

In these equations u_j^t represents any of the field variables such as u, ρ, σ_x or σ_y at time t in the cell 'j'. The quantity Δx^j is the difference between the x coordinate of the jth and (j-1)th cell at time t. The operators γ and δ are defined as

$$\gamma \bar{f}(x) = \frac{1}{2}\left[\bar{f}\left(x + \frac{\Delta x}{2}\right) + \bar{f}\left(x - \frac{\Delta x}{2}\right) \right] \tag{38}$$

and

$$\delta \bar{f}(x) = \left[\bar{f}\left(x + \frac{\Delta x}{2}\right) - \bar{f}\left(x - \frac{\Delta x}{2}\right) \right] \tag{39}$$

with

$$\bar{f}\left(x + \frac{\Delta x}{2}\right) = \frac{1}{2}\left[\bar{f}\left(x + \Delta x^{j+1}\right) + \bar{f}(x) \right] \tag{40}$$

and

$$\bar{f}\left(x - \frac{\Delta x}{2}\right) = \frac{1}{2}\left[\bar{f}(x) + \bar{f}\left(x - \Delta x^{j}\right) \right] \tag{41}$$

in 'j' notation,

$$\gamma \bar{f}_j = \frac{1}{4}\left[\bar{f}_{j+1} + 2\bar{f}_j + \bar{f}_{j-1} \right] \tag{42}$$

Similarly,

$$\delta \bar{f}_j = \frac{1}{2}\left[\bar{f}_{j+1} - \bar{f}_{j-1} \right] \tag{43}$$

Then,

$$\underset{\sim}{u}^*_j = \frac{1}{4}\left(\underset{\sim}{u}^t_{j+1} + 2\,\underset{\sim}{u}^t_j + \underset{\sim}{u}^t_{j-1} \right) + \frac{\Delta t}{4\Delta x} A\left(\gamma \underset{\sim}{u}^t\right)\left(\underset{\sim}{u}^t_{j+1} - \underset{\sim}{u}^t_{j-1} \right) \tag{44}$$

where A (γu^t) is the appropriate coefficient term. The corrector term is derived as follows:

$$\underset{\sim}{u}^{t+\Delta t} = \underset{\sim}{u}^{t} + \frac{\Delta t}{\Delta x} A(\gamma \underset{\sim}{u}^{*}) \delta \underset{\sim}{u}^{*} \tag{45}$$

where

$$\delta \underset{\sim}{u}^{*} = \underset{\sim}{u}^{*}(x + \frac{\Delta x}{2}) - \underset{\sim}{u}^{*}(x - \frac{\Delta x}{2}) = \frac{1}{2}(\underset{\sim}{u}^{*}_{j+1} - \underset{\sim}{u}^{*}_{j-1}) \tag{46}$$

and

$$\gamma \underset{\sim}{u}^{*} = \frac{1}{2}\left[\underset{\sim}{u}^{*}(x + \frac{\Delta x}{2}) + \underset{\sim}{u}^{*}(x - \frac{\Delta x}{2})\right]$$

$$= \frac{1}{4}(\underset{\sim}{u}^{*}_{j+1} + 2\underset{\sim}{u}^{*}_{j} + \underset{\sim}{u}^{*}_{j-1}) \tag{47}$$

The final form of predictor-corrector equations can be written as follows:

$$\underset{\sim}{u}^{*}_{j} = \frac{1}{4}\left\{\underset{\sim}{u}^{t}_{j+1} + 2\underset{\sim}{u}^{t}_{j} + \underset{\sim}{u}^{t}_{j-1} + \frac{\Delta t}{\Delta x}(\underset{\sim}{u}^{t}_{j+1} - \underset{\sim}{u}^{t}_{j-1}) A(\gamma \underset{\sim}{u}^{t})\right\} \tag{48}$$

$$\underset{\sim}{u}^{t+\Delta t}_{j} = \left\{\underset{\sim}{u}^{t} + \frac{\Delta t}{2\Delta x}(\underset{\sim}{u}^{*}_{j+1} - \underset{\sim}{u}^{*}_{j-1}) A(\gamma \underset{\sim}{u}^{*})\right\} \tag{49}$$

The predictor-corrector equations for the velocity u are

$$u^{*}_{j} = \frac{1}{4}\left\{u^{t}_{j+1} + 2u^{t}_{j} + u^{t}_{j-1} + 4\frac{\Delta t}{\Delta x}\left(\frac{\sigma_x{}^{t}_{j+1} - \sigma_x{}^{t}_{j-1}}{\rho^{t}_{j+1} + 2\rho^{t}_{j} + \rho^{t}_{j-1}}\right)\right\} \tag{50}$$

and

$$u^{t+\Delta t}_{j} = \left\{u^{t} + 2\frac{\Delta t}{\Delta x}\left(\frac{\sigma_x{}^{*}_{j+1} - \sigma_x{}^{*}_{j-1}}{\rho^{*}_{j+1} + 2\rho^{*}_{j} + \rho^{*}_{j-1}}\right)\right\} \tag{51}$$

Similarly, the corresponding equations for other unknowns are as follows:

$$\rho_j^* = \frac{1}{4}\left\{ \rho_{j+1}^t + 2\rho_j^t + \rho_{j-1}^t + \frac{\Delta t}{4\Delta x}\left(u_{j+1}^t - u_{j-1}^t \right) \right.$$
$$\left. \left(\rho_{j+1}^t + 2\rho_j^t + \rho_{j-1}^t \right) \right\} \qquad (52)$$

$$\rho_j^{t+\Delta t} = \rho_j^t + \frac{\Delta t}{8\Delta x}\left(u_{j+1}^* - u_{j-1}^* \right)\left(\rho_{j+1}^* + 2\rho_j^* + \rho_{j-1}^* \right) \qquad (53)$$

Equations for σ_x and σ_y follow a similar pattern. In these equations appropriate functions f_1, f_2 and f_3 have to be chosen in the pressure-density relationships. The space coordinates, i.e., the Euler coordinates are also written in a two step predictor-corrector form. In the case of one dimensional analysis, these are

$$x_j^* = \frac{1}{4}\left\{ x_{j+1}^t + 2x_j^t + x_{j-1}^t + \frac{\Delta t}{2}\left(u_{j+1}^t + 2u_j^t + u_{j-1}^t \right) \right\} \qquad (54)$$

and

$$x_j^{t+\Delta t} = x_j^t + \Delta t\left(u_j^{*t} \right) \qquad (55)$$

Initialization

At time t=0, $\rho = \rho_o$ (initial density) and u = 0. The stress in the x-direction at the left boundary is equal to the applied stress σ. The speed of sound is calculated as

$$c = \sqrt{\frac{\rho \frac{df}{d\rho} + \frac{4G}{3}}{\rho}} \qquad (56)$$

The time step

$$\Delta t = \frac{\Delta x}{c} (CFL) \qquad (57)$$

is evaluated for both layers and the smaller Δt is chosen for computation to account for the stability. In the equation CFL is the Courant-Levy-Fredrichs Number.

Calculation Routine for 2 Layered Material

The following procedure is used in developing a computer program.

1. The material constants for the two layers (the locking material and the solid) such as ρ_o, ρ_ℓ , G are assigned.
2. The number of space regions (j) and their coordinates in the two layers are assigned.
3. The types of boundaries are identified .
4. Boundary conditions are read.
5. The initial conditions for stresses, velocities and densities are specified.
6. The initial time increment is calculated.
7. The 'predictor' equations are used first at the boundary points and then for the interior points. These are to evaluate the space coordinate, velocity, density, and the stresses.
8. Following the 'predictor' equations, the 'corrector' equations are used at the boundary points and for the interior points. Yield conditions are now used to account for plasticity. The values of the field variables at the new time step are now known.
9. The new value of the speed of sound is evaluated.
10. Based on the new position coordinates and the calculated speed of sound, the new time step is determined for the next cycle of calculation.
11. The evaluated values of stresses, density, and the velocity are tabulated for desired time steps.

Discussion of Results

The first step of numerical analysis is to examine the capability and the efficiency of the locking material as a counter measure for the mine blasts. In such an analysis, the

specified items include the peak impact stress and the unloading pattern of the stress wave impinging on the locking material. It is also necessary to specify the initial density of the selected locking materials. The locking density ρ_ℓ is usually fixed for a given locking material. The results of the numerical analysis can then be used to explain the peak stress and the stress distribution in different locking materials for various times after impact and unloading at the boundary.

In the numerical experiments, aluminum locking materials have been selected. Some of the properties of aluminum locking materials have been extensively investigated[3]. A pressure density relationship as shown in Figure 11 has been assumed. The locking density ρ_ℓ is equal to 2.72 gms/c.c. Various initial densities have been considered. Results have been presented for ρ_0 = 1.39, 1.604, 1.818 and 2.1 gms/c.c. There are three distinct branches of the pressure-density relationship. Equations for these branches are as follows:

$$p = P_1 \left(\frac{\rho_1}{\rho_0}\right)\left(\frac{\rho_0 - \rho}{\rho_0 - \rho_1}\right)\left[1 + b\left(\frac{\rho_0}{\rho}\right)\left(\frac{\rho_1 - \rho}{\rho_0 - \rho_1}\right)\right] \qquad \rho_0 < \rho < \rho_1 \qquad (58)$$

$$p = P_1 + \frac{K}{R}\left[\left(\frac{\rho}{\rho_1}\right)^R - 1\right] \qquad \rho_1 < \rho < \rho_\ell \qquad (59)$$

$$p = A\left(\frac{\rho}{\rho_G} - 1\right) + B\left(\frac{\rho}{\rho_G} - 1\right)^2 \qquad \rho_\ell < \rho \qquad (60)$$

In the last of these equations ρ_G is the intersection of the p-ρ curve with ρ-axis as shown in the Figure 11. The appropriate constants were selected from reference 3. For all $\rho > \rho_\ell$, the unloading is assumed to follow the slope of the solid p-ρ curve as shown in Figure 11.

Two types of loading have been considered. The first type of loading consists of a step loading followed by step unloading. It has been assumed that a peak compressive stress of σ_1 is applied at time t=0 to the left boundary of the slab of a locking material. For purposes of illustration, a value of σ_1=100,000 psi has been assumed. The applied stress is reduced to zero by step unloading at time t=0.2 μsec. This loading pattern is illustrated in Figure 12 and will be called loading pattern 'a'. The second type of loading consists of a step loading of

a compressive stress of magnitude σ_1 at t=0 followed by an exponential unloading at the left boundary. For purposes of illustration σ_1 has been assumed to be equal to 100,000 psi. The applied stress is assumed to be maintained at $\sigma = \sigma_1$ for a duration of 0.02 microseconds. Then the exponential decay of the applied load, at the left boundary, decreases the magnitude of σ_1 to .05 σ_1 at 0.2 secs. This loading pattern is illustrated in Figure 13 and will be called loading pattern 'b'.

First, a solid material slab of initial thickness 0.5 inch has been considered. The thickness has been divided into 100 cells. In this case the solid density is ρ_ℓ =2.72 gms/c.c. The transient response of this slab to the loading pattern 'a' has been studied by using the developed computer program and the results are illustrated in Figure 14. This figure is a plot of the stress σ_x as a function of the thickness at two different instants of time t=0.21 μsecs and t=0.68 μ secs. As can be seen in the figure, the stress at a distance of 0.14 inch from the initial left boundary is still approximately 100,000 psi. This is equal to the applied peak stress. No significant attenuation has taken place during the travel of the stress wave through the thickness equal to 0.14 inch.

Next, a locking material, of initial density ρ_o = 2.1 gms/c.c. and locking density ρ_ℓ =2.72 gms/c.c., has been considered. The thickness and division into cells are identical to those for the solid. The transient response to the loading pattern 'a' has been computed and illustrated in Figure 15. The stress distribution as a function of the distance from the left boundary has been illustrated for t=0.13 μsec, 0.54 μsec, 1.17 μsec. and 2.22 μsec. It can been seen that the peak stress has been reduced by approximately 35% during the travel of the shock wave over a distance of 0.09 inch from the left boundary. In this figure the elastic forerunner wave can also be seen. Similar stress distributions for locking materials of initial density ρ_o=1.818 gms/c.c., 1.604 gms/c.c. and 1.39 gms/c.c. have been illustrated in Figures 16, 17 and 18. If these locking materials are considered as countermeasures in front of a given structure, the peak impact stress has been reduced by an amount as much as 50% when the shock wave has propagated a distance of 0.013 inch (Figure 18). It can also be observed that the locking material of lower initial density has the potential of attenuating the impact peak stress by a larger percentage when compared with the locking material of higher initial density.

As a next step, the loading pattern 'b' has been considered. The results of the study of transient response through a solid has been illustrated in Figure 19. The results are similar to those for the loading pattern 'a'. The peak impact stress has not attenuated during the passage of the stress wave over a distance of 0.15 inch. Similar stress distributions for

loading pattern 'b' has been illustrated in Figures (20-23) for different locking materials of initial density ρ_0=2.1 gms/c.c., 1.818 gms/c.c., 1.604 gms/c.c. and 1.39 gms/c.c. The Figure 20 is for a locking material with initial density 2.1 gms/c.c. Over a shock wave traverse of .045 inch the peak stress has been attenuated by 60%. This means the peak stress has been reduced to 40,000 psi. However, the locking material with initial density of 1.3 gms/c.c. can attenuate the peak stress by almost 90%, during the shock traverse of 0.05". This is illustrated in Figure 23. The unloading waves and the elastic forerunners can be identified in all these pictures.

VI. COMPUTER SIMULATION OF LOCKING MATERIALS UNDER CONDITIONS OF AXISYMMETRY

The following governing equations can be written for the analysis of the transient dynamic response of locking materials under conditions of axisymmetry and large deformations

$$\frac{\partial z}{\partial t} = w \tag{61}$$

$$\frac{\partial r}{\partial t} = u \tag{62}$$

$$\frac{\partial w}{\partial t} = \frac{1}{\rho}\frac{\partial \sigma_{zz}}{\partial z} + \frac{1}{\rho}\frac{\partial \tau_{zr}}{\partial r} + \frac{1}{\rho}\frac{\tau_{zr}}{r} \tag{63}$$

$$\frac{\partial u}{\partial t} = \frac{1}{\rho}\frac{\partial \tau_{zr}}{\partial z} + \frac{1}{\rho}\frac{\partial \sigma_{rr}}{\partial r} + \frac{1}{\rho}\frac{\sigma_{rr} - \sigma_{\theta\theta}}{r} \tag{64}$$

$$\frac{\partial \sigma_{zz}}{\partial t} = -\dot{p} + \frac{4G}{3}\frac{\partial w}{\partial z} - \frac{2G}{3}\frac{\partial u}{\partial r} - \frac{2G}{3}\frac{u}{r} \tag{65a}$$

$$\frac{\partial \sigma_{rr}}{\partial t} = -\dot{p} - \frac{2G}{3}\frac{\partial w}{\partial z} + \frac{4G}{3}\frac{\partial u}{\partial r} - \frac{2G}{3}\frac{u}{r} \tag{66a}$$

$$\frac{\partial \sigma_{\theta\theta}}{\partial t} = -\dot{p} - \frac{2G}{3}\frac{\partial w}{\partial z} - \frac{2G}{3}\frac{\partial u}{\partial r} + \frac{4G}{3}\frac{u}{r} \tag{67a}$$

$$\frac{\partial \tau_{zr}}{\partial t} = G\frac{\partial u}{\partial z} + G\frac{\partial w}{\partial r} \tag{68}$$

$$\frac{\partial \rho}{\partial t} = -\rho\frac{\partial w}{\partial z} - \rho\frac{\partial u}{\partial r} - \rho\frac{u}{r} \tag{69a}$$

$$p = p(\rho) \tag{70}$$

$$(\sigma_{zz} + p)^2 + (\sigma_{rr} + p)^2 + (\sigma_{\theta\theta} + p)^2 + 2\tau_{zr}^2 \leq \frac{2}{3}Y_o^2 \tag{71}$$

In these equations, the initial positions of the various points have been used as Lagrangian coordinates. The coordinate directions z and r represent the depth and the radial coordinate as shown in Figure 24. The circumferential direction has been denoted by θ. The other quantities in the equations are as follows:

z,r	current positions of the coordinate
w	velocity in z-direction
u	velocity in r-direction
σ_{zz}	normal stress in z-direction
σ_{rr}	normal stress in r direction
$\sigma_{\theta\theta}$	normal stress in θ direction
τ_{zr}	shear stress
ρ	density
p	hydrostatic pressure
G	modulus of rigidity
Y_o	yield stress in simple tension

The equation (71) is the yield condition. An elastic-ideal plastic condition has been assumed. The pressure p is a function of the density. The functional form is identical to the one assumed in the previous chapter and illustrated in Figure 11.

This set of governing equations can be replaced by the following equivalent set of equations

$$\frac{\partial z}{\partial t} = w \tag{61}$$

$$\frac{\partial r}{\partial t} = u \tag{62}$$

$$\frac{\partial w}{\partial t} = \frac{1}{\rho}\frac{\partial \sigma_{zz}}{\partial z} + \frac{1}{\rho}\frac{\partial \tau_{zr}}{\partial r} + \frac{1}{\rho}\frac{\tau_{zr}}{r} \tag{63}$$

$$\frac{\partial u}{\partial t} = \frac{1}{\rho}\frac{\partial \tau_{zr}}{\partial z} + \frac{1}{\rho}\frac{\partial \sigma_{rr}}{\partial r} + \frac{1}{\rho}\frac{\sigma_{rr} - \sigma_{\theta\theta}}{r} \tag{64}$$

$$\frac{\partial \sigma_{zz}}{\partial t} = \left(\rho\frac{dp}{d\rho} + \frac{4G}{3}\right)\frac{\partial w}{\partial z} + \left(\rho\frac{dp}{d\rho} - \frac{2G}{3}\right)\frac{\partial u}{\partial r} + \left(\rho\frac{dp}{d\rho} - \frac{2G}{3}\right)\frac{u}{r} \tag{65b}$$

$$\frac{\partial \sigma_{rr}}{\partial t} = \left(\rho\frac{dp}{d\rho} - \frac{2G}{3}\right)\frac{\partial w}{\partial z} + \left(\rho\frac{dp}{d\rho} + \frac{4G}{3}\right)\frac{\partial u}{\partial r} + \left(\rho\frac{dp}{d\rho} - \frac{2G}{3}\right)\frac{u}{r} \tag{66b}$$

$$\frac{\partial \sigma_{\theta\theta}}{\partial t} = \left(\rho\frac{dp}{d\rho} - \frac{2G}{3}\right)\frac{\partial w}{\partial z} + \left(\rho\frac{dp}{d\rho} - \frac{2G}{3}\right)\frac{\partial u}{\partial r} + \left(\rho\frac{dp}{d\rho} + \frac{4G}{3}\right)\frac{u}{r} \tag{67b}$$

$$\frac{\partial \tau_{zr}}{\partial t} = G\frac{\partial u}{\partial z} + G\frac{\partial w}{\partial r} \tag{68}$$

$$p = -\frac{1}{3}\left(\sigma_{zz} + \sigma_{rr} + \sigma_{\theta\theta}\right) \tag{69b}$$

$$p = p(\rho) \tag{70}$$

$$(\sigma_{zz} + p)^2 + (\sigma_{rr} + p)^2 + (\sigma_{\theta\theta} + p)^2 + 2\tau_{zr}^2 \leq \frac{2}{3}Y_o^2 \tag{71}$$

Note the continuity equation can be obtained by adding equations (65b), (66b), (67b) and using equation (69b). The above set of governing equations also can be rewritten as follows

$$\frac{\partial}{\partial t}\{u\} = [A]\frac{\partial}{\partial z}\{u\} + [B]\frac{\partial}{\partial r}\{u\} + [C]\{u\} \qquad (72)$$

$$p = -\frac{1}{3}(\sigma_{zz} + \sigma_{rr} + \sigma_{\theta\theta}) \qquad (69b)$$

$$p = p(\rho)$$

$$(\sigma_{zz} + p)^2 + (\sigma_{rr} + p)^2 + (\sigma_{\theta\theta} + p)^2 + 2\tau_{zr}^2 \leq \frac{2}{3}Y_o^2 \qquad (71)$$

where

$$\{u\}^T = \{ z, r, w, u, \sigma_{zz}, \sigma_{rr}, \sigma_{\theta\theta}, \tau_{zr} \}^T$$

The matrices [A], [B] and [C] are not constants. They are functions of the density, $p(\rho)$ and the radial coordinate. Specifically,

$$[A]=\begin{bmatrix}
0 & 0 & 0 & 0 & 0 & 0 & 0 & 0 \\
0 & 0 & 0 & 0 & 0 & 0 & 0 & 0 \\
0 & 0 & 0 & 0 & 1/\rho & 0 & 0 & 0 \\
0 & 0 & 0 & 0 & 0 & 0 & 0 & 1/\rho \\
0 & 0 & \rho\frac{dP}{d\rho}+\frac{4G}{3} & 0 & 0 & 0 & 0 & 0 \\
0 & 0 & \rho\frac{dP}{d\rho}-\frac{2G}{3} & 0 & 0 & 0 & 0 & 0 \\
0 & 0 & \rho\frac{dP}{d\rho}-\frac{2G}{3} & 0 & 0 & 0 & 0 & 0 \\
0 & 0 & 0 & G & 0 & 0 & 0 & 0
\end{bmatrix}$$

$$[B]=\begin{bmatrix}
0 & 0 & 0 & 0 & 0 & 0 & 0 & 0 \\
0 & 0 & 0 & 0 & 0 & 0 & 0 & 0 \\
0 & 0 & 0 & 0 & 0 & 0 & 0 & 1/\rho \\
0 & 0 & 0 & 0 & 0 & 1/\rho & 0 & 0 \\
0 & 0 & 0 & \rho\frac{dP}{d\rho}-\frac{2G}{3} & 0 & 0 & 0 & 0 \\
0 & 0 & 0 & \rho\frac{dP}{d\rho}+\frac{4G}{3} & 0 & 0 & 0 & 0 \\
0 & 0 & 0 & \rho\frac{dP}{d\rho}-\frac{2G}{3} & 0 & 0 & 0 & 0 \\
0 & 0 & G & 0 & 0 & 0 & 0 & 0
\end{bmatrix}$$

$$[C]=\begin{bmatrix}
0 & 0 & 1 & 0 & 0 & 0 & 0 & 0 \\
0 & 0 & 0 & 1 & 0 & 0 & 0 & 0 \\
0 & 0 & 0 & 0 & 0 & 0 & 0 & 1/\rho r \\
0 & 0 & 0 & 0 & 0 & 1/\rho r & -1/\rho r & 0 \\
0 & 0 & 0 & (\rho\frac{dP}{d\rho}-\frac{2G}{3})/r & 0 & 0 & 0 & 0 \\
0 & 0 & 0 & (\rho\frac{dP}{d\rho}-\frac{2G}{3})/r & 0 & 0 & 0 & 0 \\
0 & 0 & 0 & (\rho\frac{dP}{d\rho}+\frac{4G}{3})/r & 0 & 0 & 0 & 0 \\
0 & 0 & 0 & 0 & 0 & 0 & 0 & 0
\end{bmatrix}$$

In all these equations, it has been assumed that the stress tensor can be divided into a hydrostatic pressure p and stress deviators. Then,

$$\begin{aligned} \sigma_{zz} &= -p + S_{zz} \\ \sigma_{rr} &= -p + S_{rr} \\ \sigma_{\theta\theta} &= -p + S_{\theta\theta} \end{aligned} \qquad (76)$$

The quantities S_{zz}, S_{rr} and $S_{\theta\theta}$ are the diagonal components of the stress deviator. The yield condition (71) can be rewritten in the following form

$$S_{zz}^2 + S_{rr}^2 + S_{\theta\theta}^2 + 2\tau_{zr}^2 \leq \frac{2}{3} Y_0^2 \qquad (77)$$

Numerical Scheme

The differential equations have been numerically integrated by an optimally stable explicit finite difference scheme which is locally one dimensional. This scheme can be classified as a Strang type of scheme that provides results to a second order of accuracy in time. The scheme can be formally written as follows:

$$\{u\}^{t+2\Delta t} = L_z \quad L_r \quad L_r \quad L_z \quad \{u\}^t \qquad (78)$$

In this equation L_z is the optimally stable finite difference operator in one space dimension z for the equation

$$\frac{\partial}{\partial t}\{u\} = [A]\frac{\partial}{\partial z}\{u\} + [D]\{u\} \qquad (79)$$

and L_r is the optimally stable finite difference operator in one space dimension r for the equation

$$\frac{\partial}{\partial t}\{u\} = [B]\frac{\partial}{\partial r}\{u\} + [F]\{u\} \qquad (80)$$

It is to be noted that

$$[C] = [F] + [D] \tag{81}$$

The operators L_z and L_r are derived by using the two step formulation suggested by Mac Cormack

$$\{u^*\} = \{u\}^t + \frac{\partial}{\partial t}\{u\}^t \Delta t \tag{82}$$

and

$$\{u\}^{t+\Delta t} = \frac{1}{2}\left[\{u\}^t + \{u^*\}\right] + \frac{\Delta t}{2}\frac{\partial}{\partial t}\{u^*\} \tag{83}$$

The operator L_z can now be derived from equations (79), (82) and (83)

$$\{u^*\} = \{u\}^t + \left[[A]^t \frac{\partial}{\partial z}\{u\}^t + [D]^t \{u\}^t\right] \Delta t \tag{84}$$

$$\{u\}^{t+\Delta t} = \frac{1}{2}\left[\{u\}^t + \{u^*\}\right] + \frac{1}{2}\left[[A]^* \frac{\partial}{\partial z}\{u\}^* + [D]^* \{u\}^*\right] \Delta t \tag{85}$$

Similar expressions can be written for L_r. The next step is to obtain the spacial finite difference form for $\frac{\partial}{\partial r}\{u\}$ and $\frac{\partial}{\partial z}\{u\}$. Because Lagrangian coordinates have been used, the finite difference mesh work deforms with time. The traditional central difference expressions are difficult to use and are not accurate unless a convected coordinates and suitable transformation relationships, are used. However, an integral definition of the partial derivitives can be used. Then

$$\frac{\partial F}{\partial z} = -\frac{1}{A}\left\{F_{12}(r_1 - r_2) + F_{23}(r_2 - r_3) + F_{34}(r_3 - r_4) + F_{41}(r_4 - r_1)\right\} \tag{86}$$

$$\frac{\partial F}{\partial r} = \lim_{A \to 0} \frac{1}{A} \int F(\underline{n} \cdot \underline{i})\, ds \approx \frac{1}{A}\left\{F_{12}(z_1 - z_2) + F_{23}(z_2 - z_3) + F_{34}(z_3 - z_4) + F_{41}(z_4 - z_1)\right\} \tag{87}$$

$$F_{ij} = \frac{1}{2}(F_i + F_j) \tag{88}$$

The locations of the points 1, 2, 3 and 4 are illustrated in Figure 24.

Solution Procedure

1. The first step is to obtain all the input data including the material characteristics, geometry, size of the finite difference mesh work, initial and boundary conditions.
2. The second step is to set up the finite difference grid work and initialize all the field variables. In this step, the size of the first time step Δt is also established from stability considerations.
3. All the field variables are calculated at the boundary and interior points for the first time step Δt^{o}. The concept of the point condition code are used to consider different types of boundaries.
4. The yield condition is now checked and the appropriate stress deviators are adjusted to the yield surface.
5. Then, the appropriate rotational corrections are introduced to account for the finite rotations and the appropriate stress rates.
6. New time step Δt is computed and the calculations are started at step 3.

Numerical results

A circular cylindrical slab of locking material has been considered (Figure 25). The dimensions of the slab are .06 inch in diameter and .03 inch thick. The locking behavior is identical to the one considered in the case of one dimensional strain. The p-ρ diagram is illustrated in Figure 11. It is assumed that the boundary which is initially at r = .03 inch is assumed to be fixed. The boundary z = .03 inch is assumed to be fixed. At the boundary that is initially at z = 0 a compressive normal stress σ_z=100,000 psi is applied during time $0 \leq t \leq .2114$ μsec and $\sigma_z = 0$ for $t > .2114$ μsec. σ_z, σ_r at = .005 inch and at three different timeshave been plotted as a function of z in Figure 26 to 27. The stress τ_{rz} at r = .015 inch has been plotted in Figure 28. The displacements z at boundary that is initially at z = 0 have been plotted at time t = .3875 μsec as a function of original r coordinates (Lagrangian coordinates) in Figure 29.

VII. STATE - SPACE APPROACH

The state-variable method as applied to automatic control theory is well known. In such an analysis, a set of variables is selected and expressed as a state vector. The future state of the vector is predicted from a knowledge of the present state of the vector, input disturbances and a knowledge of system matrix and output distribution matrix. In such an analysis the state vector changes as a function of time. In the present analysis, however, a state-space vector is selected. The state of this vector changes as a function of an independent space coordinate such as z. In any specific problem, the state-space variables and the state space vector need to be selected. At present, the problem of concern is to predict the dynamic response of locking material or a locking material-structure combination by using a state-space approach.

The basic objective of selecting a state-space vector is to reduce the three dimensional field equations that govern the dynamic behavior of a thick slab or layer of slabs to a set of equations involving only two space coordinates. As a special case, an axisymmetric problem has been considered in this section. In such a case, two independent coordinates r and z will be reduced to one independent coordinate r . The slab can undergo finite deformations. A set of Lagrangian coordinates have been used. The initial positions have been selected as the Lagrangian coordinates. The material is assumed to have either a pressure-density behavior of a locking material or that of an elastic solid. It is also assumed to be elastic-plastic.

In the past, there have been many attempts to eliminate one of the coordinates, usually the thickness coordinate, from the set of governing equations. The classical plate theory is one such attempt. This is an approximation and can deal with only thin plates. Attempts have been made to consider thick slabs by including transverse shear deformation and rotary intertia effects. These are again approximations to the three dimensional theory and they consider only small deformations. Furthermore, these theories are inaccurate when layered slabs are considered. The state space approach, however, is an asymptotic expansion of the complete three dimensional equations of motion. By matching the interlayer boundary conditions, layered slabs can be analyzed.

In the past, the analysis has been used to investigate elastostatic problems and elastodynamic problems involving vibrations of structures. The reported analysis has considered only small deformations. The results of the investigations that are reported here are concerned with exploring the feasibility of the application of the state-space approach

to study the transient response of elastic-plastic-locking material involving large deformations.

Outline of the Method

The first step is to select a state-space vector.

$$\{Q\} = \begin{Bmatrix} q_1 \\ q_2 \\ . \\ . \\ q_n \end{Bmatrix} \tag{89}$$

Then, the state-space vector at a given space coordinate c_2 is expressed in terms of the state-space vector at another coordinate c_1.

$$\{Q\}_{\text{coordinate } c_2} = [L]\,\{Q\}_{\text{coordinate } c_1} \tag{90}$$

where $[L]$ is the transfer matrix .

As applied to a locking material slab under axi-symmetric conditions the state-space vector can be written as follows

$$\{Q\} = \begin{Bmatrix} u_t \\ w_t \\ \sigma_z \\ \tau_{rz} \end{Bmatrix} \tag{91}$$

In this equation, u_t is the particle velocity in x-direction, w_t is the particle velocity in z direction, σ_z is the normal stress and τ_{rz} is the shear stress. The dependent field variables that have not been selected as state variables are the stress σ_r, the stress σ_θ and the density ρ. Then, the state vector at any value of $\bar{z}$ can be expressed in terms of the state variable at z=0.

$$\begin{Bmatrix} u_t \\ w_t \\ \sigma_z \\ \tau_{rz} \end{Bmatrix}_{z=\bar{z}} = \begin{bmatrix} L_{uu} & L_{uw} & L_{uz} & L_{uR} \\ L_{wu} & L_{ww} & L_{wz} & L_{wR} \\ L_{zu} & L_{zw} & L_{zz} & L_{zR} \\ L_{Ru} & L_{Rw} & L_{Rz} & L_{RR} \end{bmatrix} \begin{Bmatrix} u_t \\ w_t \\ \sigma_z \\ \tau_{rz} \end{Bmatrix}_{z=0} \tag{92}$$

When specific boundary conditions are known the preceding equations take the following form

$$\begin{Bmatrix} 0 \\ 0 \\ \sigma_z \\ \tau_{rz} \end{Bmatrix}_{z=z_2=H} = \begin{bmatrix} [A_{11}] & [A_{12}] \\ [A_{21}] & [A_{22}] \end{bmatrix} \begin{Bmatrix} u_t \\ w_t \\ -q \\ 0 \end{Bmatrix}_{z=z_1(0)} \tag{93}$$

Where $\sigma_z = -q$ is the applied load on the top surface. This surface is denoted by $z = z_1$. The surface $z_1(0)$ i.e., z_1 at time $t = 0$ is the initial position of the top surface. The velocities u_t and w_t are prescribed to be zero at the fixed surface $z = z_2 = H$. In a similar way, any combination of surface conditions can be prescribed at the top and bottom surfaces $z = z_1(t)$ and $z = z_2(t)$. Then a set of differential equations can be written for u_t and w_t at $z = z_1(0)$.

Then a set of differential equations can be written for u_t and w_t at $z = z_1(0)$

$$\begin{Bmatrix} 0 \\ 0 \end{Bmatrix} = [A_{11}] \begin{Bmatrix} u_{t_o} \\ w_{t_o} \end{Bmatrix} + [A_{12}] \begin{Bmatrix} -q \\ 0 \end{Bmatrix} \tag{94}$$

where $u_t\big|_{z=z_1(0)} = u_{t_o}$ and $w_t\big|_{z=z_1(0)} = w_{t_o}$

This set of differential equations can be integrated to obtain u_{to} and w_{to} as functions of r and time. The remaining field variables at any value of z, r and t can be expressed in terms of $u_{to}(r,t)$ and $w_{to}(r,t)$.

State Space Approach To Axisymmetric Problems

The shear stresses $\tau_{r\theta}$ and $\tau_{\theta z}$ are identically zero because of the assumption of axisymmetry. The remaining stresses σ_r, σ_θ, σ_z and τ_{rz} are independent of θ. The following field equations can be written.

Equations of motion:

$$\frac{\partial \sigma_r}{\partial r} + \frac{\partial \tau_{rz}}{\partial z} + \frac{\sigma_r - \sigma_\theta}{r} = \rho \frac{\partial u_t}{\partial t} \tag{95}$$

$$\frac{\partial \tau_{rz}}{\partial r} + \frac{\partial \sigma_z}{\partial z} + \frac{\tau_{rz}}{r} = \rho \frac{\partial w_t}{\partial t} \tag{96}$$

Conservation of Mass:

$$-\frac{\dot{\rho}}{\rho} = \frac{\partial u_t}{\partial r} + \frac{u_t}{r} + \frac{\partial w_t}{\partial z} \qquad (97)$$

Stress - Strain Relations:

$$\dot{\sigma}_r = \frac{2G}{3}\left(2\frac{\partial u_t}{\partial r} - \frac{u_t}{r} - \frac{\partial w_t}{\partial z}\right) - \dot{p} \qquad (98)$$

$$\dot{\sigma}_\theta = \frac{2G}{3}\left(-\frac{\partial u_t}{\partial r} + 2\frac{u_t}{r} - \frac{\partial w_t}{\partial z}\right) - \dot{p} \qquad (99)$$

$$\dot{\sigma}_z = \frac{2G}{3}\left(-\frac{\partial u_t}{\partial r} - \frac{u_t}{r} + 2\frac{\partial w_t}{\partial z}\right) - \dot{p} \qquad (100)$$

$$\dot{\tau}_{rz} = G\left(\frac{\partial u_t}{\partial z} + \frac{\partial w_t}{\partial r}\right) \qquad (101)$$

Yield Condition:

$$S_r^2 + S_\theta^2 + S_z^2 + 2\tau_{rz}^2 - \frac{2}{3}Y^2 \leq 0 \qquad (102)$$

In the equations (98) to (101) that represent stress-strain relations, G is the modulus of rigidity and p is the hydrostatic pressure. In equation (102) Y is the yield stress in simple tension. It has been assumed that the stress tensor can be separated into a stress deviator and a hydrostatic pressure. The deviator stress components are denoted by S_r, S_θ and S_z. The pressure density relations are assumed in the form as in the case of one dimensional analysis

$$p = P_1\left(\frac{\rho_1}{\rho_0}\right)\left(\frac{\rho_0 - \rho}{\rho_0 - \rho_1}\right)\left[1 + b\left(\frac{\rho_0}{\rho}\right)\left(\frac{\rho_1 - \rho}{\rho_0 - \rho_1}\right)\right] \qquad (103)$$

$$\rho_0 < \rho < \rho_1$$

$$p = P_1 + \frac{K}{R}\left[\left(\frac{\rho}{\rho_1}\right)^R - 1\right] \qquad \rho_1 < \rho < \rho_\ell \qquad (104)$$

$$p = A\left(\frac{\rho}{\rho_G} - 1\right) + B\left(\frac{\rho}{\rho_G} - 1\right)^2 \qquad \rho_\ell < \rho \qquad (105)$$

In these equations, P_1, b, K, R, A and B are constants that characterize pressure-density relations as shown in Figure 11.

From equations of motion and stress-strain relations, the following relationship can be obtained

$$\frac{\partial}{\partial z}\{u\} = [L_1]\{u\} + [L_2]\{\bar{u}\} \qquad (106)$$

In this equation

$$\{u\} = \begin{Bmatrix} u_t \\ w_t \\ \sigma_z \\ \tau_{rz} \end{Bmatrix} \qquad (107)$$

$$\{\bar{u}\} = \begin{Bmatrix} f(\rho) \\ \sigma_r \\ \sigma_\theta \end{Bmatrix} \qquad (108)$$

$$[L_1] = \begin{bmatrix} 0 & -\frac{\partial}{\partial r} & 0 & \frac{1}{G}\frac{\partial}{\partial t} \\ \frac{1}{2r} + \frac{1}{2}\frac{\partial}{\partial r} & 0 & \frac{3}{4G}\frac{\partial}{\partial t} & 0 \\ 0 & \rho\frac{\partial}{\partial t} & 0 & -\frac{\partial}{\partial r} - \frac{1}{r} \\ \rho\frac{\partial}{\partial t} & 0 & 0 & 0 \end{bmatrix} \qquad (109)$$

and

$$[L_2] = \begin{bmatrix} 0 & 0 & 0 \\ \frac{3}{4G}\frac{\partial}{\partial t} & 0 & 0 \\ 0 & 0 & 0 \\ 0 & -\frac{\partial}{\partial r} - \frac{1}{r} & \frac{1}{r} \end{bmatrix} \qquad (110)$$

In equation (106), the partial derivatives of the state-space vector $\{u\}$ with respect to z have been expressed in terms of partial derivatives of the state-space vector $\{u\}$ and associated vector $\{\bar{u}\}$ with respect to r and t. Such an equation is extremely useful in axisymmetric problems where the boundary conditions are prescribed at given values of z coordinates.

The Maclaurin series expansions for the elements of the state-space vector are now written in terms of the z-coordinate. To do this, the necessary derivatives with respect to z are obtained from equation (106)

$$\frac{\partial^2}{\partial z^2}\{u\} = [L_1]\frac{\partial}{\partial z}\{u\} + [L_2]\frac{\partial}{\partial z}\{\bar{u}\}$$

The operator elements of matrices $[L_1]$ and $[L_2]$ are independent of z. Using equation (106) again

$$\frac{\partial^2}{\partial z^2}\{u\} = [L_1]^2\{u\} + [L_2]\frac{\partial}{\partial z}\{\bar{u}\} + [L_1][L_2]\{\bar{u}\}$$

$$\frac{\partial^3}{\partial z^3}\{u\} = [L_1]^3\{u\} + [L_2]\frac{\partial^2}{\partial z^2}\{\bar{u}\} + [L_1][L_2]\frac{\partial}{\partial z}\{\bar{u}\}$$

$$+ [L_1]^2[L_2]\{\bar{u}\} \qquad (111)\ \text{contd.}$$

$$\frac{\partial^4}{\partial z^4}\{u\} = [L_1]^4\{u\} + [L_2]\frac{\partial^3}{\partial z^3}\{\bar{u}\} + [L_1][L_2]\frac{\partial^2}{\partial z^2}\{\bar{u}\}$$

$$+ [L_1]^2[L_2]\frac{\partial}{\partial z}\{\bar{u}\} + [L_1]^3[L_2]\{\bar{u}\} \qquad (111)$$

These expressions can be substituted to replace the partial derivatives with respect to the z coordinate of the state-space vector by the partial derivatives with respect to r and t only.

Then the Maclaurin series expansions for u_t, w_t, σ_z and τ_{rz} are as follows

$$u_t = u_{t_o} + z\left(\frac{\partial u}{\partial z}\right)_o + \frac{z^2}{2!}\left(\frac{\partial^2 u}{\partial z^2}\right)_o + \frac{z^3}{3!}\left(\frac{\partial^3 u}{\partial z^3}\right)_o + \frac{z^4}{4!}\left(\frac{\partial^4 u}{\partial z^4}\right)_o + O(z^5)$$

$$w_t = w_{t_o} + z\left(\frac{\partial w}{\partial z}\right)_o + \frac{z^2}{2!}\left(\frac{\partial^2 w}{\partial z^2}\right)_o + \frac{z^3}{3!}\left(\frac{\partial^3 w}{\partial z^3}\right)_o + \frac{z^4}{4!}\left(\frac{\partial^4 w}{\partial z^4}\right) + O(z^5)$$

$$\sigma_z = \sigma_{z_o} + z\left(\frac{\partial \sigma_z}{\partial z}\right)_o + \frac{z^2}{2!}\left(\frac{\partial^2 \sigma_z}{\partial z^2}\right)_o + \frac{z^3}{3!}\left(\frac{\partial^3 \sigma_z}{\partial z^3}\right)_o + O(z^4) \qquad (112)$$

$$\tau_{rz} = \tau_{rz_o} + z\left(\frac{\partial \tau_{rz}}{\partial z}\right)_o + \frac{z^2}{2!}\left(\frac{\partial^2 \tau_{rz}}{\partial z^2}\right)_o + \frac{z^3}{3!}\left(\frac{\partial^3 \tau_{rz}}{\partial z^3}\right)_o + O(z^4)$$

Writing equations (112) in the matrix form

$$\begin{Bmatrix} u_t \\ w_t \\ \sigma_z \\ \tau_{rz} \end{Bmatrix}_{\text{any } z} = \begin{bmatrix} L_{uu} & L_{uw} & L_{uz} & L_{ur} \\ L_{wu} & L_{ww} & L_{wz} & L_{wr} \\ L_{zu} & L_{zw} & L_{zz} & L_{zr} \\ L_{ru} & L_{rw} & L_{rz} & L_{rr} \end{bmatrix} \begin{Bmatrix} u_{to} \\ w_{to} \\ -q \\ 0 \end{Bmatrix} + \begin{Bmatrix} F_u \\ F_w \\ F_z \\ F_r \end{Bmatrix} \qquad (113)$$

Where L_{uu}, L_{uw} etc., are elements containing differential operators with respect to r and t only. The quantities F_u, F_w, F_z and F_r are derivatives of σ_r, σ_θ and ρ with respect to r, z and t.

The expressions for other field variables σ_r, σ_θ and ρ can be written in terms of the variables u_t, w_t and σ_z by using equations (97), (98) and (99).

$$\frac{\partial \sigma_r}{\partial t} = G\left(\frac{\partial u_t}{\partial r} - \frac{u_t}{r}\right) - \frac{1}{2}\frac{\partial \sigma_z}{\partial t} - \frac{1}{2}\frac{\partial f}{\partial t} \qquad (114)$$

$$\frac{\partial \sigma_\theta}{\partial t} = G\left(\frac{u_t}{r} - \frac{\partial u_t}{\partial r}\right) - \frac{1}{2}\frac{\partial \sigma_z}{\partial t} - \frac{1}{2}\frac{\partial f}{\partial t} \qquad (115)$$

$$\frac{\partial \rho}{\partial t} = \frac{3}{2}\left(\frac{u_t}{r} + \frac{\partial u_t}{\partial r}\right) + \frac{3}{4G}\left(\frac{\partial \sigma_z}{\partial t} + \frac{\partial f}{\partial t}\right) \qquad (116)$$

Solution of equations:

The surface conditions prescribed at $z = z_1$ and $z = z_2 = H$ are as follows.

$$\begin{aligned} -\sigma_z &= q_t \;;\; \tau_{rz} = 0 \quad \text{at} \quad z = z_1 \\ u_t &= 0 \;;\; w_t = 0 \quad \text{at} \quad z = z_2 = H \end{aligned} \qquad (117)$$

Using relations expressed in the form of equations (113)

$$L_{uu}\,U_{to} + L_{uw}\,W_{to} + L_{uz}\,(-q) + F_u = 0 \qquad (118)$$

$$L_{wu}\,U_{to} + L_{ww}\,W_{to} + L_{wz}\,(-q) + F_w = 0 \qquad (119)$$

These are a set of two partial differential equations with respect to independent variables r and t. Once u_{to} and w_{to} are evaluated at every coordinate r and at any time t, the corresponding quantities along with σ_z and τ_{rz} are known at any z by means of equation

(113). σ_r, σ_θ and ρ are evaluated by directly integrating equations (114), (115) and (116) respectively.

Solution Procedure:

The given geometry is divided into Lagrangian cells in r and z directions. The following procedure is adopted to calculate the values of the field variables at time $t + \Delta t$ from the corresponding known values at time t to a first order accuracy.

1. Equations (118) and (119) are solved for u_{to} and w_{to} at time $t + \Delta t$ based on corresponding values at time t.
2. Using equations (113), the field variables u_t, w_t, σ_z and τ_{rz} are evaluated at any coordinate z and for different values of r.
3. By integration of equations (114), (115) and (116), the remaining field variables σ_r, σ_θ and ρ are obtained at any z and r.
4. The check on yield criterion is applied and the stresses are suitably modified.
5. The coordinates r and z are updated for each Lagrangian cell.
6. In order to account for finite deformations, appropriate rotational corrections are incorporated wherever necessary.
7. The time step Δt is updated from stability considerations.
8. Appropriate new values of coordinates z_1 and z_2 are established for all cells for calculations during the next time step. Reassignment of cells are done where necessary.
9. The above steps, beginning at 1, are repeated with the new value of the time step Δt and the new coordinates r and z for each cell.

Numerical Calculations

Because of its inherent stable characteristics, an implicit method of numerical solution is adopted to solve the equations (118) and (119). In keeping with the differential operators in these two equations, a set of eight first order differential equations in t is written as follows:

$$\frac{\partial u_t}{\partial t} = (u_t)_t$$

$$\frac{\partial (u_t)_t}{\partial t} = (u_t)_{tt} \qquad (120) \text{ contd.}$$

$$\frac{\partial (u_t)_{tt}}{\partial t} = (u_t)_{ttt}$$

$$\frac{\partial (u_t)_{ttt}}{\partial t} = f_1$$

$$\frac{\partial w_t}{\partial t} = (w_t)_t$$

$$\frac{\partial (w_t)_t}{\partial t} = (w_t)_{tt} \qquad (120)$$

$$\frac{\partial (w_t)_{tt}}{\partial t} = (w_t)_{ttt}$$

$$\frac{\partial (w_t)_{ttt}}{\partial t} = f_2$$

Where f_1 and f_2 are functions of u_t, $(u_t)_t$, $(u_t)_{tt}$, $(u_t)_{ttt}$, w_t, $(w_t)_t$, $(w_t)_{tt}$ and $(w_t)_{ttt}$ and are obtained from equations (118) and (119) respectively.

The implicit solution that is written to correspond to n + 1 and n time steps takes the form

$$u_t^{n+1} = u_t^n + \frac{\Delta t}{2} \left[(u_t)_t^n + (u_t)_t^{n+1} \right] \qquad (121)$$

$$(u_t)_t^{n+1} = (u_t)_t^n + \frac{\Delta t}{2} \left[(u_t)_{tt}^n + (u_t)_{tt}^{n+1} \right] \qquad (122)$$

$$(u_t)_{tt}^{n+1} = (u_t)_{tt}^n + \frac{\Delta t}{2} \left[(u_t)_{ttt}^n + (u_t)_{ttt}^{n+1} \right] \qquad (123)$$

$$(u_t)^{n+1}_{ttt} = (u_t)^{n}_{ttt} + \frac{\Delta t}{2}\left[f_1^n + f_1^{n+1} \right] \qquad (124)$$

$$w_t^{n+1} = w_t^n + \frac{\Delta t}{2}\left[(w_t)_t^n + (w_t)_t^{n+1} \right] \qquad (125)$$

$$(w_t)_t^{n+1} = (w_t)_t^n + \frac{\Delta t}{2}\left[(w_t)_{tt}^n + (w_t)_{tt}^{n+1} \right] \qquad (126)$$

$$(w_t)_{tt}^{n+1} = (w_t)_{tt}^n + \frac{\Delta t}{2}\left[(w_t)_{ttt}^n + (w_t)_{ttt}^{n+1} \right] \qquad (127)$$

$$(w_t)^{n+1}_{ttt} = (w_t)^{n}_{ttt} + \frac{\Delta t}{2}\left[f_2^n + f_2^{n+1} \right] \qquad (128)$$

By successive substitution of $(u_t)_t^{n+1}$ from equation (122), $(u_t)_{tt}^{n+1}$ from equation (123) into equation (121), an expression for $(u_t)_{ttt}^{n+1}$ is obtained as

$$(u_t)^{n+1}_{ttt} = -(u_t)^{n}_{ttt} - 2\left(\frac{2}{\Delta t}\right)(u_t)^n_{tt} - 2\left(\frac{2}{\Delta t}\right)(u_t)^n_t - \left(\frac{2}{\Delta t}\right)^3 (u_t)^n + \left(\frac{2}{\Delta t}\right)^3 u_t^{n+1} \qquad (129)$$

Similarly, using equations (125), (126) and (127), the expression for $(w_t)_{ttt}^{n+1}$ is obtained as

$$(w_t)^{n+1}_{ttt} = -(w_t)^{n}_{ttt} - 2\left(\frac{2}{\Delta t}\right)(w_t)^n_{tt} - 2\left(\frac{2}{\Delta t}\right)^2 (w_t)^n_t - \left(\frac{2}{\Delta t}\right)^3 (w_t)^n + \left(\frac{2}{\Delta t}\right)^3 w_t^{n+1} \qquad (130)$$

Equating equation (124) with equation (129),

$$F_1\left(u_t^{n+1}, w_t^{n+1}\right) = u_t^{n+1} - \left(\frac{\Delta t}{2}\right)^3 \left[2(u_t)_{ttt}^n + 2\left(\frac{2}{\Delta t}\right)(u_t)_{tt}^n + 2\left(\frac{2}{\Delta t}\right)^2 (u_t)_t^n + \left(\frac{2}{\Delta t}\right)^3 (u_t)^n \right] - \left(\frac{\Delta t}{2}\right)^4 \left[f_1^n + f_1^{n+1} \right]$$

$$= 0 \qquad (131)$$

Similarly, equating (128) with (130) gives

$$F_2\left(u_t^{n+1}, w_t^{n+1}\right) = w_t^{n+1} - \left(\frac{\Delta t}{2}\right)^3 \left[2(w_t)_{ttt}^n + 2\left(\frac{2}{\Delta t}\right)(w_t)_{tt}^n + 2\left(\frac{2}{\Delta t}\right)^2 (w_t)_t^n + \left(\frac{2}{\Delta t}\right)^3 (w_t)^n \right] - \left(\frac{\Delta t}{2}\right)^4 \left[f_2^n + f_2^{n+1} \right]$$

$$= 0 \qquad (132)$$

In equations (131) and (132), the quantities at time step n are known and the unknowns are u_t^{n+1}, w_t^{n+1}, f_1^{n+1} and f_2^{n+1}. To solve the set of these two equations, Newton's iterative method [32] is adopted.

Using a fixed point iteration, i.e., by choosing an initial approximation for u_t^{n+1} and w_t^{n+1} for a fixed n, the successive approximations are generated according to Newton's method by means of the relations

$$\begin{Bmatrix} \tilde{u}_t^{m+1} \\ \tilde{w}_t^{m+1} \end{Bmatrix} = \begin{Bmatrix} \tilde{u}_t^m \\ \tilde{w}_t^m \end{Bmatrix} - \begin{bmatrix} \frac{\partial F_1^m}{\partial \tilde{u}_t} & \frac{\partial F_1^m}{\partial \tilde{w}_t} \\ \frac{\partial F_2^m}{\partial \tilde{u}_t} & \frac{\partial F_2^m}{\partial \tilde{w}_t} \end{bmatrix} \begin{Bmatrix} F_1^m \\ F_2^m \end{Bmatrix} \qquad (133)$$

$$m = 0, 1, 2, \ldots$$

where $\tilde{u}_t = u_t^{n+1}$ for a fixed n.

The iterations using equations (133) are carried out till a satisfactory convergence is achieved for the values of u_t and w_t. These values are then utilized as the initial values u_{to}^{n+1} and w_{to}^{n+1} and solution is carried out further on.

Non-dimensionalization Process:

The displacements u and w are non-dimensionalized as

$$\bar{u} = \frac{u}{H}$$
$$\bar{w} = \frac{w}{H} \qquad (134)$$

With time t being non-dimensionalized as $\bar{t}$ using the relation

$$\bar{t} = \frac{1}{R}\sqrt{\frac{G}{\rho_0}}\, t \qquad (135)$$

the non-dimensionalized velocities are

$$\bar{u}_t = \frac{R}{H}\sqrt{\frac{\rho_0}{G}}\, u_t$$
$$\bar{w}_t = \frac{R}{H}\sqrt{\frac{\rho_0}{G}}\, w_t \qquad (136)$$

In these expressions, H is the total thickness of the slab and R is its radius. The other non-dimensionalized quantities are successively written as

$$\bar{u}_{tt} = \frac{1}{H}\left[R\sqrt{\frac{\rho_o}{G}}\right]^2 u_{tt}$$

$$\bar{u}_{ttt} = \frac{1}{H}\left[R\sqrt{\frac{\rho_o}{G}}\right]^3 u_{ttt}$$

$$\bar{u}_{tttt} = \frac{1}{H}\left[R\sqrt{\frac{\rho_o}{G}}\right]^4 u_{tttt}$$

(137)

$$\bar{w}_{tt} = \frac{1}{H}\left[R\sqrt{\frac{\rho_o}{G}}\right]^2 w_{tt}$$

$$\bar{w}_{ttt} = \frac{1}{H}\left[R\sqrt{\frac{\rho_o}{G}}\right]^3 w_{ttt}$$

$$\bar{w}_{tttt} = \frac{1}{H}\left[R\sqrt{\frac{\rho_o}{G}}\right]^4 w_{tttt}$$

The pressure p, the normal stresses $\sigma_r, \sigma_\theta, \sigma_z$, the shear stress τ_{rz} and the deviator stresses S_r, S_θ and S_z are all non-dimensionalized with respect to the magnitude of the applied load intensity q i.e.,

$$\bar{p} = \frac{p}{q}$$

$$\bar{\sigma}_r = \frac{\sigma_r}{q}$$

$$\bar{\sigma}_\theta = \frac{\sigma_\theta}{q}$$

$$\bar{\sigma}_z = \frac{\sigma_z}{q}$$

(138) Contd.

$$\bar{\tau}_{rz} = \frac{\tau_{rz}}{q}$$

$$\bar{S}_r = \frac{S_r}{q}$$

$$\bar{S}_\theta = \frac{S_\theta}{q} \qquad (138)$$

$$\bar{S}_z = \frac{S_z}{q}$$

Computer programming:

1. The number of Lagrangian cells, their r and z coordinates are established.
2. All displacements and their time derivatives are initially set to zero.
3. The initial densities of all cells are set to the prescribed value of ρ_o.
4. After the initial guess for u_t and w_t for the first time step, the values of u_{to} and w_{to} are obtained after a sufficient number of iterations using Newton's method.
5. With these initial functions u_{to} and w_{to} at any time step n, the field variables u_t, w_t, σ_z, and τ_{rz}, are evaluated at every z and for every coordinate r.
6. With the known values of u_t, σ_z and p, of the previous time step the current values of other field variables σ_r, σ_θ and p are obtained after applying suitable yield check.
7. All the field variables along with the displacements u and w are printed out.
8. The time step is updated based on stability criterion and steps from 4 onwards repeated.

Numerical results:

A slab of locking material of diameter 2 inches and thickness 0.2 inch has been considered. The lower boundary surface which is initially at z_2 = 0.2 inch has been assumed to be fixed. A stress of q = 100,000 psi is applied at the upper boundary surface located at z

$= z_1(0) = 0$. The material properties are the same as described in chapters V and VI. The functional form of $f(\rho)$ is described by Figure 11 and the associated equations (103), (104) and (105). For purposes of illustration, a yield stress = 20,000 psi is assumed. The results of the transient response is shown in Figure 30 .

VIII. CONCLUSIONS

It has been shown that a locking material shield has the potential of protecting a given structure from dynamic loads that have a time history similar to that of mine blasts. This conclusion is based on the analysis under conditions of one dimensional strain and the studies under conditions of axisymmetry. In order to provide a tool for designing the locking material shield, a second order computationally efficient numerical scheme has been developed. The numerical scheme is capable of considering large deformations and locking phase transition. The accuracy of the procedure has been checked by comparing the results with known solutions.

In order to further improve the computational efficiency, a state-space approach has been developed to study the axisymmetric transient response of locking material slabs subjected to dynamic loads. The present stage of the analysis is still in a preliminary stage. Accuracy of the results still needs to be established. Prelimary computations have demonstrated the stability of the computer simulation and a superior computational efficiency. The results can be obtained at a rate approximately five times faster than other known techniques.

The following items have been suggested as recommended additional tasks to follow the present work.

A first task is to develop point condition codes for locking material-structure combinations. The reliability of the resulting computer program should be established by comparing the results with some known solutions. A second task will be to improve the accuracy and computational efficiency during phase transition and unloading. In addition, the shock wave can be steepened by employing newer techniques such as the method of artificial compression. The third task will be to consider non-ideal plasticity. A very important additional task will be to investigate the accuracy of the state-space approach and the needed modifications.

REFERENCES

1. Hanagud, S., "A Contribution to the Theory of Isotropic Locking" Sudaer Report No. 152, Stanford University, California, 1963.
2. Hanagud, S. "Finite Amplitude Spherical Shock Waves in Locking Solids" Proc. 5th U.S. National Congress, 1966. (Invited Sectional Lecture).
3. Linde, R.K., and D.N. Schmidt, "Attenuation of Shockwaves in Distended Solids" AFWL-TR-66-13, 1966.
4. Hanagud, S., G.S. Sidhu and B. Ross, "Elastic-Plastic Impart of Compactible Rods and Plates" Israel Journal of Technology, 1969.
5. Von Neumann, J., and R.D. Richmyer, "A Method for the Numerical Calculation of Hydrodynamic Shocks", J. Appl. Phys. Vol. 21, 1950, pp. 232-237.
6. Richtmyer, R.D., and K.W. Morton, "Finite Difference Methods for Initial Value Problems", Interscience - Wiley, New York, 1967.
7. Wilkins, M.L., "Calculation of Elastic-Plastic Flow" UCRL-7322, Physics UC-34 HD-
8. Cole, J.D., "New Math of Mechanics", Proc. U.S. Natl, Congr. Appl. Mech. 1970, p. 3-10.
9. Ross, B., and S. Hanagud "Penetration Studies" final report, NWRC 7000-452-4, Naval Warfare Research Center, S.R.I. Menlo Park, Calif., 1969.
10. Hanagud, S., G.S. Sidhu and B. Ross, "Elastic-Plastic Impart of Compactible Plates and Paper presented at the sixth U.S. National Congress of Applied Mechanics, 1976.
11. Lax, P., and B. Wendroff, "Difference Schemes for Hyperboilc Equations with High Order of Accuracy", Comm. pure. Apply. Math, 17, 1964, pp. 381-390.
12. Strang, G. "Accurate Partial Difference Methods", Numer. Math. 1964, p. 37.
13. Strang, G., "On the Construction and Comparison of Difference Schemes", SIAM. J. Numer. Anal., 5, 1968, p. 506.
14. Gottlieb, D., "Strang Type Difference Schemes for Multidimensional Problems", SIAM. J. Num. Anal., 9, 1972, pp. 650-661.
15. Gourlay, A.R. and Mitchell, "A Classification of Split Difference Methods for Hyperbolic Equation in Several Space Dimensions", SIAM J. Numer. Math., Vol. 6, 1969, pp. 62-71.
16. Gourlay, A.R. and Morris, J.L., "Multistep Formulation of the Optimized Method for Nonlinear Hyperbolic System in Two Space VAriables", J. Comp. Phys., 5, 1970, pp. 229-243.
17. Turkel, E., "Multidimensional Difference Schemes of Fourth-Order Accuracy" Abarbanil, Gttlieb, J. Comp. Phys., Vol. 21, 1976, pp. 85-113.

18. Turkel, E., "Phase Error and Stability of Second Order MEthods for Hyperbolic Problems I", J. Comp. Phys., Vol. 15, 1974, pp. 226-250.

19. Gottlieb, D. and Turkel, E., "Phase Error and Stability of Second Order Methods for Hyperbolic Problems II", Comp. Phys., Vol. 15, 1974, pp. 251-265.

20. Conley and Smoller, "Shock Waves as Limits of Progressive Wave Solutions of Higher Order Equations", Comm. Pure Appl. Math., Vol. 24, 1971, pp. 459-472.

21. Warming and Hyatt, "The Modified Equation Approach to the Stability and Accuracy Analysis of Finite-Difference Methods", J. Comp. Phys., Vol. 14, 1974, pp. 159-179.

22. Gottlieb, D., and Turkel, E., "On Acceleration of Mac Cormack's Scheme", J. Comp. Phys., Vol. 26, 1978, pp. 252-256.

23. Glimm, J., "Solution in the Large for Nonlinear Hyperbolic Systems of Equations", Comm.Pure. Appl. Math., 18, 1965, pp. 697-715.

24. Chorin, J.A., "Random Choice Solution of Hyperbolic Systems", J. Comp. Phys., 22, 1976, pp. 517-533.

25. Harten, A., "The Artificial Compression Method for Shocks and Contact Discontinuities", Comm. Pure. Appl. Math., 30, 1977, pp. 611-630.

26. Harten, A., "The Method of Artificial Compression" U.S. Atomic Energy Commission, contract report at (11-1)-3077, 1979.

27. Gottlieb, D. and Turkel, E., "Boundary Conditions for Multistep Finite-Difference Methods for Time-Dependent Equation", J. Comp. Phys., Vol. 26, 1978, pp. 181–196.

28. McGuire, G.R., and Morris, J.L., "Restarting Order of Accuracy for Multilevel Scheme for Nonlinear Hyperbolic System in Many Variables", J. Inst. Math. Appl, 17, 1976, pp. 53-67.

29. Gakenheimer, D.C., and J. Miklowitz, "Transient Excitation of an Elastic Half Space by a Point Load Traveling on the Surface", J. Appl. Mech., Vol. ??, 1969, pp. 505-515.

30. Gakenheimer, D.C., "Numerical Results for Lamb's Point Load Problem", J. Appl. Mech., Vol. ??, 1970, pp. 522-524.

31. Varley, E. (Ed), "Propagation of Shock Waves in Solids", AMD Vol. 17, ASME, New York, 1976.

32. Conte, S.D., and C. deBoor, "Elementary Numerical Analysis - An Algorithmic Approach", McGraw Hill Book Company, 1980, pp 216, 403.

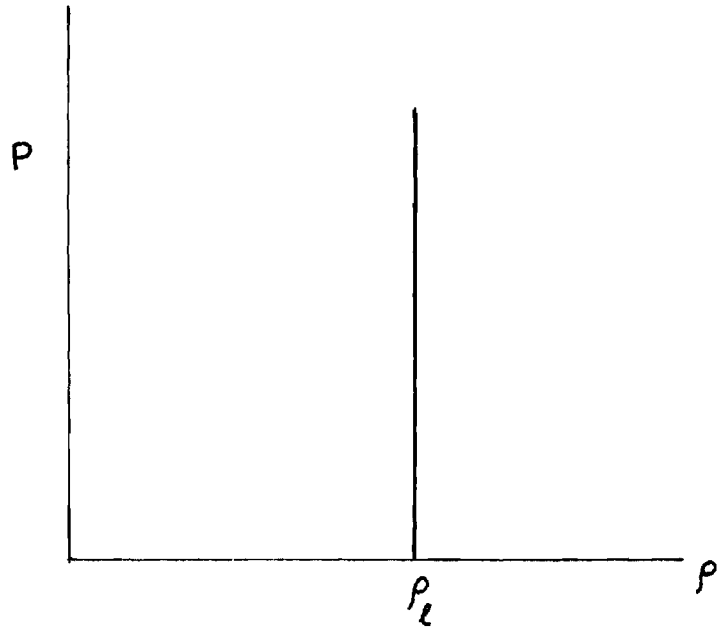

FIG . 1 a simple locking material

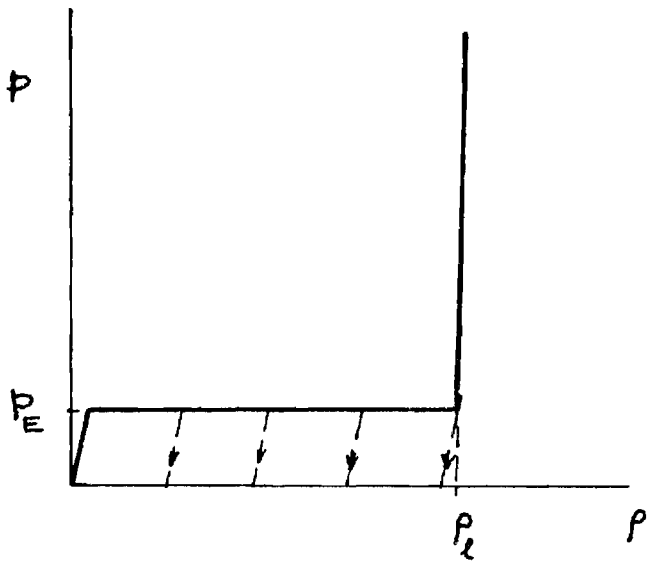

FIG. 2 an elastic locking solid

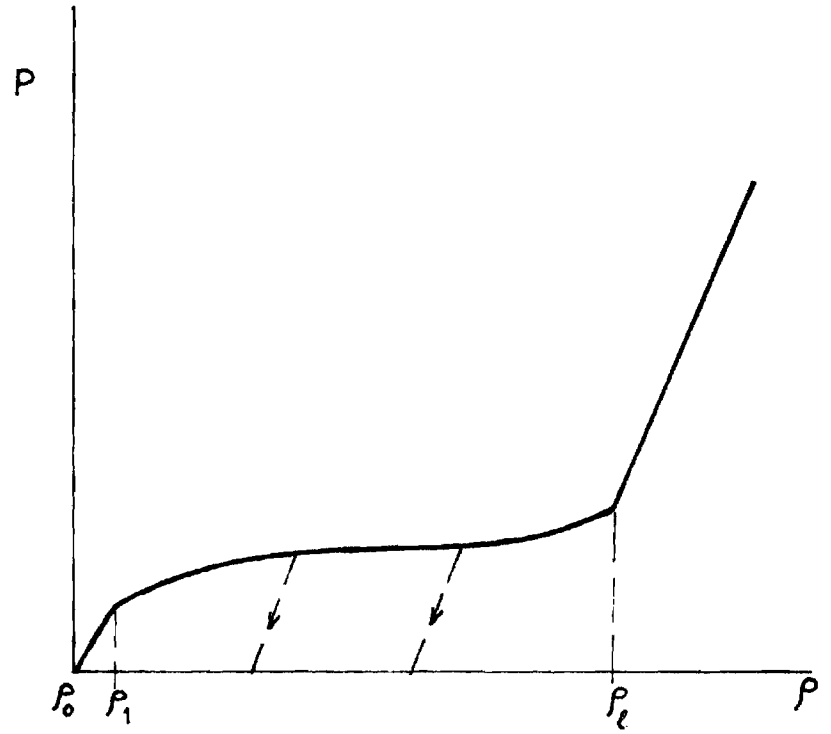

FIG. 3 experimental $p-\rho$ diagram for locking materials

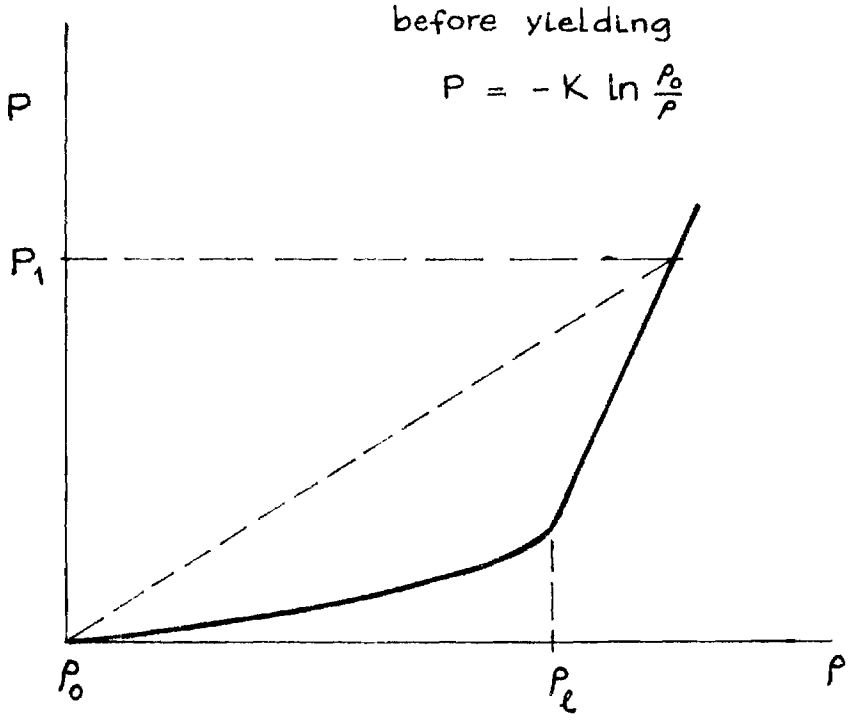

FIG. 4 pressure density relationship

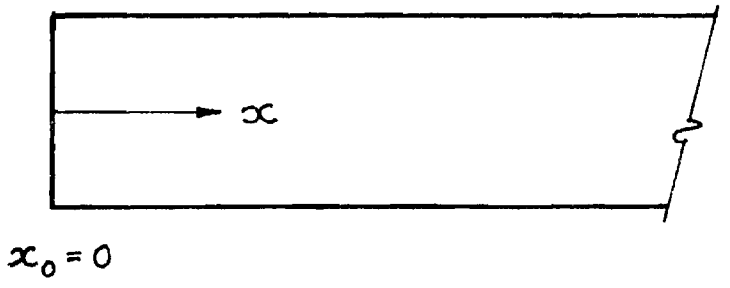

FIG. 5 material geometry

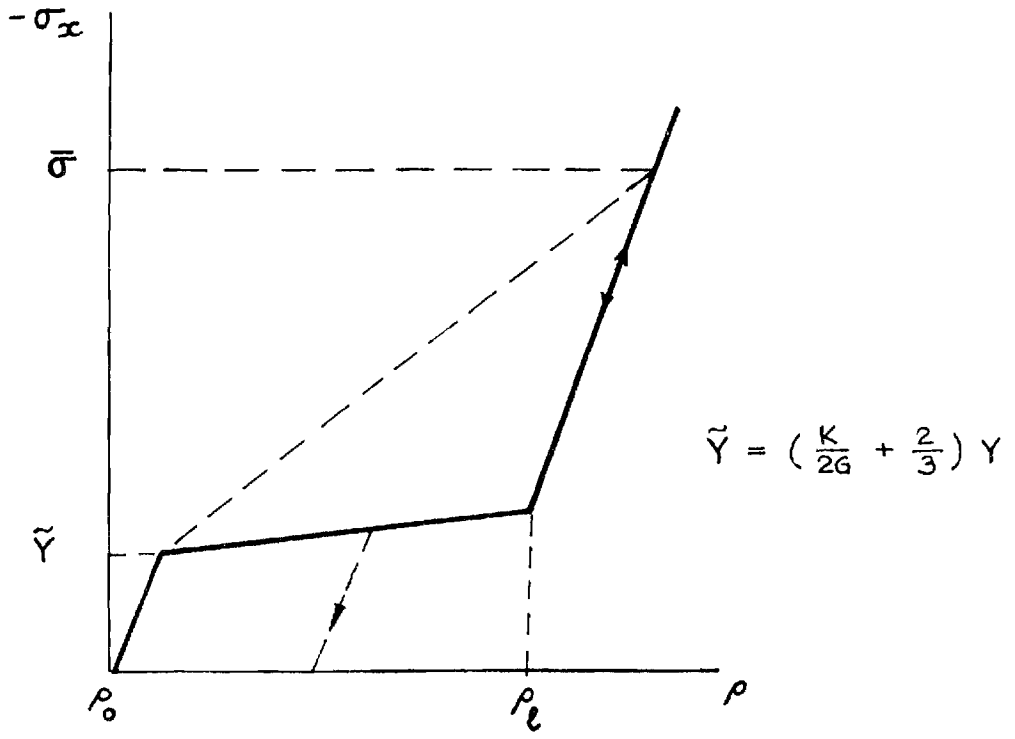

FIG. 6 $\sigma_x - \rho$ relationship

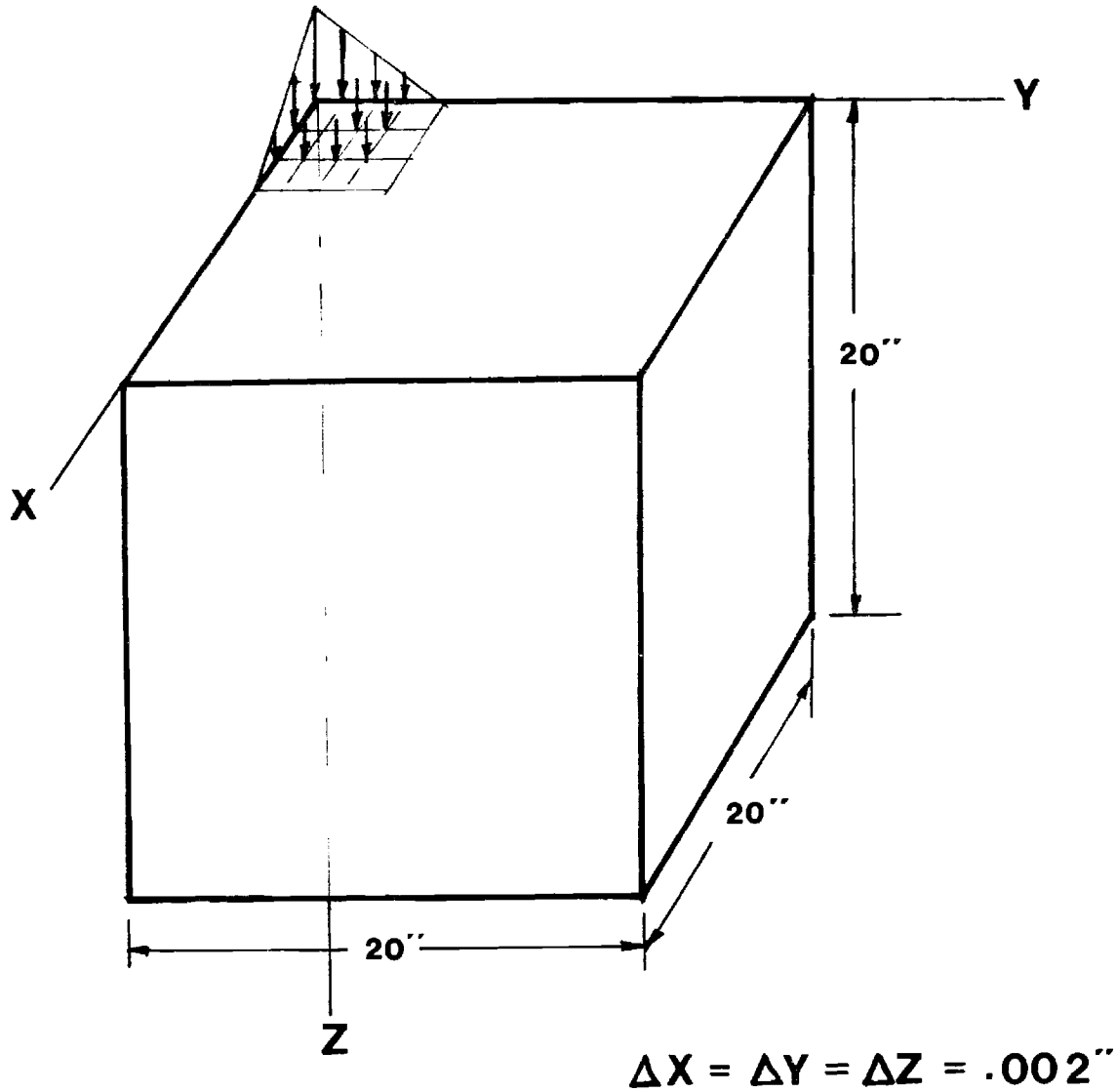

FIG. 7 geometry of 3-D problem

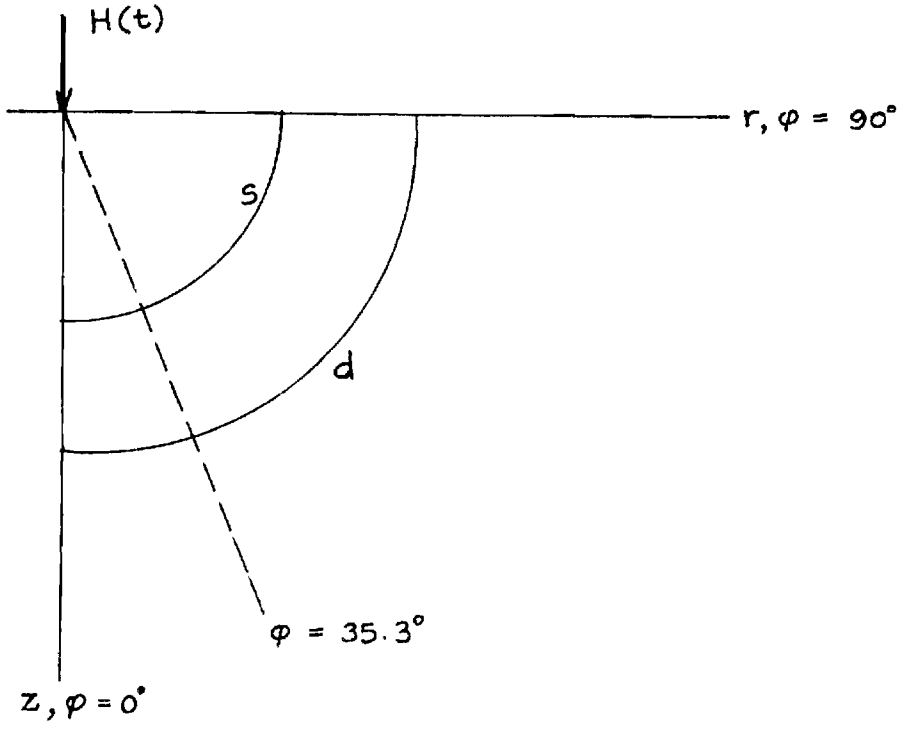

FIG. 8 polar coordinates

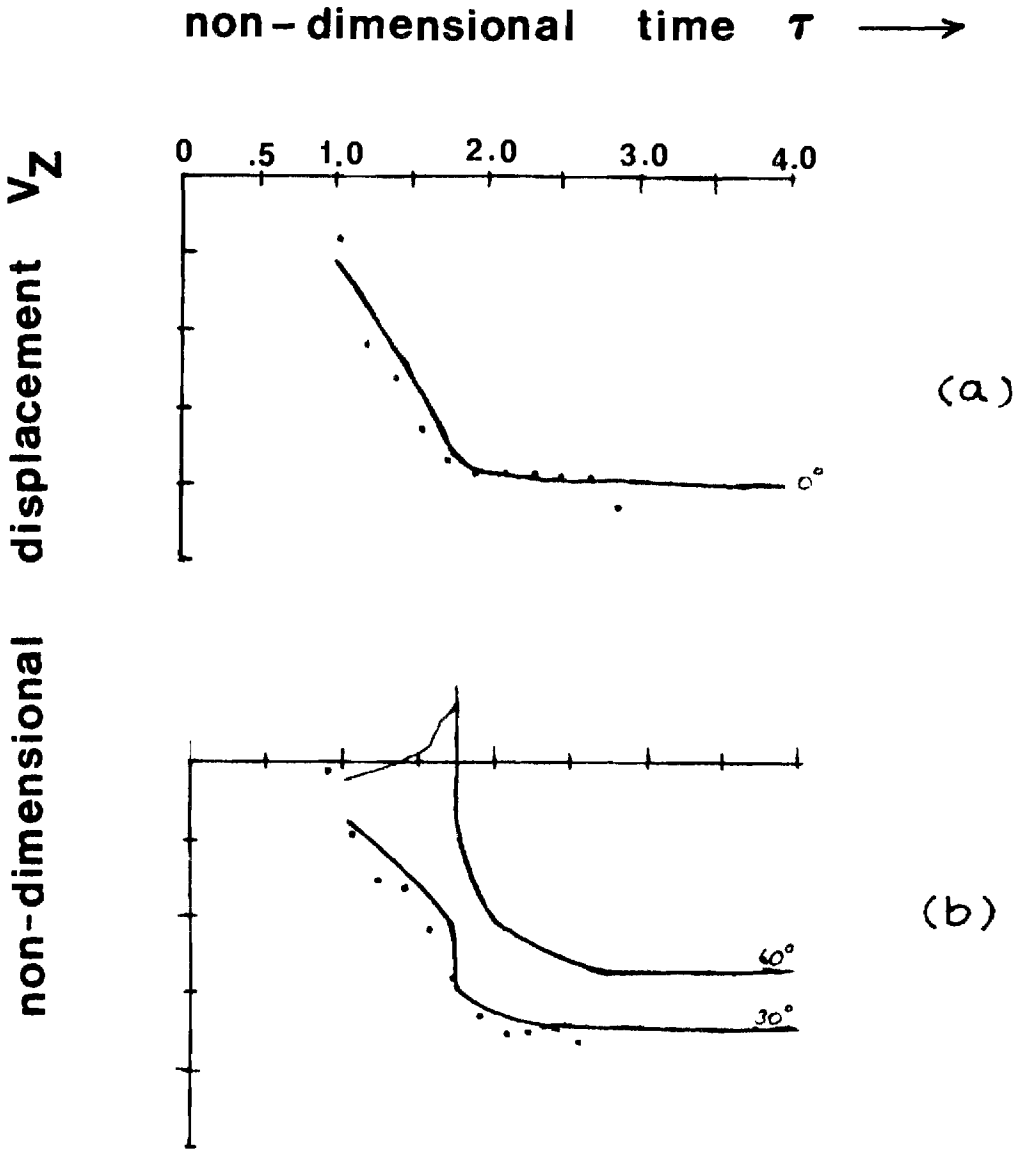

FIG. 9 variation of v_z with τ

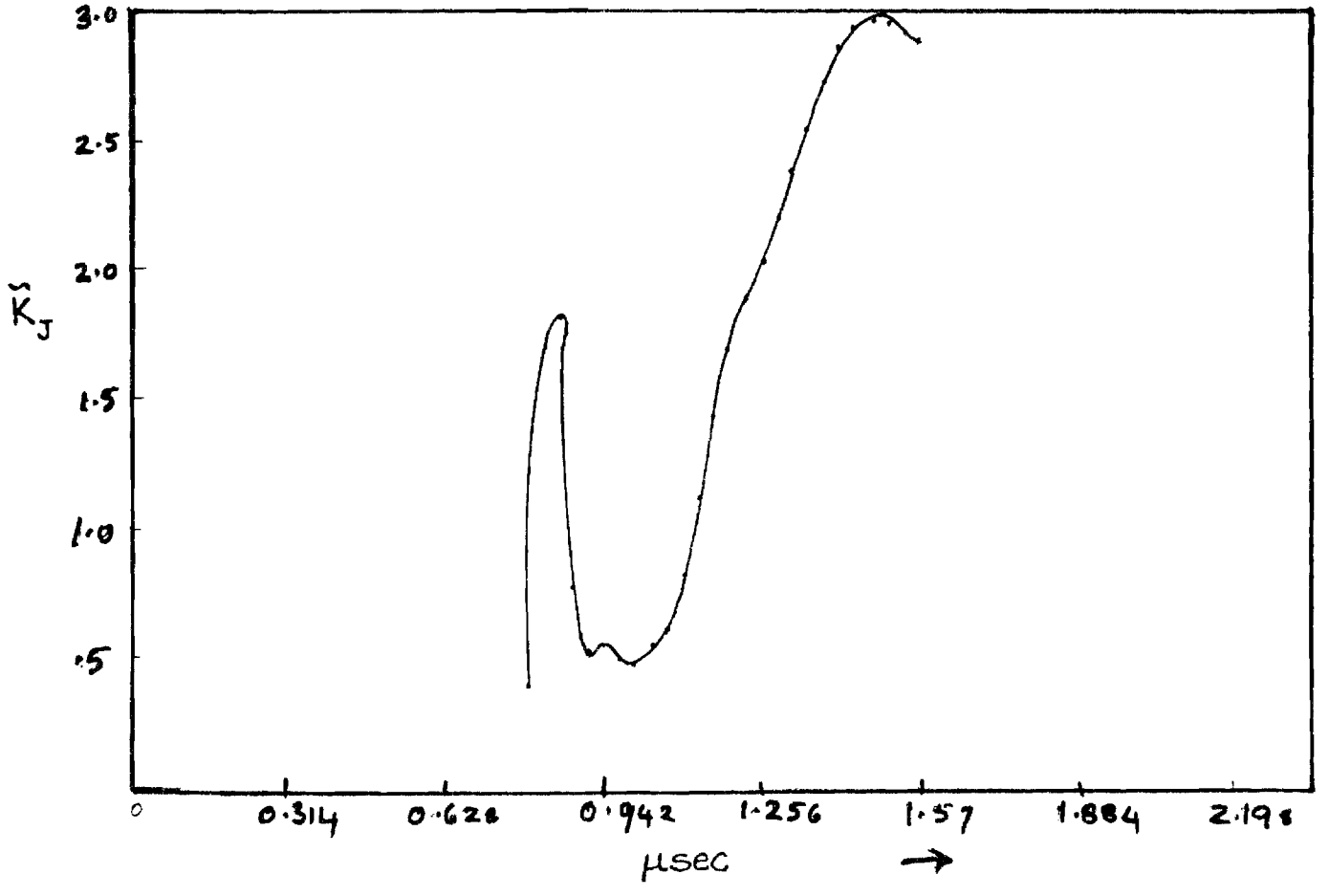

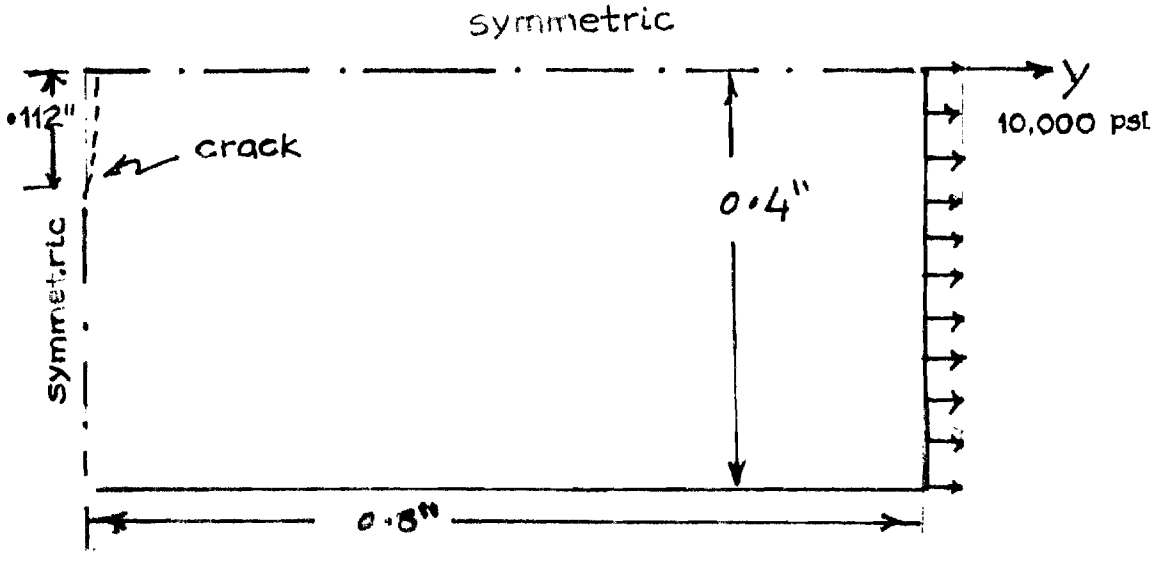

FIG.10 variation of stress intensity factor with time

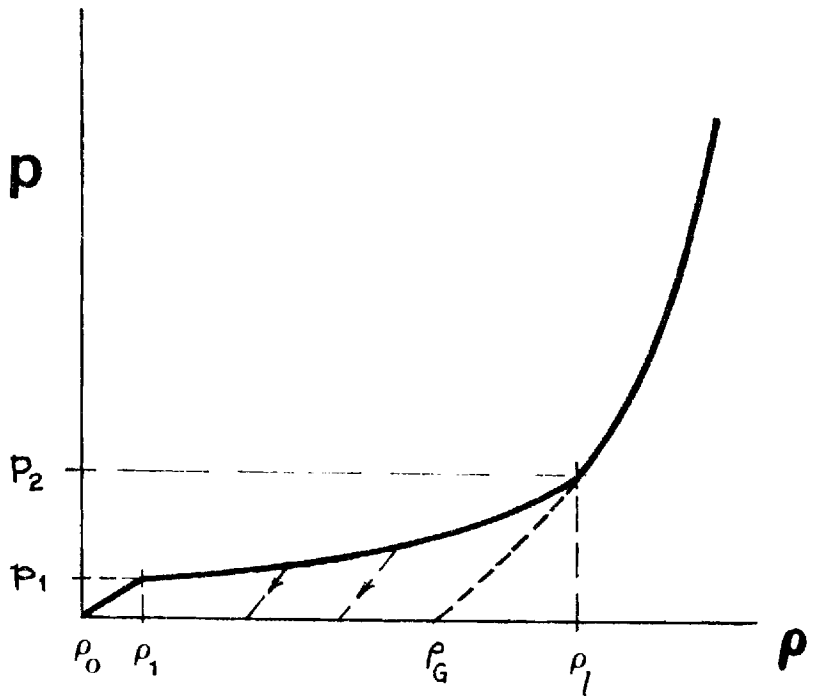

FIG.11 pressure – density curve

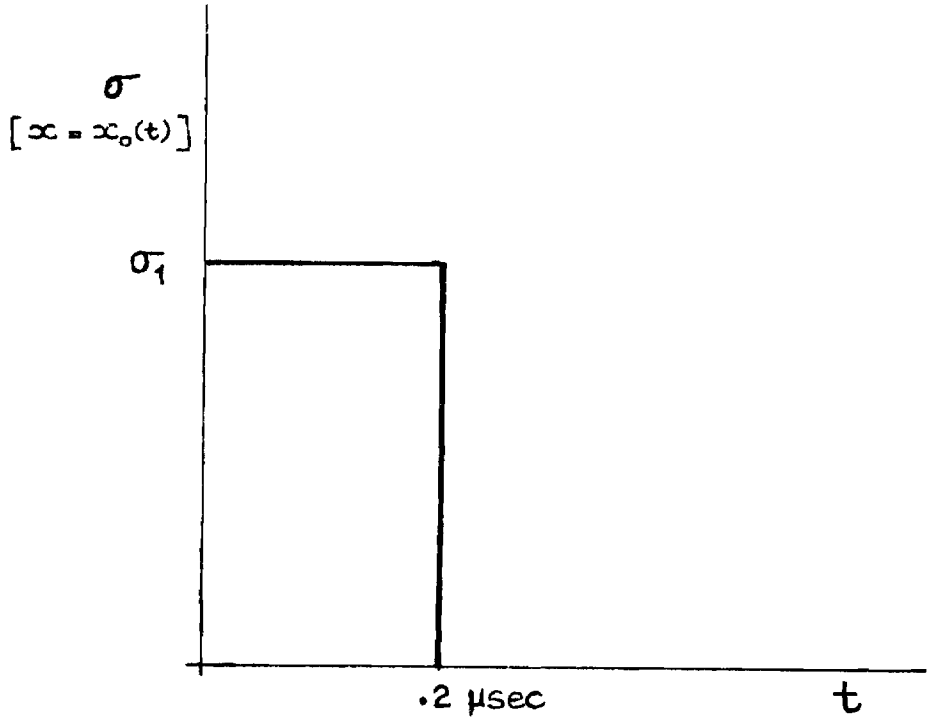

FIG. 12 step loading, pattern "a"

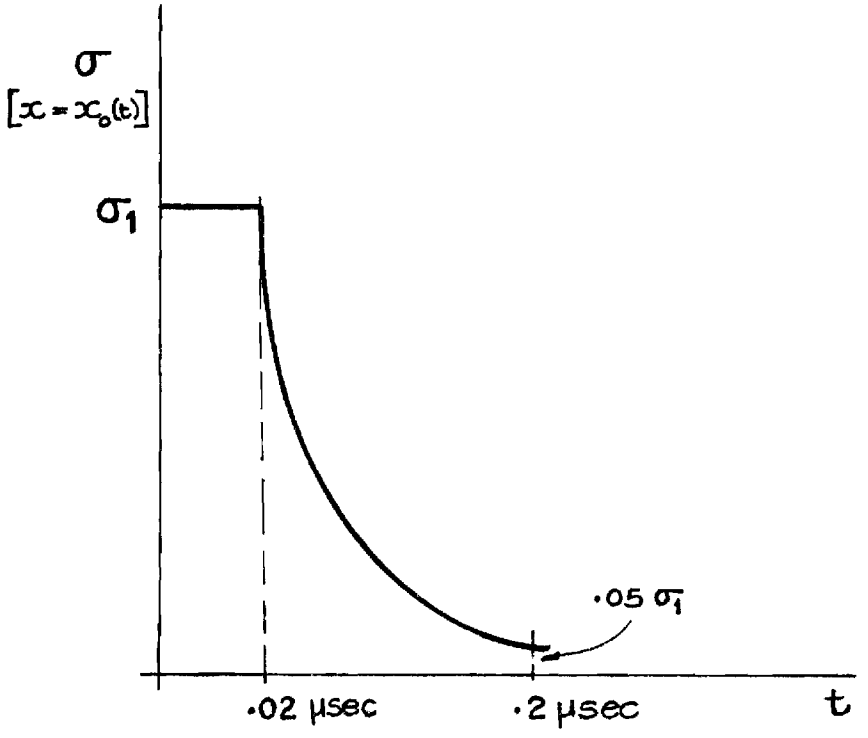

FIG.13 exponential decrease of load, pattern "b"

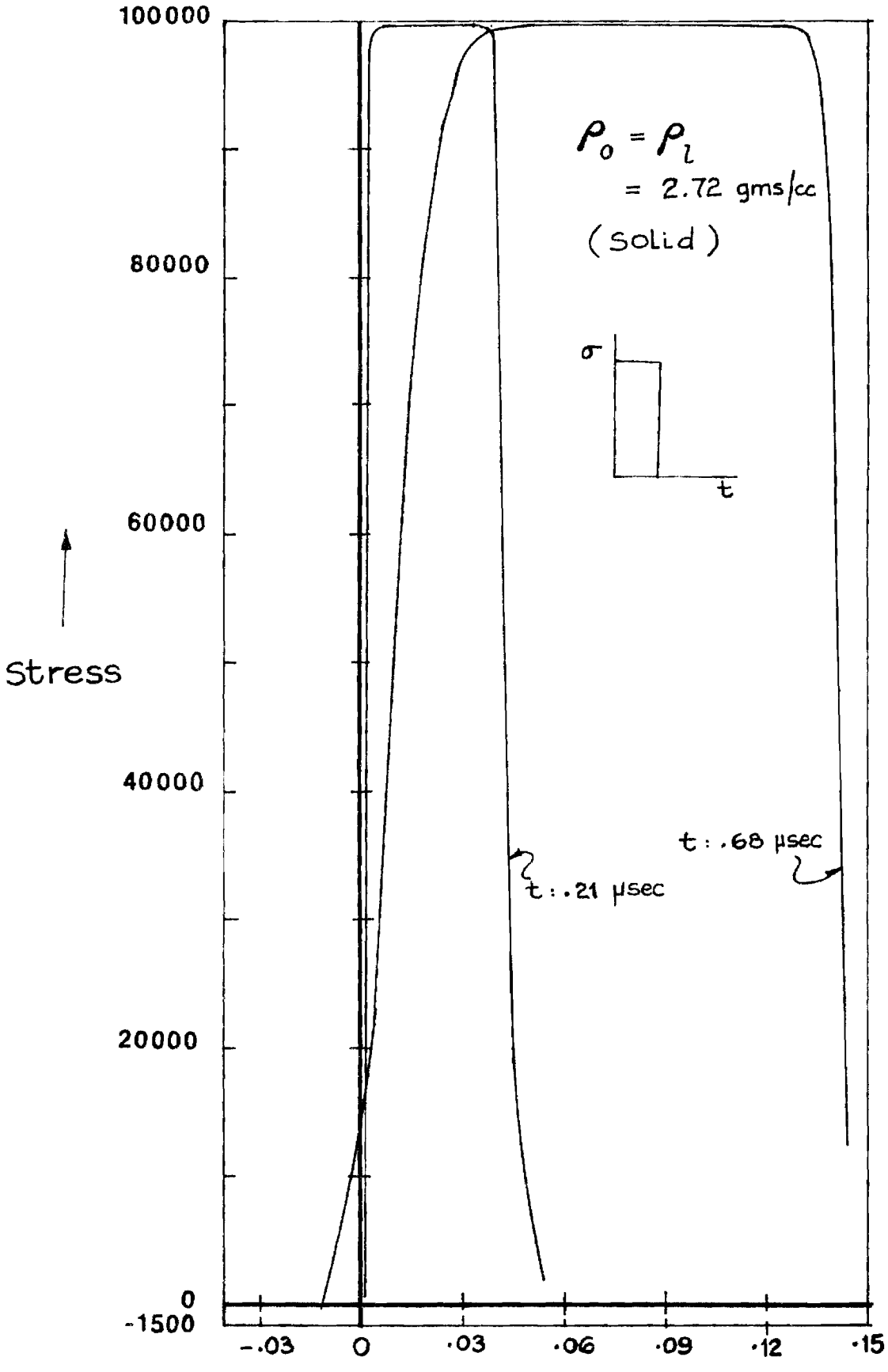

FIG.14 stress distribution at various times

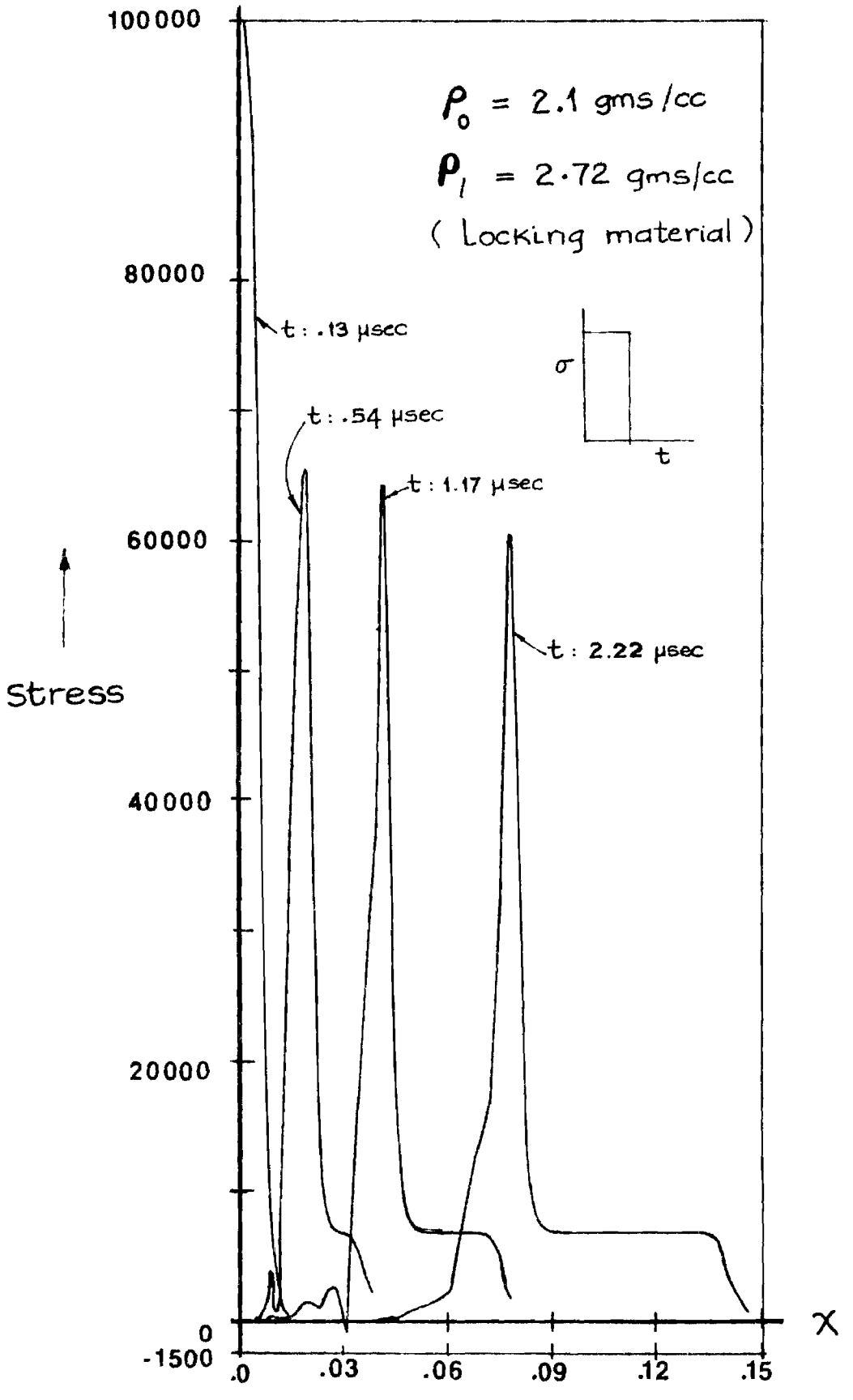

FIG.15 stress distribution at various times

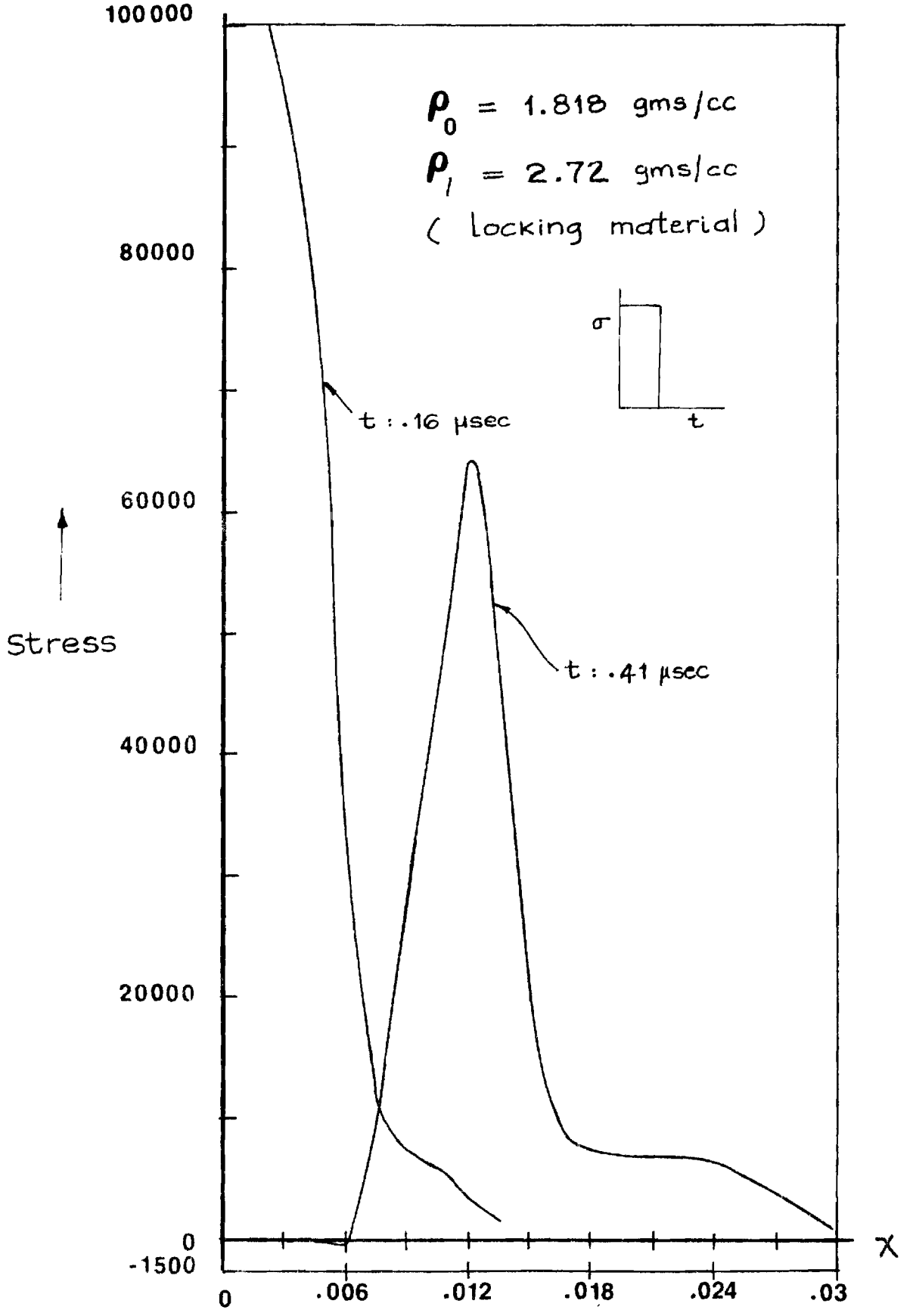

FIG. 16 stress distribution at various times

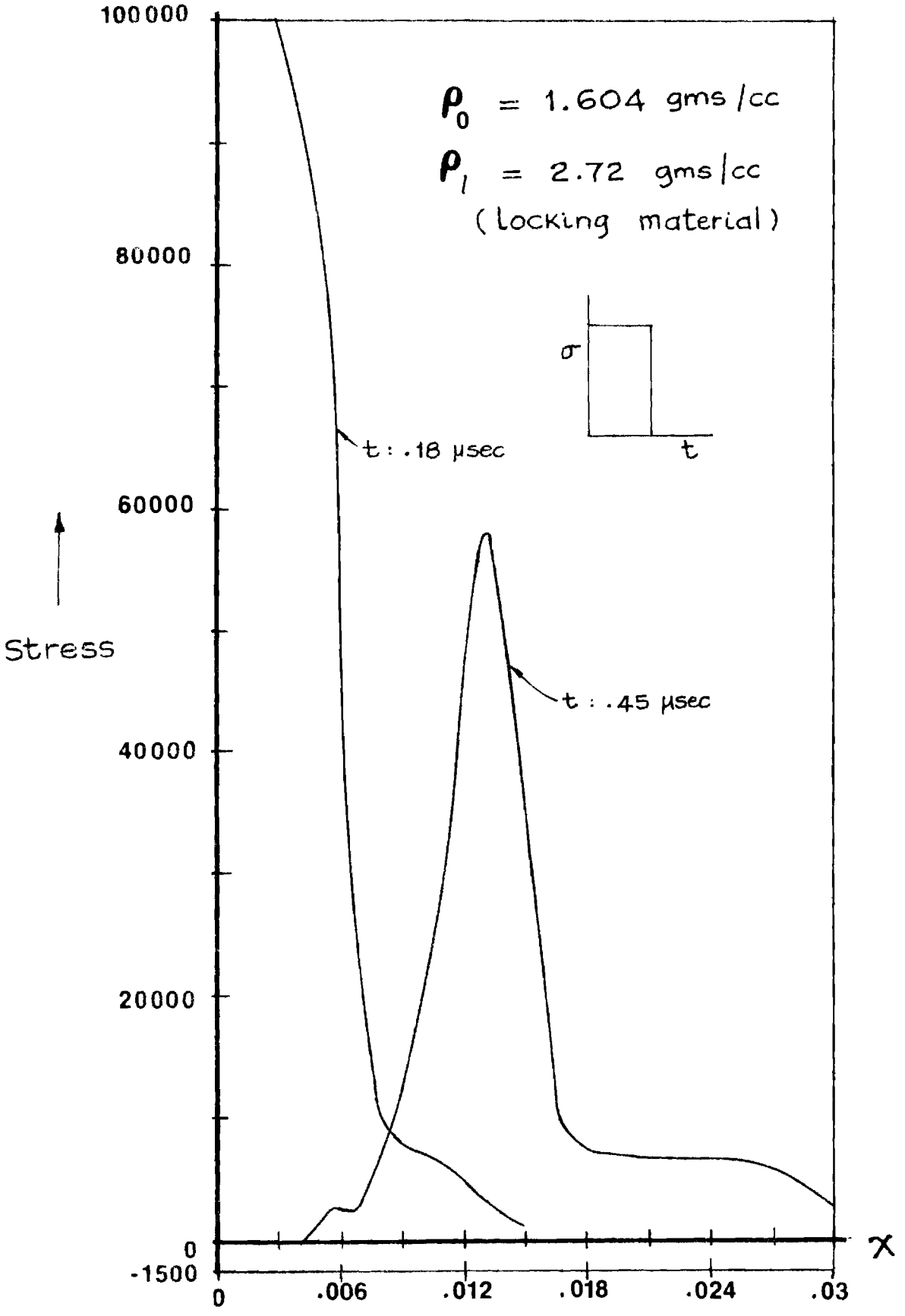

FIG.17 stress distribution at various times

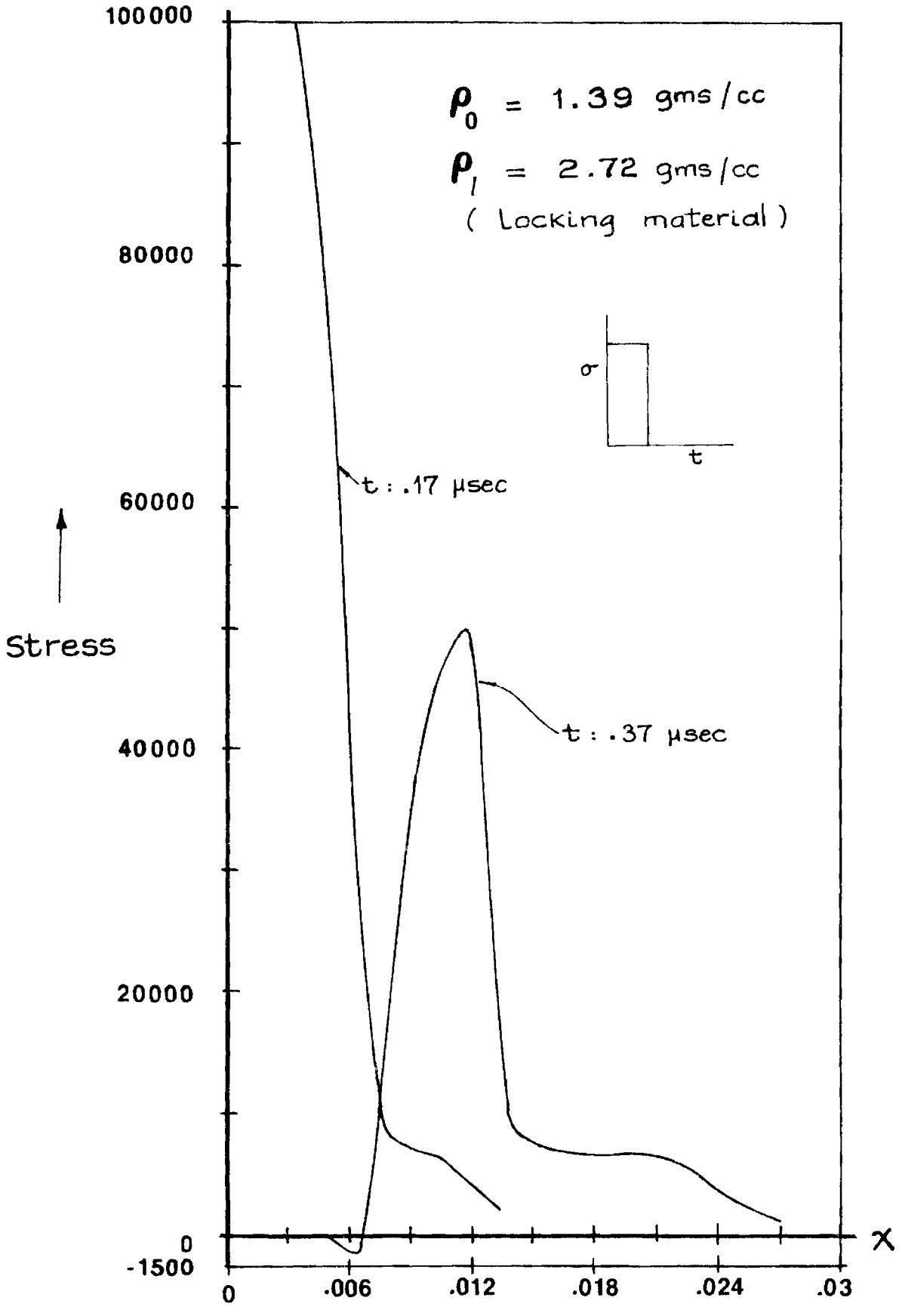

FIG.18 stress distribution at various times

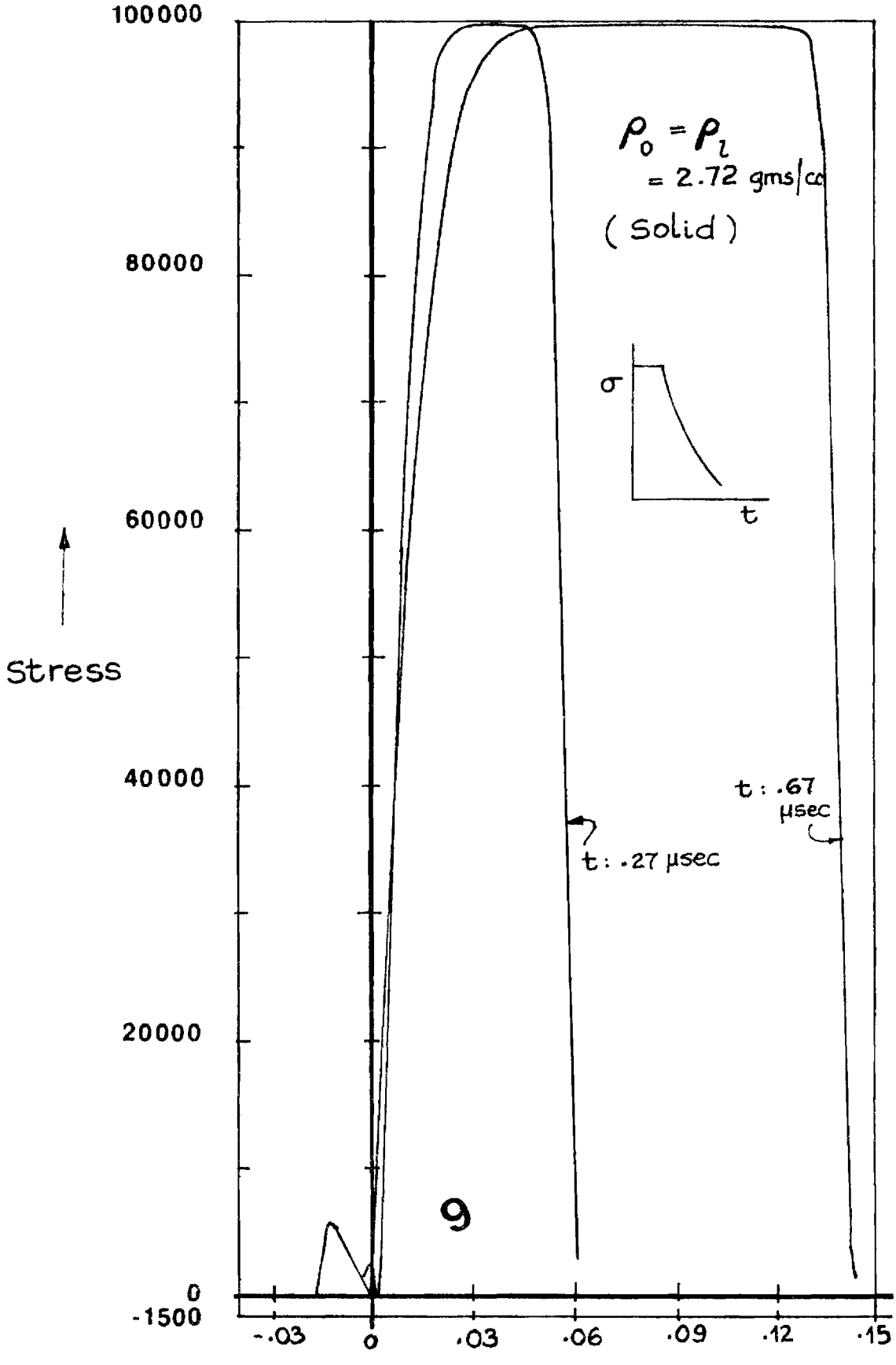

FIG. 19 stress distribution at various times

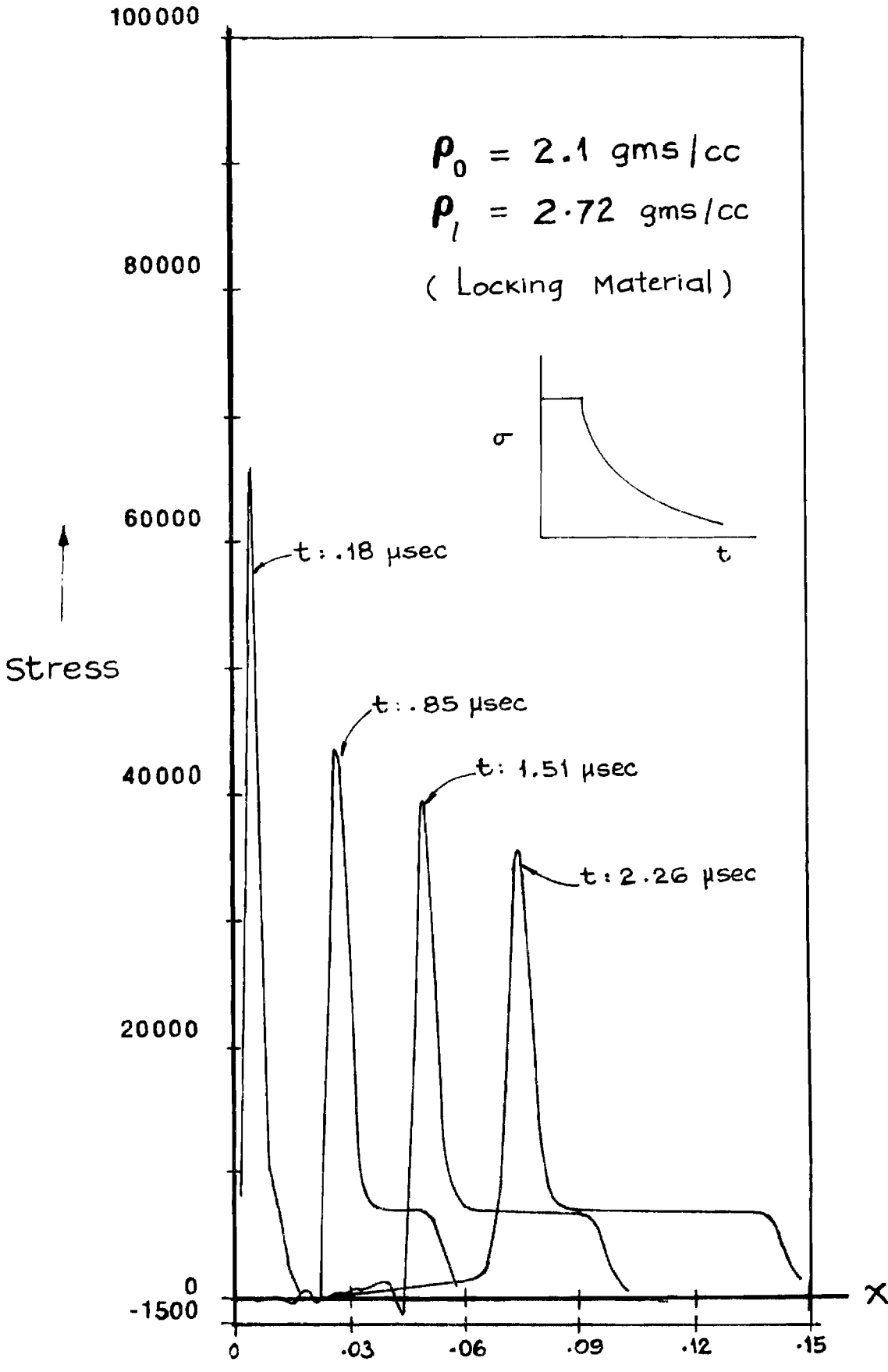

FIG. 20 stress distribution at various times

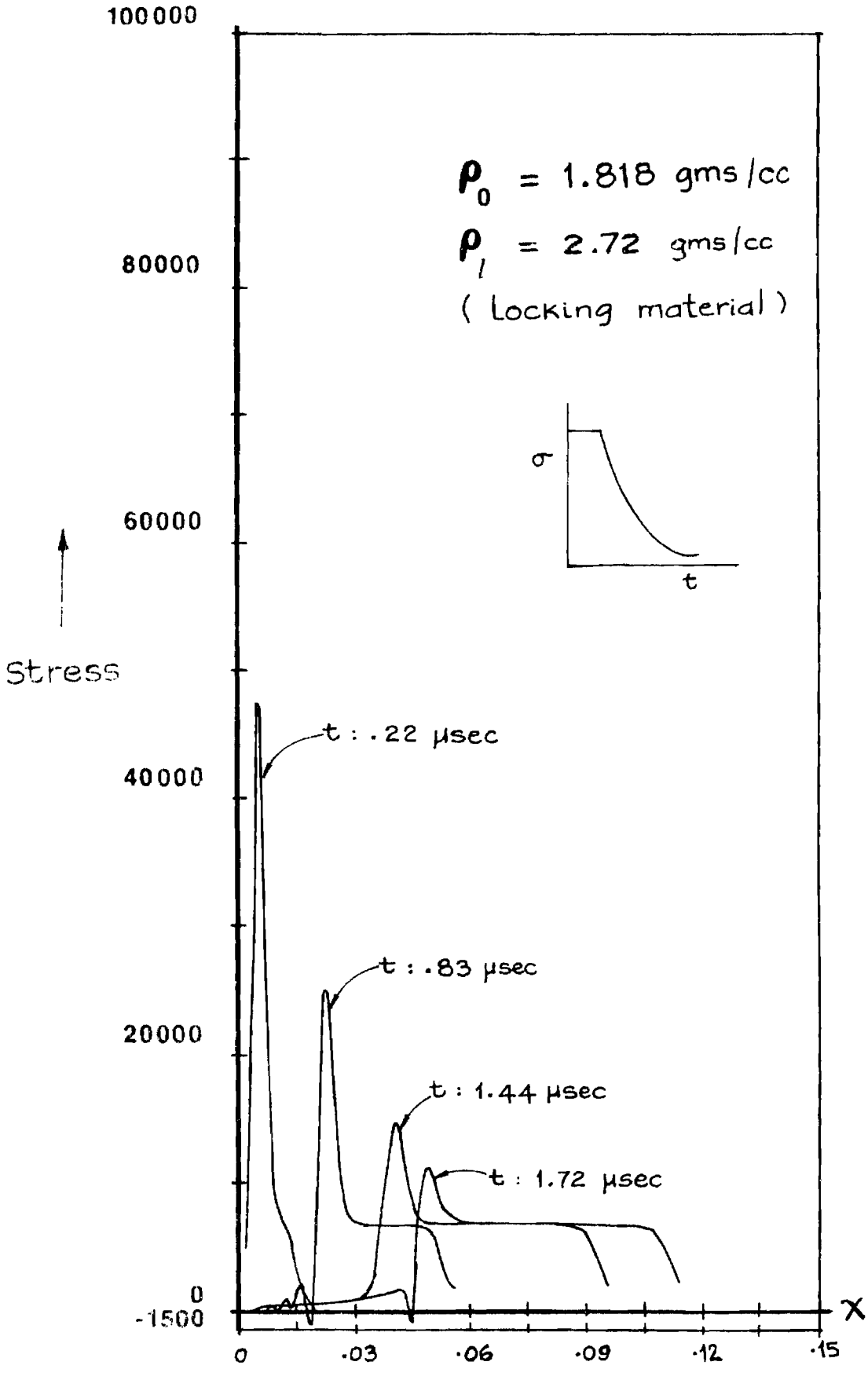

FIG. 21 stress distribution at various times

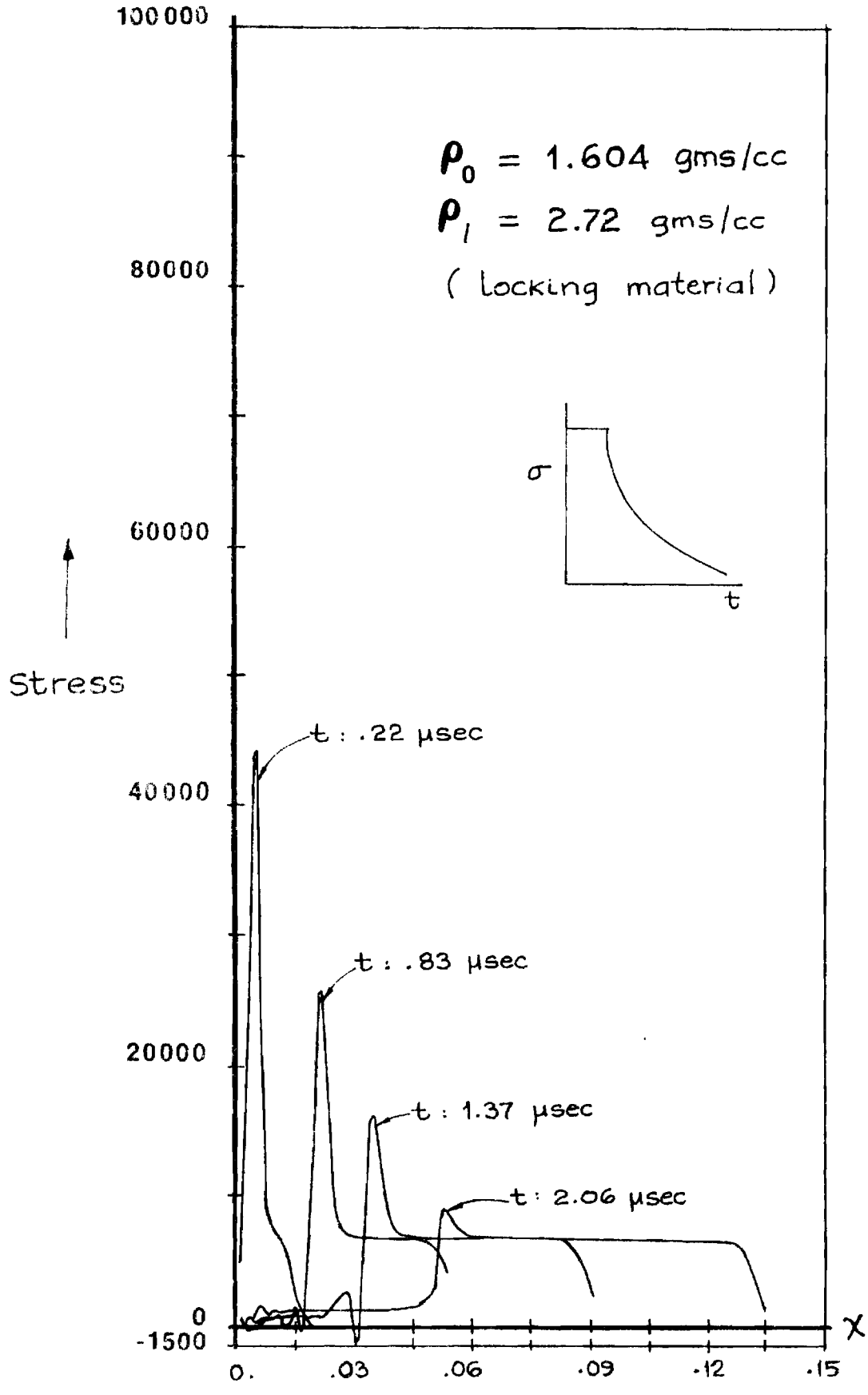

FIG.22 stress distribution at various times

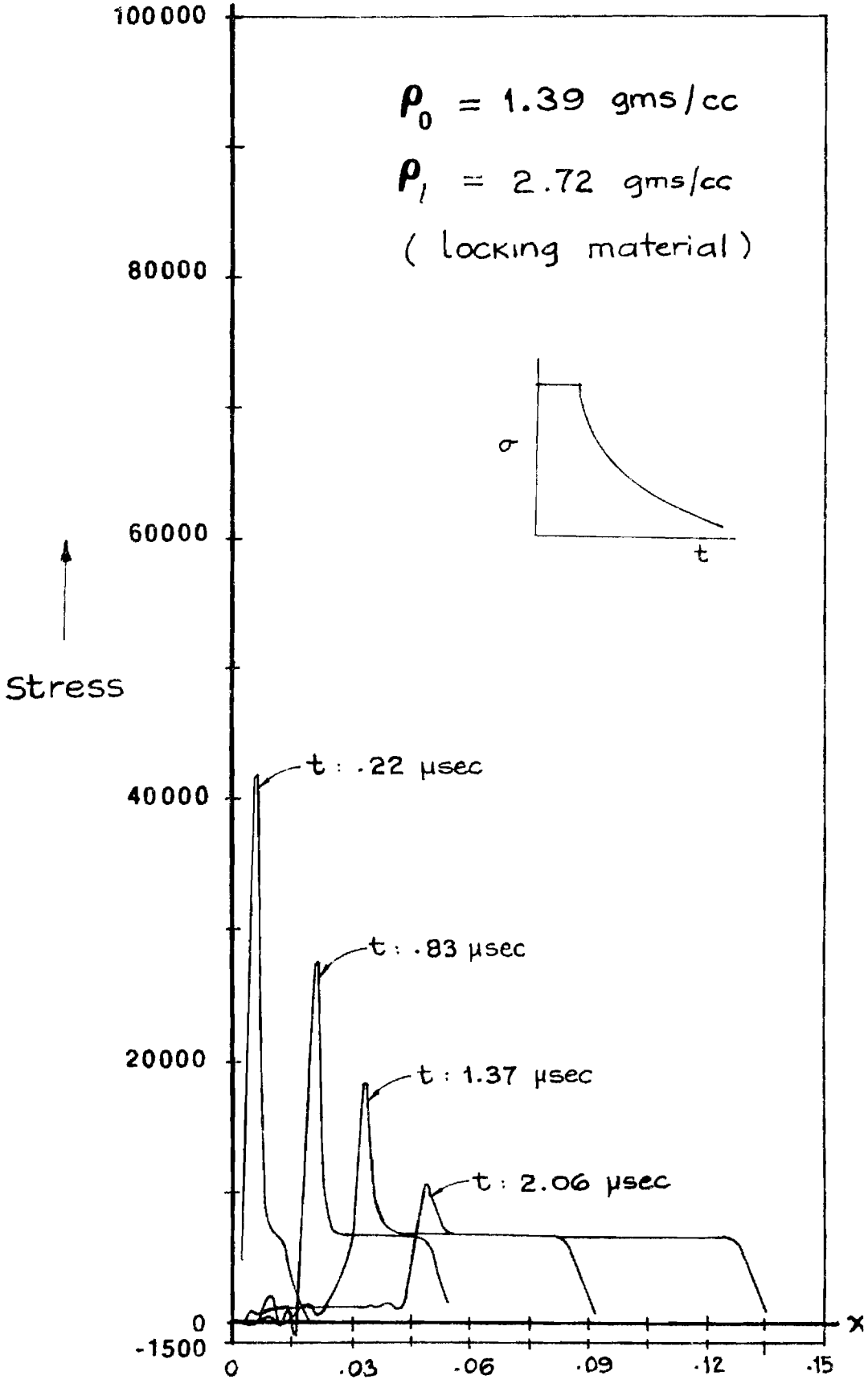

FIG. 23 stress distribution at various times

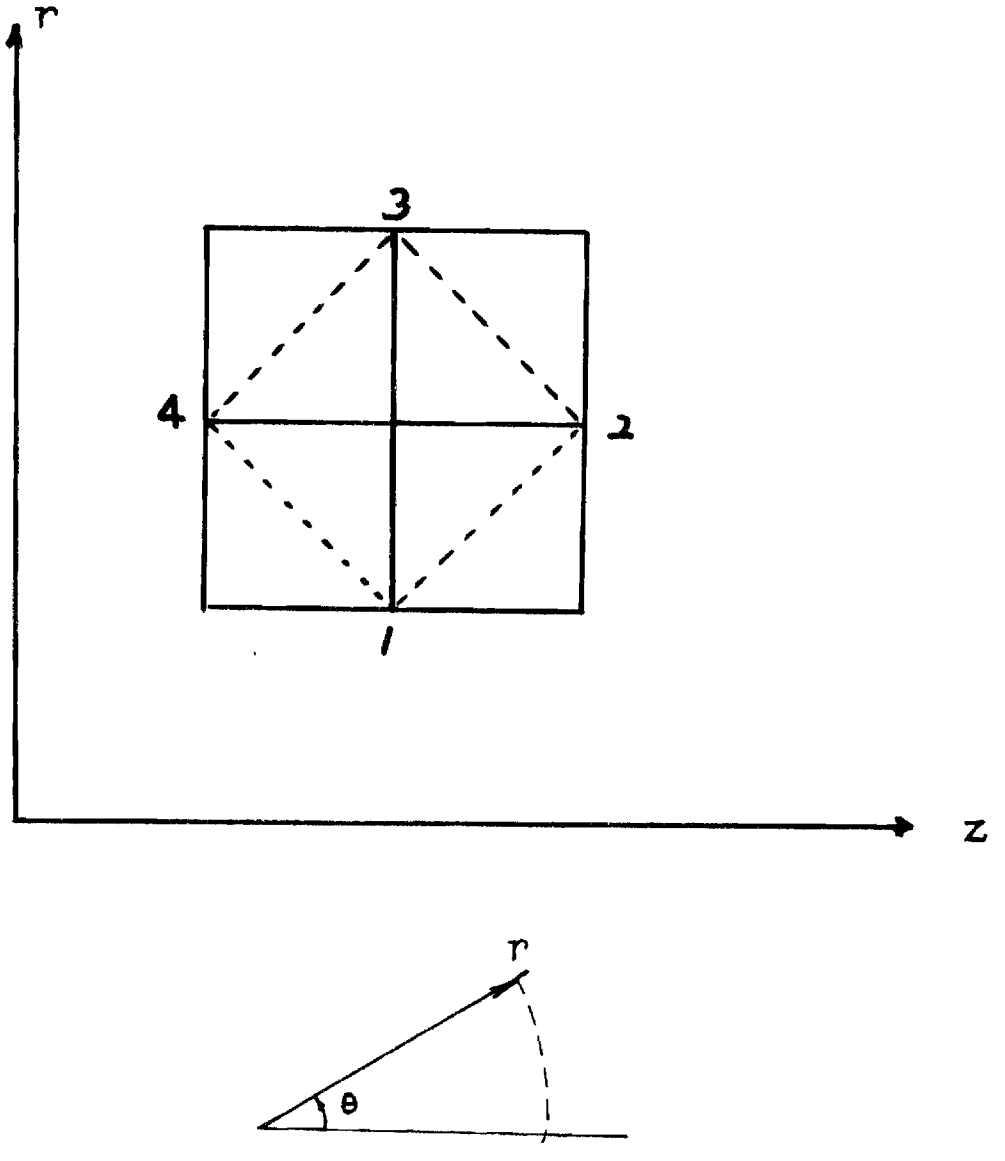

FIG. 24 finite difference grid of an interior point

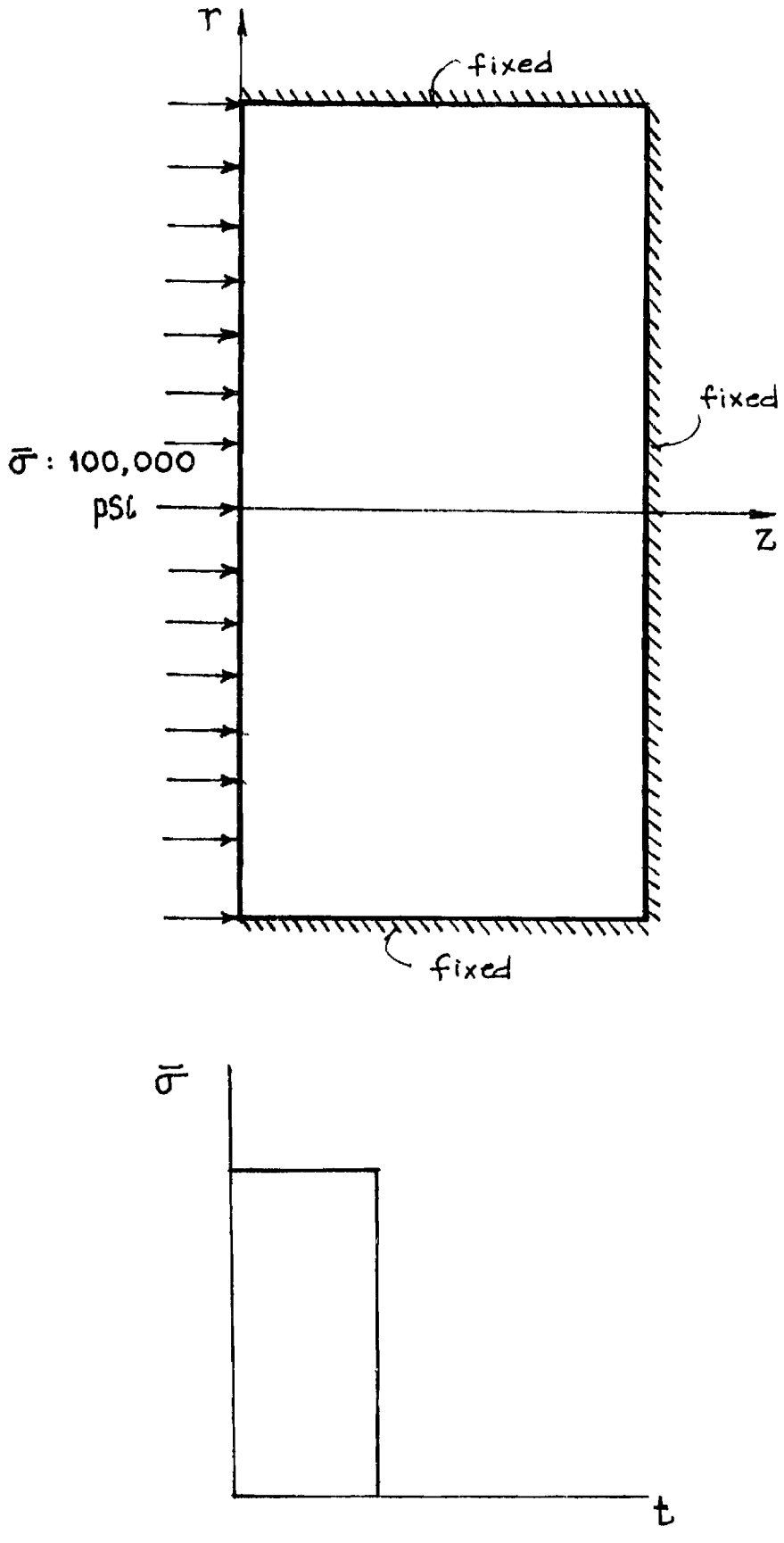

FIG. 25 · geometry and loading

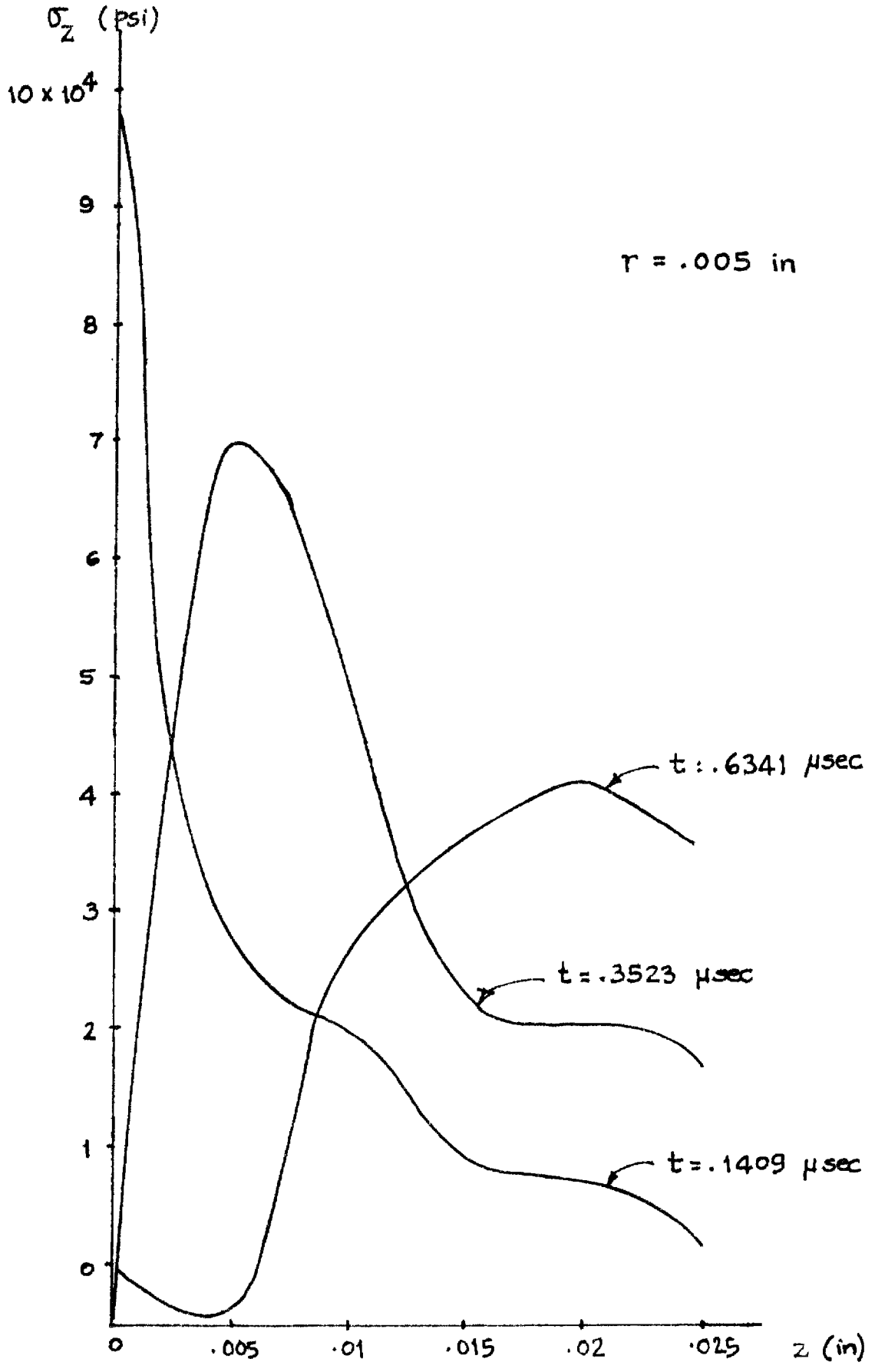

FIG. 26 σ_z variation with time

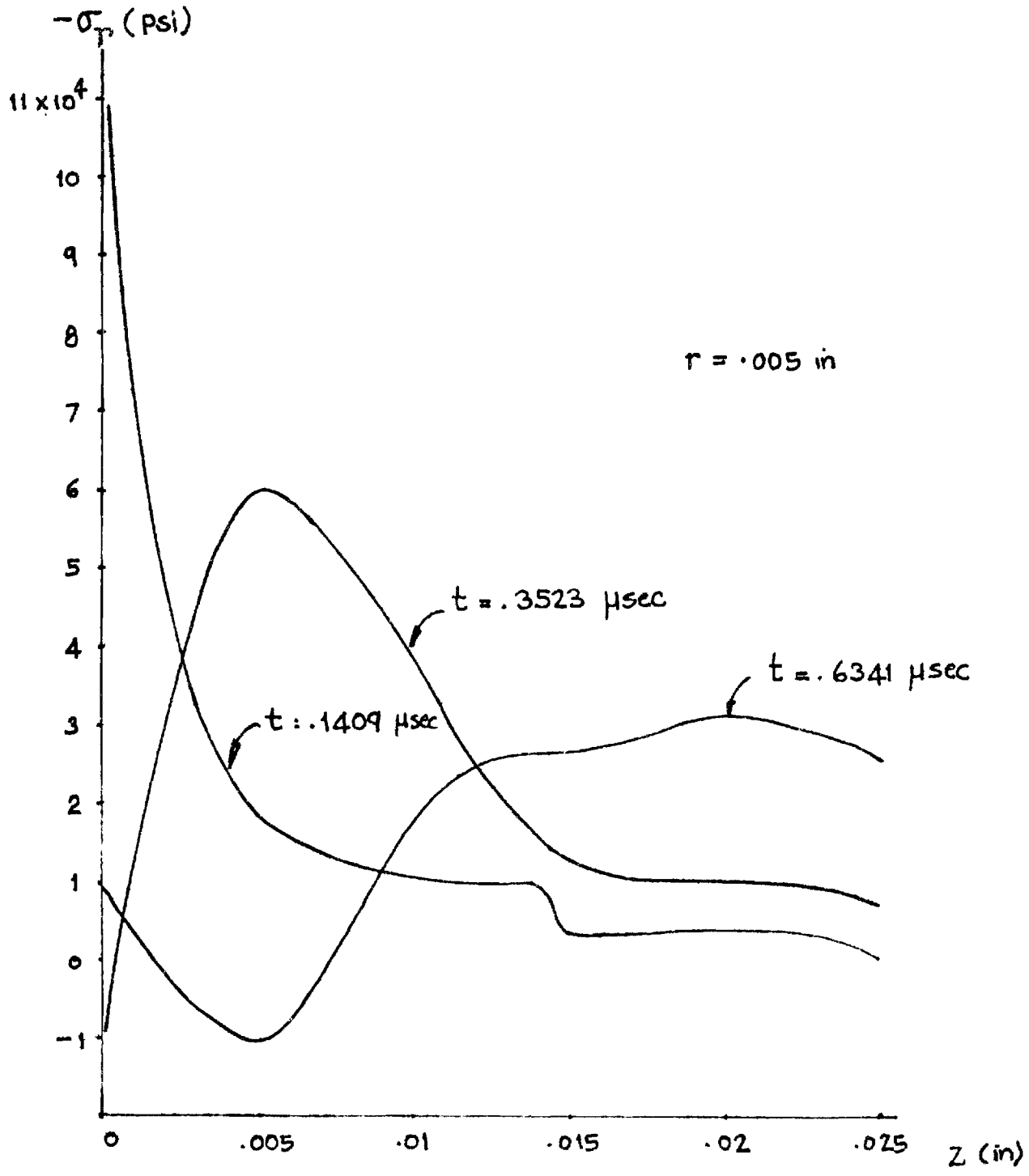

FIG. 27 σ_r variation with time

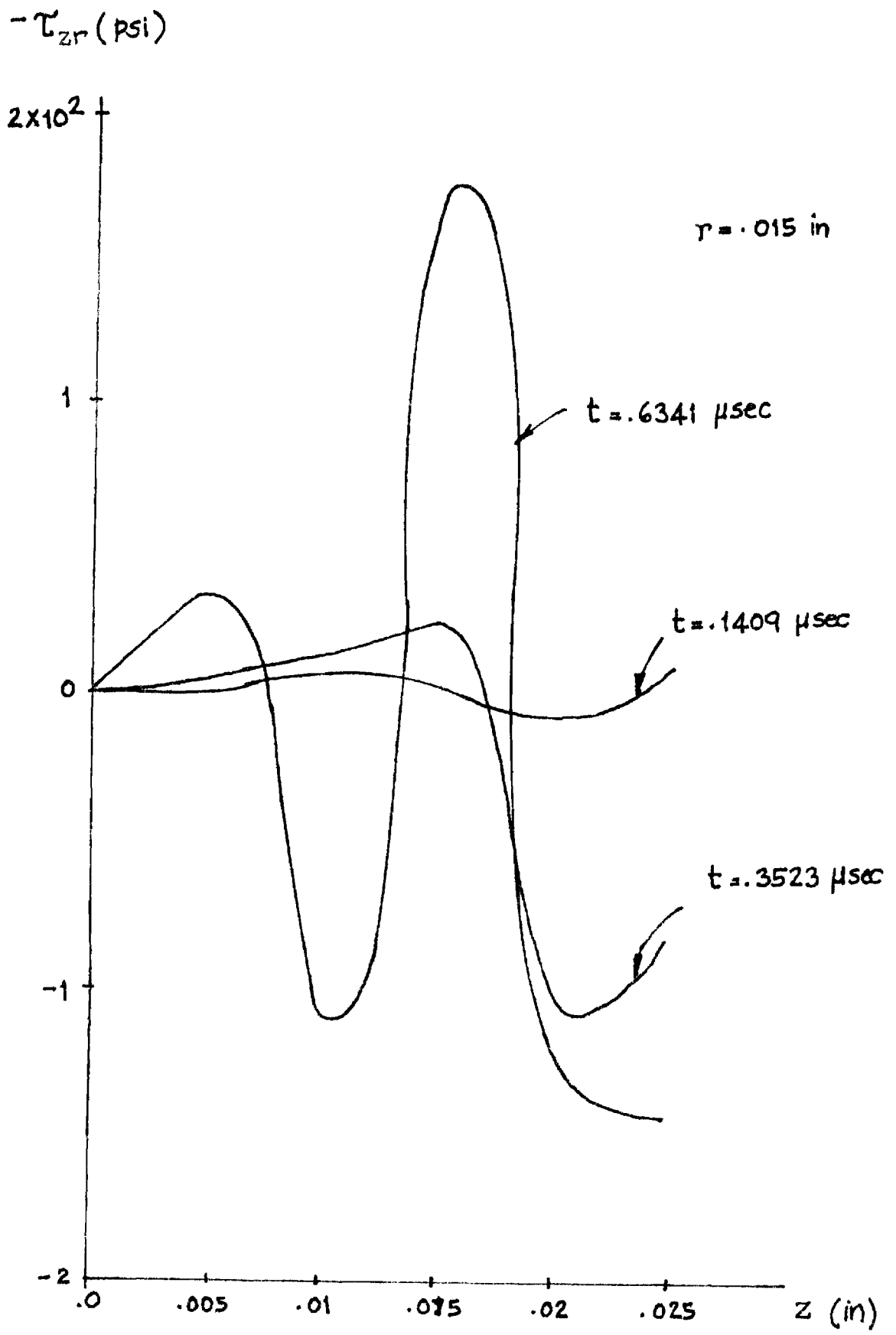

FIG. 28 τ_{zr} variation with time

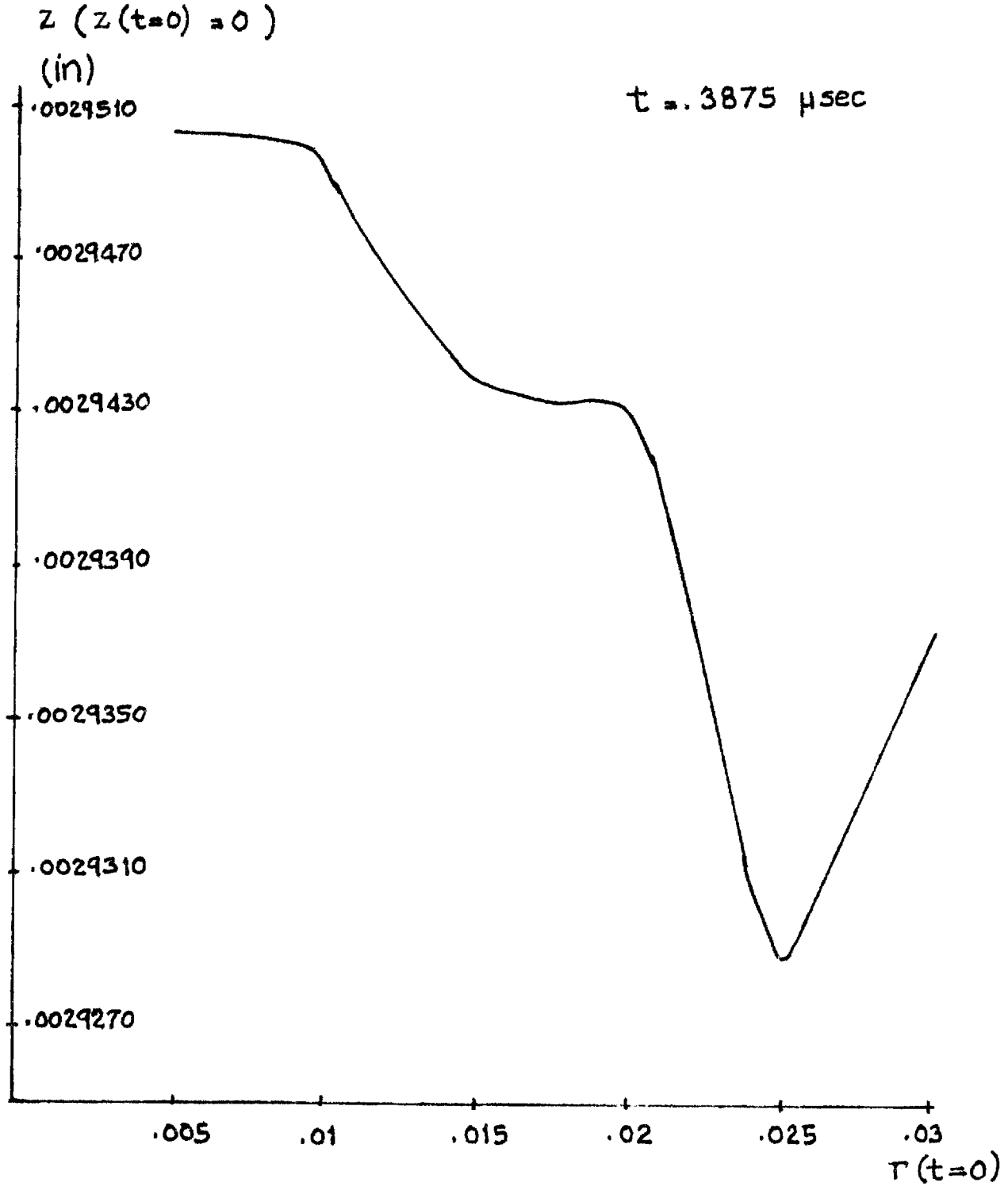

FIG . 29 displacement of top surface

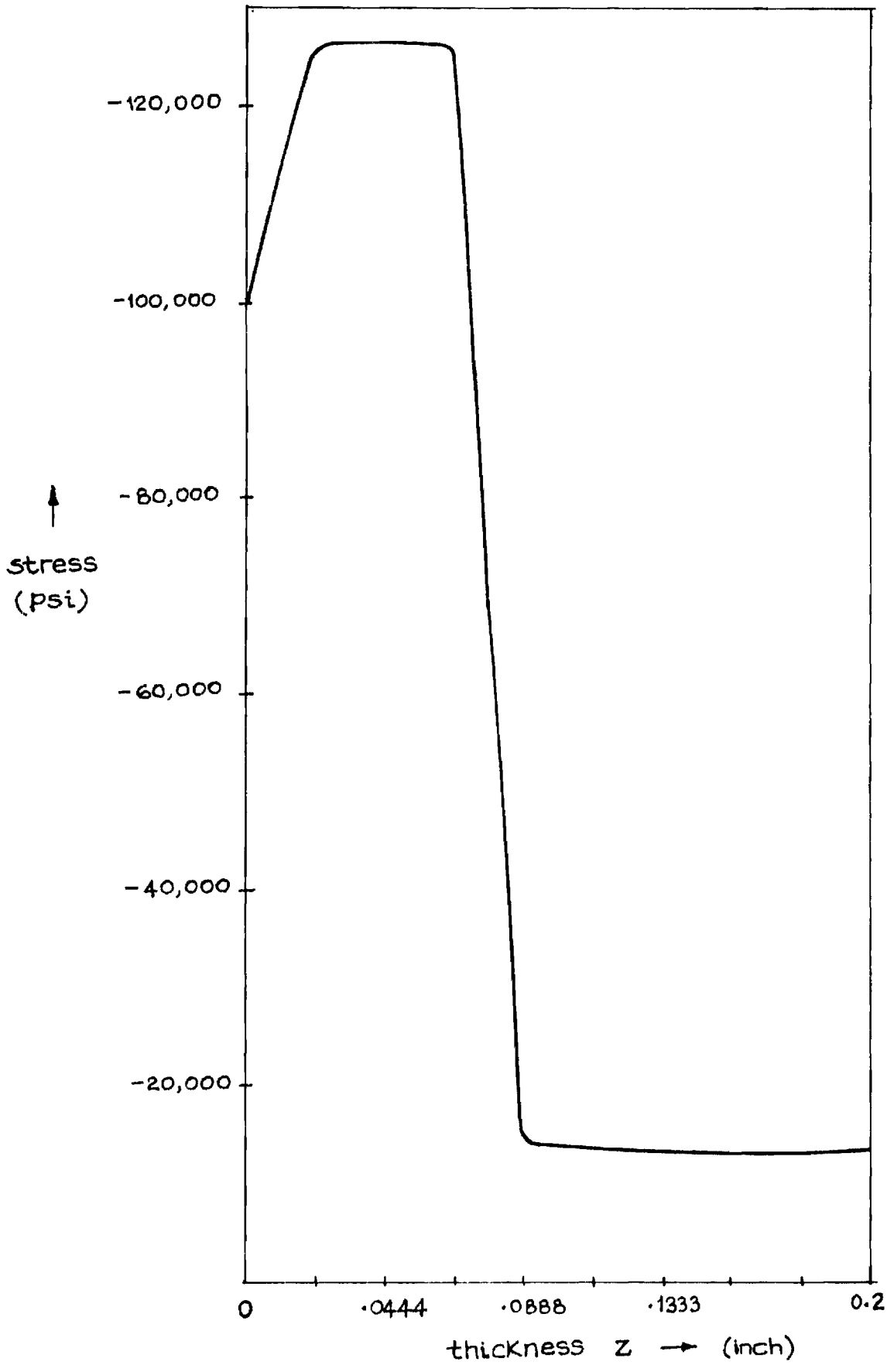

FIG. 30 state space approach

Appendix I

Appendix I

User Guide For ZLAX3S and ZLAX3LS

Program Modules

LW

This is the main program and does nothing but call the subroutines that perform the calculations. The subroutines called are, INPTT, GRIDD, and SOLVE.

INPTT

This subrountine reads the identification, control parameters, and material properties For example, the first card inputs an identification which consists of any identifier. The second card contains the special option flags and is entered as an octal number, with each bit having a special meaning. Other input data are discussed in a separate section.

GRIDD

This subroutine reads the data that is used to setup the mesh work to be used. This read data include, the number of mesh points in each direction, the size of mesh spacing, the factor relating spatial mesh spacing to temporal time spacing, and the point condition code assigned to each mesh point. It also reads user defined point condition codes definitions, and the initial conditions which for the current version serve as the boundary condition for later times as well.

SOLVE

This subroutine is called after the initial phases, when the problem is defined, and controls the execution of the finite difference equations until completion. Its primary function is to call the subroutines that perform the seperate steps of the Strang type of operator, and in a proper order. In addition, it calls the routine that produces output of the results and updates the program counters, such as the current cycle and the elapsed time. The routines called are XPASS, YPASS, ZPASS, PRNT and STATUS.

XPASS

This routine performs all the operations associated with the one-dimensional Lax-Wendroff operator in the x-direction. It does this by scanning each y and z constant line of

the mesh in turn, and performing the finite difference operations for each point along it. Two passes are made over each line. The first, and the final Mac Cormack step are performed in two steps. The routine then moves to the next line.

At every scanned point, the exact nature of the finite difference operation to be performed, forward or backward difference, boundary value, and equations to use, are determined by the point condition code associated with the mesh point. A more detailed explanation of the point condition codes will be given later. The routines called by XPASS are BNDRY, VFB1, VFB2, VBF1 and VBF2.

YPASS

This routine and ZPASS are almost identical to XPASS except that lines processed are different.

FLW

This function subprogram does the actual computations of finite differencing. It provides four alternate entry points other than FLW, which is never used. Each one performs a different computation on the values which are passed to it through the COMMON block EVAL.

VFB1	performs the first step of the Mac Cormack using forward differencing.
VFB2	performs the second step using backward differencing
VBF1	performs the first step using backward differencing
VBF2	performs the second step using forward differencing

BNDRY

This subroutine, which is called by XPASS, YPASS, and ZPASS before every line pass, updates the boundary conditions for the half-step arrays of the field variables. This is necessary because the half-step values exist only for the duration of a single pass.With a small amount of modification, this routine could be expanded to accomodate time dependent boundary conditions.

PRNT

This routine outputs the results of the computation, at specified intervals. It has two forms of output, formatted and unformatted (binary) which may be selected independently. The formatted output is the printed results and the unformatted output is machine readable output intended for use by other programs, such as a plotting program.

STATUS

This subroutine is included for purposes of monitoring the progress of the program after it has started running, and in no way affects the computations. It will operate only on certain CDC computers and calls the subroutine FSYS.

Point Condition Codes

Every mesh point is assigned, by input, a point condition code, which defines the differencing properties of the point. It gives information as to whether the point does forward or backward differences at each Mac Cormack half-step, whether it has a fixed value (such as at a boundary), or whether it is to be skipped entirely. It is used primarily to separate interior and boundary points.

Included in the BLOCK DATA subroutine SETUP, there is a set of pre-defined point codes. These may be used, or modified. Also, the user may input a set of temporary codes with the input data, up to the maximum allowed by the array IUEQNS.

In the routine XPASS, YPASS, and ZPASS, as each point is scanned, its point condition code is obtained, from an array IPT, which has an entry for each mesh point. This code is used to locate the point code definition in the tables IEQNS and IUEQNS. From this data, the proper differencing can be performed. Positive codes are in IEQNS and negative codes are in IUEQNS. A zero code means no operation.

Definition Table Format

The arrays IEQNS and IUEQNS are three-dimensional arrays that contain the data which control differencing at each mesh point, through that point's point condition code.

IEQNS (<# field variables> , < # codes > , < # dimensions >)

where

<# field variables>

is the number of field variables for which the solutions are sought. For a three-dimensional problem this is 9. The second subscript,

codes

is the point code index. Then last subscript,

dimensions

is the number of spatial dimensions.

For example, for an interior point in three-dimensions, the definition for its code would be,

XPASS: 1,2,3,4,5,6,7,8,9
YPASS: 1,2,3,4,5,6,7,8,9
ZPASS: 1,2,3,4,5,6,7,8,9

The entries, numbered 1-9, are the index used in the routine XPASS, YPASS, ZPASS in the completed "Go to" statements to solve the correct equation. The values 1-9 indicate that it is an interior point. Values of 10-18 indicate a lower boundary, e.g. i = 1, j = 1, or k = 1. Values of 19-27 indicate an upper boundary. Therefore, 10-18 are always forward z difference and 19-27 are always backward z difference, 1-9 are interior points and thus alternate at each half-step. Additionally, if any value in the definition has a negative value, then XPASS, YPASS and ZPASS will not attempt any computation for that field variable. This is used for specified boundary values.

An example for two dimensions with 5 field variables is

XPASS: 1, -2, 3, 4, -5
YPASS: 6, -7, 8, 9, -10

where the field variables are; ρu_t, ρv_t, σ_{xx}, σ_{yy}, σ_{xy}. On an XPASS this point is an interior point (1-5), with ρv_t and σ_{xy} being specified values. On a YPASS this point is a lower boundary (6-10). Physically, this point repesents,

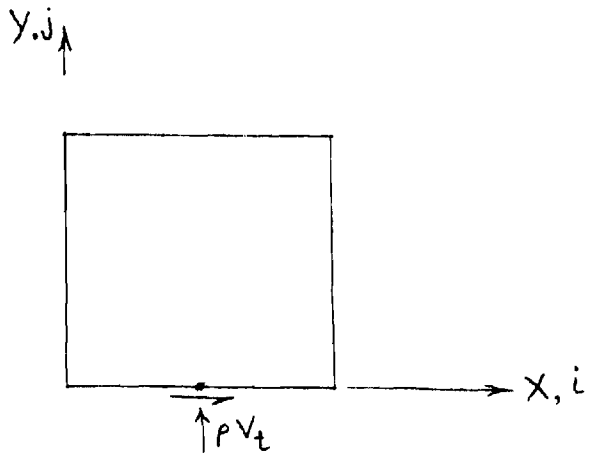

a mixed boundary where velocity in the y-direction and traction in the x-direction are specified.

Logical AND Operation

The statement,

```
ICK = IDBG . AND . 20B
```

and

```
ICK = AND(IDBG, 20B)
```

are equivalent in CDC FTN. They are both bitwise logical AND operations. The digit string followed by the letter"B" indicates the number in octal.

The purpose of these operations, which appear throughout the program, is to test the options set by the second data card (and in the variable IDBG).

Extended Memory Usage

In the 3-D version of the program, the amount of available primary memory restricts the size of the mesh that may be used. The use of a second order scheme does not require such a fine mesh. However, the need may arise where a large mesh is needed. Therefore, use is made of secondary memory (disc in this case) so that unused portions of the mesh are not in primary memory when not needed. This is handled by calls to Cyber Record Manager which allows random access to the secondary memory. The procedure was set up to optimize access to the disc, but still the amount of I/O can be large.

The routines used to process the data transfer are MGET, MPUT and SPUT. MGET will retrieve a block of memory, MPUT will store a block, and SPUT will store a single word. The data is stored in the secondary memory as a four dimensional array,

MEM(IBMX, JBMX, KBMX, 14)

where,

IBMX- the number of mesh points is x-direction
JBMX-the number of mesh points is y-direction
KBMX-the number of mesh points is z-direction

and 14 arrays from primary memory are included. These values are defined in SETUP. When values are loaded into the memory, each of the 14 data arrays has all the values for a constant K (x & y passes) or constant J (z passes). The 14 data arrays are EQUIVALENCED to the array,

CM(IBMX, MAX(JBMX, KBMX),14)

The memory transfers are handled by the GETPUT routine

GETPUT

This routine has 4 ENTRY points, GETPUT (unused), MGET (load memory), MPUT (store to disc), and SPUT (store single word to disc).

MGET

MGET(LV, IV, JV, KV, NWRDS, JK)

this routine reads NWRDS/10 words from MEM, starting at (IV, JV, KV, LV). This is equivalent to the I index varying from I = IV to I = IV + (NWRDS/10). Because the way a multidimensional array is stored in FORTRAN, always a segment of the I - column is accessed. The JK variable represents the second index for the 2-D array. For x & y passes, the K is held constant so that JK represents the J index. For Z passes, the J is held constant, so that JK is the K index. It is to be noted that NWRDS is the number of character (10 per word) to transfer; a Cyber Record Manager convention.

MPUT

This routine operates in the same manner as MGET.

SPUT

Unlike MGET & MPUT which do block transfers, this routine stores a single word to disc.

The values NXY & NXZ are defined as follows:

GRIDD @ 59-60
NXY = IBMX * JBMX * 10
NXZ = IBMX * 10
} for use in GRIDD only

SOLVE @ 56-57
NXY = (IMAX - IMIN + 1) *10
NXZ = (IMAX - IMIN + 1) *10
} for use in XPASS, YPASS, ZPASS

Input Data

The first data card contains an identification title which consists of any identifier. It is read with a format specification of 8A10, for an 80 column card. This card is used by the subroutine INPTT.

The second data card contains the special option and contains two octal numbers read with the format specification of 1X, ϕ 20, 1X, ϕ 2, where there are 20 octal digits in every

60 bit word on the CDC computer used. The first variable read, IDBG, is used to indicate several options that are available. With each bit in the variable labeled A,B,C,D,..... from right to left,

..... IHG FED CBA

and have the following meanings.

A - if set then the values read by INPTT are printed, this bit is usually set.

B - unused for the 3-D program.

C - if set then the map of the point condition codes is printed, this bit is usually set.

D - if set then formatted output is produced on unit 6.

E - if set then unformatted output (binary) is produced on unit 8.

F - specifies the units to use, 0 in English and 1 is metric.

G - specifies the Mac Cormack variant to use, 0 is the forward/backward (FB) and 1 is the backward/forward (BF).

H - is used in conjunction with G to specify the order of using each variant. A value of 0 indicates a fixed variant, that is, the variant chosen by G is used throughout execution. A value of 1 causes the application of the variants to alternate at every step. This option should normally be set to 0.

I - unused.

J - unused.

K - unused.

L - if set indicates that the intermediate passes may be printed. If this option has a value of zero then SOLVE will call the PRNT routine only after the second step has been completed. However, if set then SOLVE will call PRNT after every call to one of the PASS routines. Whether output is actually produced is still determined by the print interval data.

The remaining option bits are unused. The second variable on the data card is intended for controlling the restart capability of the program which is not used and therefore should always have a value of zero.

The third data card specifies the cycle and print control data. It reads the following variables in a free field format; MXCYCL, IPINT, IPMN, IPMX, JPMN, JPMX, KPMN, KPMX, IPCYMN, IPCYMX. These have the following meanings.

MXCYCL - is the maximum number of cycles to process. It is incremented if necessary to make it an even number.

IPINT - is the print interval. The routine PRNT will print results every IPINT 'th cycle. If the L option is zero and IPINT is odd, the odd cycles will not be printed.

IPMN, JPMN, KPMN - specify the minimum I, J, K, range to start printing.

IPMX, JPMX, KPMX - specify the maximum I, J, K range to print

IPCYMN - is the first cycle at which any output is produced.

IPCYMX - is the last cycle at which any output is produced.

Use of the variables IPMN, IPMX, JPMN, JPMX, KPMN and KPMX allow output to be produced only for a region of interest. Similarly, the IPCYMN will allow output to be suppressed until the wave arrives at the area of interest.

The fourth data card reads the values of the CFL number and the artificial viscosity coefficient. The CFL number is the stability criterion,

$$CFL \equiv C_L \frac{\Delta t}{\Delta x} \leq 1$$

where C_L is the fastest wave speed. The viscosity coefficient is generally unused.

The fifth data card reads the material constants in free field format. The variables read are; MAT, ANU, CAPE, and RHOG.

MAT - This is a 10 character material designator, enclosed in quotes.

ANU - Poisson's ratio

CAPE - Young's modulus, in English units it is given in lbs/in^2 and metric as kpa.

RHOG - density, is gm/cm^3 always.

This is also the last data card processed by INPTT.

The sixth data card, the first processed by GRIDD, gives the size of the mesh. The variables read, in free field format, are; ITOTL, JTOTL, KTOTL, DX, DY and DZ, and have the following meanings,

ITOTL - the maximum number of points in the x-direction.

JTOTL - the maximum number of points is the y-direction

KTOTL - the maximum number of points in the z-direction

DX, DY, DZ - are ΔX, ΔY, ΔZ, the grid sizes, and should normally all be equal.

The seventh data card contains a single number which indicates the number of cards that follow and contain boundary data.

The next group of cards contain the boundary data, in the form; I, J, K, TXX, TYY, TZZ, TXY, TXZ, TYZ, U, V, W, where, I, J, K, give the location and the rest give the values. It is to be noted that the array TRAC in /PCODE/ common block must be large enough to hold all the data, as the program makes no checks.

The next group of cards are the point condition codes that define the geometry. These are arranged in groups of constant K, then each card is a constant I, with J locations across the card. If I=J=K=2 then the cards would be,

K=1

I=1 J=1 J=2

I=2 J=1 J=2

K=2

I=1 J=1 J=2

I=2 J=1 J=2

so that the location of each code is given by,

(1,1,1) (1,2,1)

(2,1,1) (2,2,1)

(1,1,2) (1,2,2)

(2,1,2) (2,2,2)

The first card after the point code contains a single number, which may be zero, this gives the number of user specified point codes. It must not be larger than the maximum number of entries that the array IUEQNS in common block /EQNS/ can hold, which the program does not check.

The final group of cards contains the definitions of the user defined point condition codes. The data is free field, with the first number being the positive value of the code number. It is to be noted that user codes are entered as negative numbers in the point condition code map as read by GRIDD. The remaining numbers on the card define the code. They are grouped as XPASS, YPASS, ZPASS. For the 3-D codes there are 28 values per card, including the code number itself. For example, if the standard code 1, which represents an interior point, were entered as a user defined code, with a code number of -8 then the data card for it would be,

8, 1,2,3,4,5,6,7,8,9, 1,2,3,4,5,6,7,8,9, 1,2,3,4,5,6,7,8,9,

Point Condition Codes - Predefined Values

Using a cube as the model, there are three different z-constant cross-sections. These will be called z-lower, for the lower face, z-mid, for the interior planes and z-upper, for the upper face. When, z-lower is defined as the K=1 face and z-upper is defined as the K=KTOTL face. These give,

z-lower

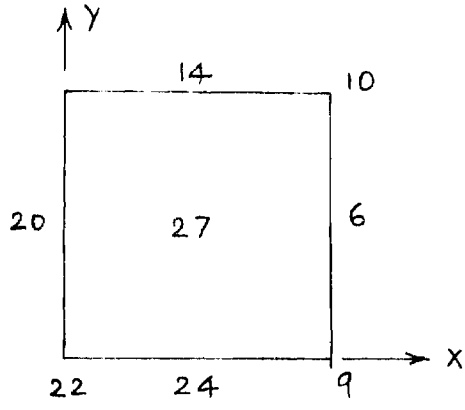

z-mid

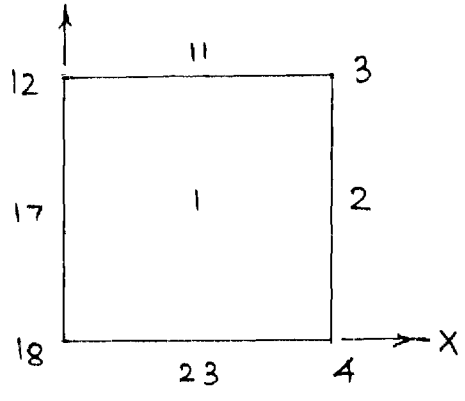

z-upper

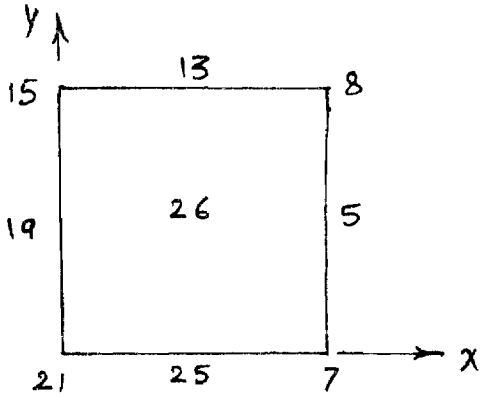

where all boundaries are traction boundaries.

As an example, code 17 is on a lower boundary, an interior y, and an interior z. Therefore, the definition for 17 is,

	ρu_t	ρv_t	ρw_t	σ_{xx}	σ_{yy}	σ_{zz}	σ_{xy}	σ_{yz}	σ_{xz}
XPASS	10	11	12	-13	14	15	-16	17	-18
YPASS	1	2	3	14	5	6	-7	8	-9
ZPASS 1	2	3	-4	5	6	-7	8	-9	

where,

σ_{xx} is a defined value, -13, -4, -4
σ_{yx} is a defined value, -16, -7, -7
σ_{xz} is a defined value, -18, -9, -9

As another example, code 6 is an upper x boundary, an interior y, and a lower z boundary. It is also a traction boundary so that, for its position on an edge, all stresses, except σ_{yy}, are defined, so that its definition is,

	ρu_t	ρv_t	ρw_t	σ_{xx}	σ_{yy}	σ_{zz}	σ_{xy}	σ_{yz}	σ_{xz}
XPASS	19	20	21	-22	23	-24	-25	-26	-27
YPASS	1	2	3	-4	5	-6	-7	-8	-9
ZPASS	10	11	12	-13	14	-15	-16	-17	-18

For the case where the body is symmetric about the x and y axes, there are additional point condition codes defined. They are assigned according to the following diagram,

z lower

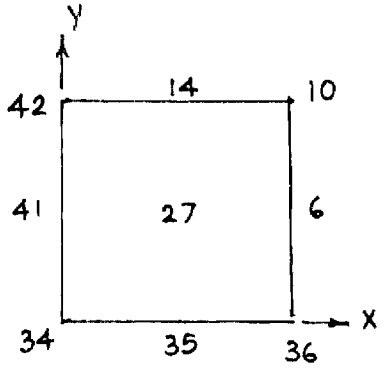

z - mid

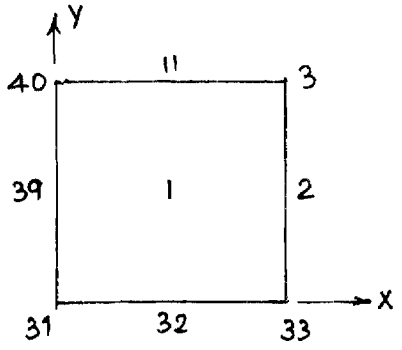

z - upper

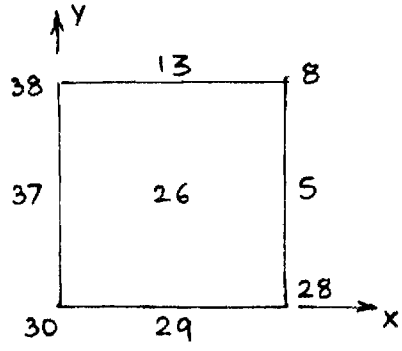

The symmetry conditon is obtained by setting appropriate velocities to zero and appropriate shear stresses to zero

—

Appendix II

Appendix II

User Guide to Axisymmetric Second Order Elastic Plastic Program*

The main program LW calls various subprograms. These subprograms may call additional subprograms as necessary. The specific subprogrmas called by LW are INPTT, GRIDD and SOLVE.

INPTT

This subprogram reads the following input data:

IPRINT: If 1 then print output per cycle.
If 2 then print output per two cycles.

IB: If 1 then the left boundary I=1, subject to step loading. If 2 then the left boundary I=1 subject to exponential loading.

TO, TI: These are the parameters of the exponential loading, only read for condition IB=2.

MXCYCL: This is the maximum number of cycles to carry out.

IPINT: This is the print increment, every IPINT th cycle is printed.

IPMN: This is the minimumX index to print.

IPMX: This is the maximum X index to print.

JPMN: This is the minimum Y index to print.

JPMX: This is the maximum Y index to print.

IPCYMN: This is the first cycle to start print.

IPCYMX: This is the last cycle to perform print.

P: The stability factor, must be less than or equal to 1.

MAT: This is a 10 character material identifier.

ANU: Poisson's ratio, ν (psi)

CAPE: Young's modulus, E (psi)

RHOG: Density, ρ (gm/cc)

YIELD: Yield stress (psi)

This routine also performs conversions of units as necessary for computations in lbin-micro sec units.

---

* In this computer program, the notations X and x refer to the Z coordinate. Similarly the notations Y and y refer to the r coordinate.

GRIDD

In this subprogram, the point conditon codes of the grids are set by reading the array IPT(I,J). There are nine different point condition codes. Every grid point corresponds to one point condition code. The definition is as follows:

Point Condition Code	Grid Points
1	Interior points
2	left boundary points
3	right boundary points
4	lower boundary points
5	upper boundary points
6	left and lower corner point
7	left and upper corner point
8	right and lower corner point
9	right and upper corner point

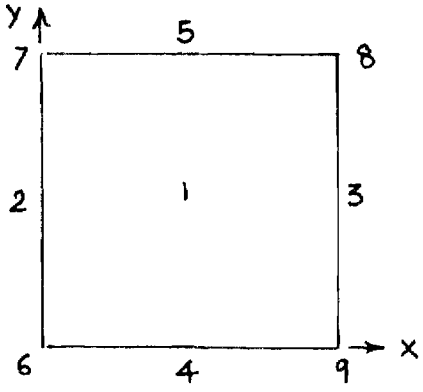

Depending upon the various point condition codes that are assigned to each grid point, the appropriate difference expressions of the spatial derivatives are formulated to execute the integration of the field equations. For example, if the point (I,J) has a point condition code 2 then the difference expressions for the spatial derivatives are formed by using data of points (I,J),(I,J-1), (I+1,J) and (I,J+1). But if point (I,J) has point condition code 8, then the spacial derivitives are formed by using data of points (I,J), (I-1,J) and (I,J+1) are expressed.

This subprogram also reads the following input data:

ITOTL: Number of grid points in X - direction

JTOTL: Number of grid points in Y - direction

DX: Cell size in X direction

DY: Cell size in Y direction

NPLT: Number of cards of initial conditon data

TRAC (L, K): This array contains the initial condition data (e.g. tractions at boundary I=1)

SETUP

This subprograms initializes the IEQNS array which contain the point conditon codes/equations and cross-reference values.

SOLVE

This routine controls the application of the Lax-Wendroff scheme. On odd cycles it performs Lx pass first, then Ly pass. For even cycles it performs Ly pass which is first followed by Lx pass. It also determines to print the results at every cycle or at every other cycle. It also determines when the last required cycle of calculations have been completed. For IB=2, it will get suitable boundary tractions by calling subroutine BUNDRYZ. The specific subprograms called by SOLVE are XPASS, YPASS, PRNTT, BUNDRYZ.

XPASS

This subprogram performs the Lx Lax-Wendroff operator and correct the stresses due to rotation and check Von Mise's yield condition. And at pass Lx(t+Dt), calculatesthe new time step Dt by calling subroutine EVADT. The subprograms called by XPASS are VALUE, RHODP, EVADT, CORECT and YIELDD.

YPASS

This subprogram performs the Ly Lax-Wendroff operator, corrects the stresses due to rotation and checks Von Mise's yield condition. The subprograms called by YPASS are VALUE, RHODP, CORECT, YIELDD.

RHODP

This subroutine is to calculate the density from the pressure-density relationship from the known pressure. This subprogram must be changed for different pressure-density relationships.

BUNDRYZ

This subprogram computes the boundary stresses due to the exponential loading case (i.e. IB=2). This module must be changed for different boundary loading conditions.

VALUE

This is a subprogram that is used to calculate the values of coefficients of the field equations and the specific derivatives. This subprogram VALUE calls the following subprograms: CODEIJ, VAREA, FDXY.

CODEIJ

This subprogram returns the specific Lagrangean coordinate indices of the vertices of elements for different point conditon codes.

VAREA

This subroutine calculates the values of areas of specific elements. It calls function TRIANG.

TRIANG

This subprogram calculates the value of areas of specific triangles.

FDXY

The subprogram returns the value of specific derivative with respect to x or y.

EVADT

This subroutine evaluates time step for every grid point on the basis of stability considerations.

CORECT

This subroutine performs the corrections to computed stresses due to rotation and finite deformation. The specific subprogram called by CORECT is OMEGA.

OMEGA

This subroutine calculates the values of $\cos(2\omega)$ and $\sin(2\omega)$, where ω is the angle of rotation.

YIELDD

This subprogram checks the Von Mise's yield condition.

PRNTT

This subprogram prints the computed values of the field variables.